BYU Civil & Environmental Engineering
IRA A. FULTON COLLEGE OF ENGINEERING

Performance Criteria for Free-Standing Timber Frames with Knee Braces

Zachary Halisky
Graduate Research Assistant

Sarah Partington
Undergraduate Research Assistant

Johnn P. Judd
Assistant Professor

November, 2022

EXECUTIVE SUMMARY

Traditional mortise and tenon timber frames have been used in modern construction for a substantial period of time with acceptable performance against weather phenomena and other hazards. However, performance criteria for this style of timber framing are not well defined in current codes and standards. To determine performance criteria for free-standing timber frames with knee-braces, four tasks were undertaken: (1) Two timber frame specimens were tested under cyclic loads to determine hysteretic behavior, damage states, and to explore rehabilitation of a damaged member using self-tapping screws. Three damage states for were identified: peg shear, tenon tearout, and post or beam splitting. Self-tapping screws were able to restore the strength of the 2-peg timber frame with the damaged beam, but not the stiffness of the frame. (2) Four timber frame mortise and tenon connection specimens were subjected to damp conditions for six months and then tested under monotonic tensile load to determine the effect of joint details. The results indicated that connection types tested had similar strength and stiffness. (3) Twelve free-standing timber frames with knee braces located at various sites across the United States were tested in the field under impulse loading to determine the fundamental period of vibration and to estimate damping. A relationship between the fundamental period and the mean roof height was fit to the test data using a power-law equation, and three sets of parameters were determined: a lower-bound equation for seismic loads, an upper-bound equation for wind loads, and mean equation for human-induced vibration performance criteria. (4) Component fragilities for timber frames were developed based on damage states derived from the cyclic and monotonic test data, and an estimate of repair procedures, repair costs, and repair time based on a survey of practicing timber framers.

ACKNOWLEDGEMENTS

Financial support for this project was provided by the Timber Frame Engineering Council (TFEC) and the Timber Framers Guild (TFG) (https://www.tfguild.org/). Funding was also provided by Brigham Young University. Fire Tower Engineered Timber (Providence, Rhode Island) provided the original full-size timber frames that were used in the cyclic tests.

The authors appreciate David Anderson, Structures Laboratory Manager in the Department of Civil and Construction Engineering, Rodney Mayo, Structures Laboratory Instrumentation Manager, Ethan Brown, Ben Meek, and Micah Harley, Laboratory Assistants, and Tate Baird and Jacob Lopez, undergraduate students, for their invaluable help in the experimental work.

The authors also wish to recognize members of the TFEC who selflessly volunteered their time to help with the vibration tests. Thank you to Eric Morley, and Larry Scarborough (Carolina Timberworks, West Jefferson, North Carolina), Tom Nehil and Chris Newman (Nehil-Sivak, Kalamazoo, Michigan), Peter Henrikson (PH Timber Framing, Grand Marais, Minnesota), Dick Schmidt (Fire Tower Engineered Timber, Laramie, Wyoming), Dave Kaplan (Elevated Design Build, Fort Collins, Colorado), and Kip Apostle (Euclid Timber Frames, Heber Valley, Utah). The authors would like to recognize Ben Brungraber, Joe Miller, and Dick Schmidt, for guidance and suggestions during the project.

Although many people made this research project possible, this report represents the opinion of the authors and not necessarily that of the TFEC or the TFG. The findings, conclusions, and recommendations expressed in this paper are those of the authors and do not necessarily reflect the views of the sponsors or the people acknowledged.

TABLE OF CONTENTS

LIST OF TABLES

LIST OF FIGURES

CHAPTER 1 INTRODUCTION

The background and motivation for the research are presented in this chapter, and the objective and scope of the research are defined. The chapter also includes a brief summary of the organization of this report.

1.1 Background

Timber frames that use large-dimension wood members with mortise and tenon connections and wood pegs are a traditional construction method that has been successfully used throughout the world for centuries. Examples of timber frames include ordinary structures, such as residential structures and free-standing structures, especially gazebos, and pavilions (Fig. 1.1).

Fig. 1.1. Examples of free-standing timber frame structures.

Other examples of timber frames include more notable structures, such as covered structures for bridges (Pierce et al. 2005), as shown in Fig. 1.2, and roof trusses, such as the roof of the Notre Dame cathedral (Courtenay 2022) shown in Fig. 1.3.

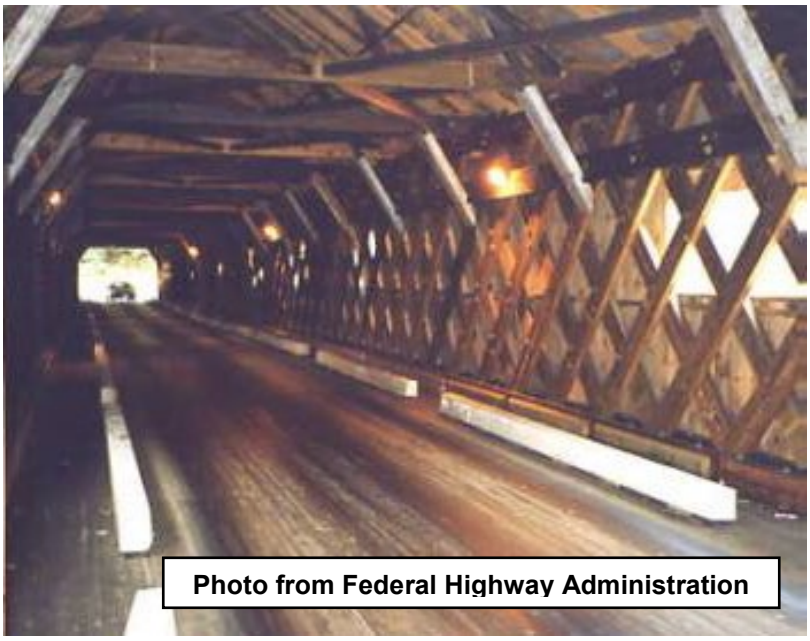

Fig. 1.2. Typical covered bridge with timber frames.

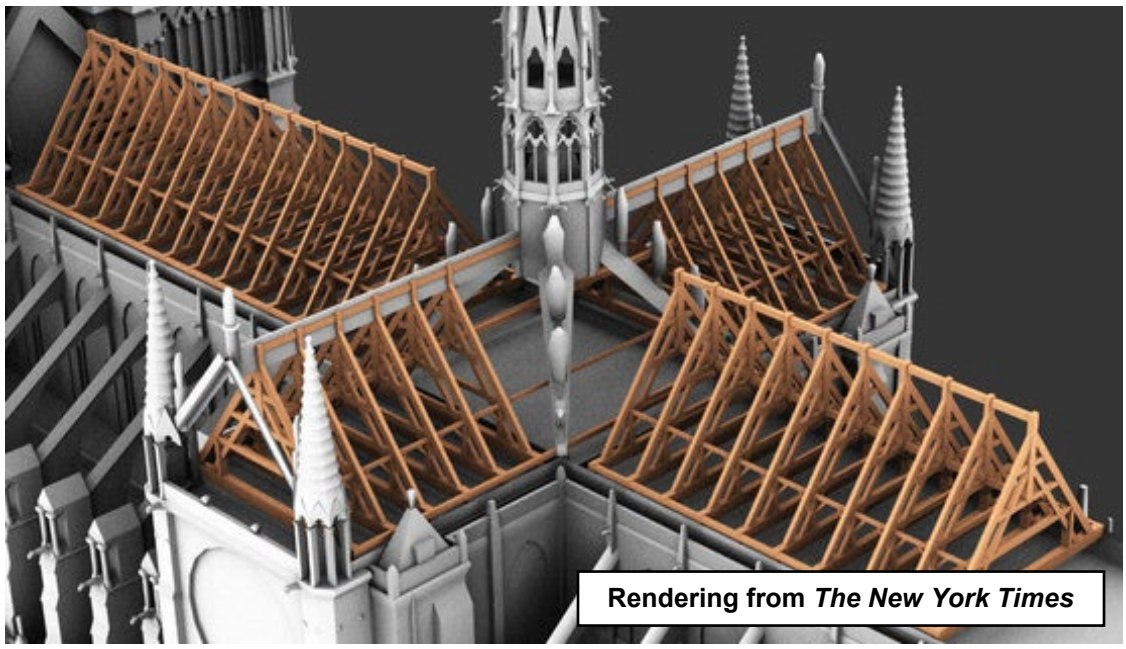

Fig. 1.3. Timber frame roof in the Notre Dame cathedral.

In addition to existing structures, timber frames are also used in new construction. For example, Fig. 1.4 shows a free-standing timber frame for a farmer's market that was built in 2013. Although modern innovations in building, including structural composite lumber, connector hardware, and mass-produced steel fasteners, have led to efficient light-frame wood construction methods that are ubiquitous in North America, there has been a resurgence in traditional timber framing (Heitz 2016).

Traditional knee-braced timber frames with mortise and tenon connections have been widely used and continue to be prevalent in both residential and commercial designs because they are relatively easy to construct and because they are an efficient frame assembly, especially for transferring shear forces (Schmidt 2007).

Fig. 1.4. Free-standing timber frame built in 2013.

An important contributor to this revival of timber framing is that the complex and time-consuming process of crafting precision timber joinery by hand has been largely automated in recent years by advancements in tooling and machinery (e.g., Wu et al. 2019, Pedersen et al. 2023). For example, Fig. 1.5 shows typical computer automated drafting (CAD) software and timber milling machinery that can be used to design and fabricate a timber frame. This automation has the potential for higher precision construction compared to hand-constructed frames. For builders, this can lead to greater productivity. For owners, this can lead to lower cost. As a result, these advancements have greatly reduced the labor required for traditional timber frame construction and made possible more widespread adoption of timber frames in aesthetic and structural applications.

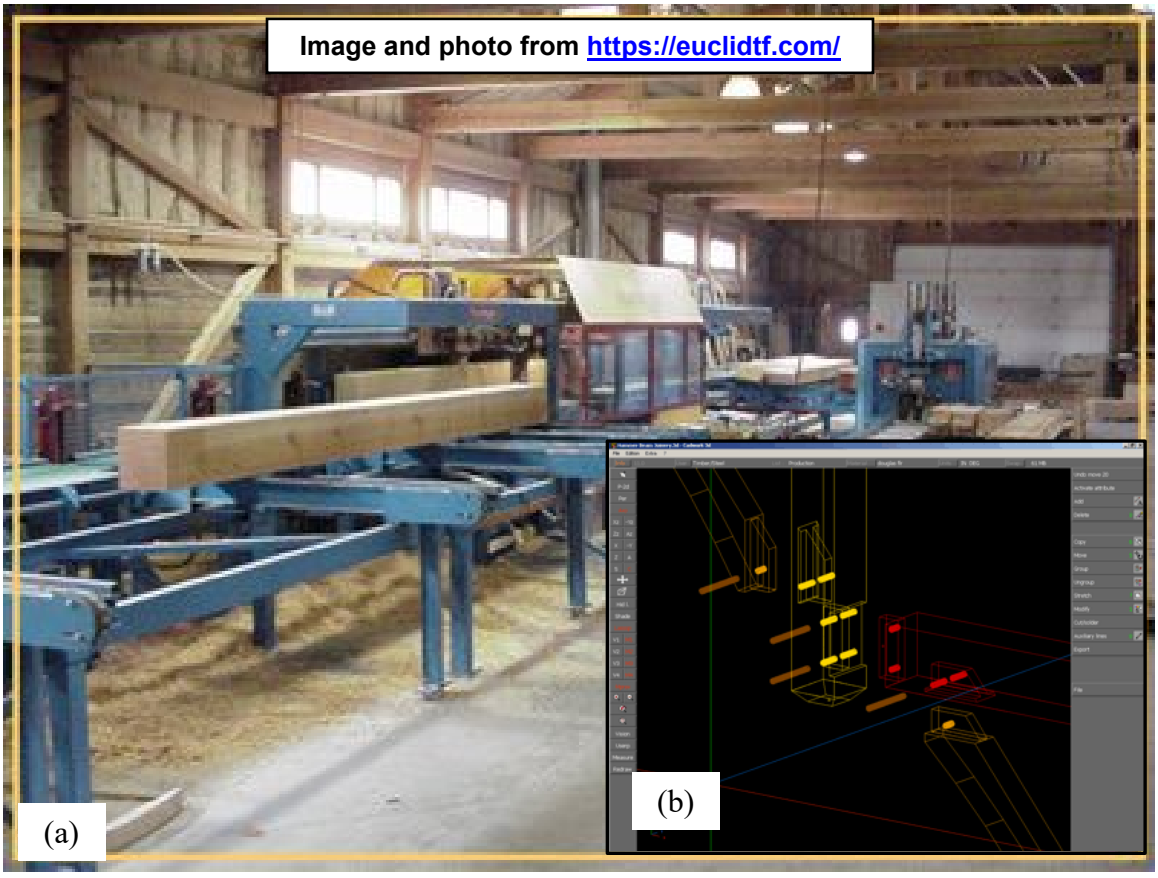

Fig. 1.5. Typical (a) timber milling machinery and (b) CAD software.

1.2 Research Motivation

Despite the prevalence of timber frames, the structural performance of timber frames is not well understood. In one of the first efforts to investigate structural behavior, Brungraber (1985) tested timber frames and joints in timber frames under static monotonic loads. Among other findings, the study showed that the joints had an adequate factor of safety for connection failure. Since that study, several efforts have been undertaken in timber frame engineering. Examples include historic timber frame construction (e.g. Feio et al. 2014, Chen 2020) and timber frames with mortise and tenon joinery (e.g. Aejaz et al. 2021).

This report covers the literature relevant to timber frames that use knee-braces for lateral resistance and that are typical of newer construction in North America. Most of this research has focused on the behavior of individual connections in timber frames. For instance, Schmidt and MacKay (1997) adapted the European yield model (Soltis and Wilkinson 1991), originally developed for dowel type connections with fasteners, to connections with wood pegs. The study concluded that some of the yield modes originally developed for steel fasteners are not applicable to pegs. Since the European yield model is partly based on the dowel bearing strength of the wood, Church and Tew (1997) examined the effect of peg diameter and grain orientation. The study determined that the bearing strength is not sensitive to either parameter. Schmidt and Daniels (1999) tested joints in timber frames to determine applicable yield modes and to establish minimum edge and end distances to prevent failure of the connected members prior to peg failure.

To establish recommendations for modeling timber frames, Bulliet et al. (1999) tested several types of connections, including mortise and tenon connections. Sandberg et al. (2000) conducted double-shear tests of oak pegs and confirmed the yield modes proposed by Schmidt and Daniels. Schmidt and Scholl (2000) tested mortise and tenon connections with wood pegs to

determine the effect of load duration and connection detailing. Similar to connections with steel fasteners (Rosowsky and Reinhold 1999), the tests show that the duration of load does not affect the yield strength of the peg connections. Schmidt and Miller (2004) tested wood peg connections loaded in tension and developed an analytical model to represent the shear stress in a peg based upon the peg and base material specific gravities. Subsequently, Miller et al. (2010) developed an additional yield mode to represent peg shear. Hindman (2019) tested pegs from a variety of wood species and for a range of diameters to determine the bending yield strength. Judd et al. (2012) tested mortise and tenon connections under tensile load. The tensile test results indicated that the European yield model with the additional peg shear yield mode was adequate to predict tensile strength.

Research on the behavior of full-scale timber frames is relatively limited. Schmidt and Erikson (2003) tested single-story and two-story timber frames with knee braces under static lateral loads. Among other findings, the test results show that the compressive behavior of the knee-brace connection is significantly stronger and has higher stiffness compared to the tensile strength of the knee-brace connection. As a result, a timber frame with knee-braces is relatively flexible under lateral loading. To maximize the lateral stiffness of the timber frame, Schmidt and Erikson recommended that the length of the knee brace be at least 914 mm, the connections use two or more pegs, and connections are detailed with adequate end and edge distances, such as those as specified in the Standard for design of timber frame structures and commentary (Timber Frame Engineering Council 2019).

Cyclic tests of full-scale timber frame knee-brace subassemblies have been conducted to investigate the effect of the number of pegs and the moisture condition of the lumber on the hysteretic behavior (Judd et al. 2018). Two types of connections (2-peg and 3-peg) and two

moisture conditions of lumber (green and dry) were examined. The results show that the timber frame subassemblies exhibited asymmetric behavior due to brace bearing in the post during compressive load excursions and dowel-type behavior of the pegs in the brace during tensile load excursions. Accordingly, the predominate modes of failure were peg shear and tenon tear out when the brace was in tension and perpendicular-to-grain tension failure of the post-to-beam connection when the brace was in compression. Specimens with 3-peg connections were stronger compared to specimens with 2-peg connections, and specimens constructed with green lumber had increased deformation capacity compared to specimens constructed with dry lumber.

Free-standing timber frames with knee braces are common and have demonstrated acceptable performance when subjected to earthquakes and windstorms, yet performance criteria for these structures has not fully investigated in the literature and it is not currently well defined in construction standards and building codes. For example, ASCE 7 *Minimum Design Loads and Associated Criteria for Buildings and Other Structures* (ASCE 2022) provides guidance for considering vertical deflections (e.g., ponding), lateral deflections (story drift), camber and floor vibrations. However, application of the guidance to free-standing timber frames with knee-braces is either not appropriate (because floor vibrations isn't a concern in many cases) or requires special attention (because the frames are usually open and story drift limits are mostly based on preventing damage in a closed structure). Building codes are similarly ambiguous. For example, the 2018 International Building Code (IBC), https://codes.iccsafe.org/content/IBC2018, the 2018 International Residential Code (IRC), https://codes.iccsafe.org/content/IRC2018, and the 1997 Uniform Building Code, International Conference of Building Officials, Whittier, California.) do not mention timber frames. As a consequence, timber framer designers lack clear and appropriate performance criteria that is afforded for other structural systems.

1.3 Research Objective

The objective of this research is to determine performance criteria for free-standing timber frames with knee-braces. The hypothesis is that free-standing timber frames can be accurately evaluated for most performance considerations based on the connection detailing, two-dimensional phenomenological models, and the fundamental frequency of the system, similar to the approach used to mitigate floor vibrations in steel and wood structures.

To accomplish the research objective, four tasks (Fig. 1.6) were created to determine performance criteria: (1) cyclic tests of timber frames were conducted to determine hysteretic behavior and to explore rehabilitation schemes for improved performance after damage due to a lateral-loading event; (2) durability tests of brace connections were conducted to determine the effect of joint details on the tensile strength and behavior of typical knee-brace connections; (3) vibration tests of timber frames in the field were conducted to determine the fundamental period of vibration and modal damping; and (4) a life-cycle analysis was conducted to determine the embodied carbon and the damage states for knee-brace connection and to establish component fragilities for performance assessment.

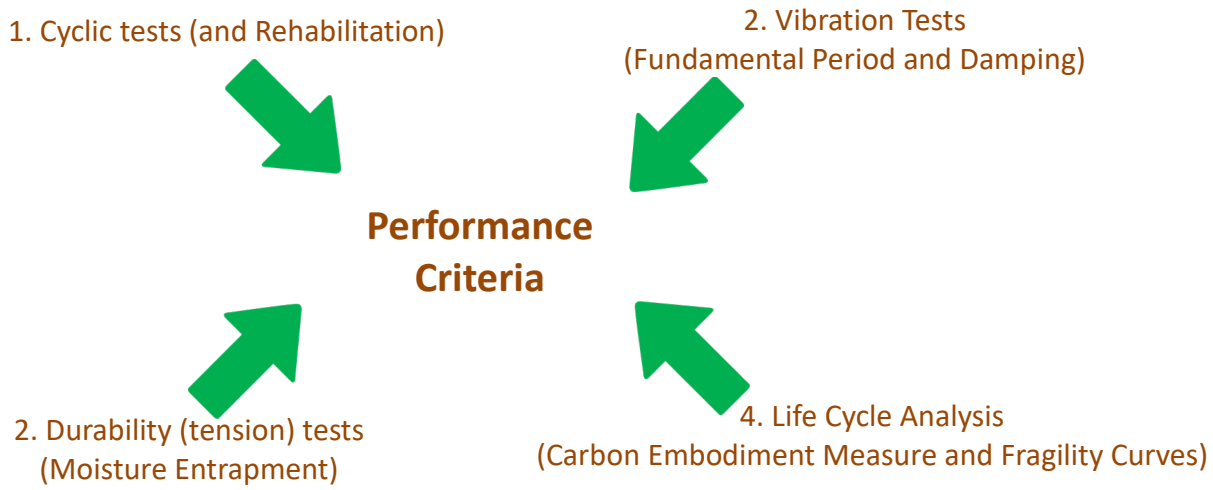

Fig. 1.6. Diaphragm of research approach.

The scope of this research is limited to performance criteria for wind and seismic loads, and for selected loads that are not clearly addressed in conventional codes and standards, such as loads imposed by human activity. The effect of water content is considered in the durability tension tests.

1.4 Report Organization

This report summarizes the research approach and findings. It is organized into seven chapters:

- Chapter 1 gives the background and motivation for the research and defines the objective and scope of the research project. The chapter also includes a brief summary of the organization of this report.

- Chapter 2 contains a literature review. Performance criteria and limit states for steel structures, concrete structures, masonry structures and timber structures are briefly discussed. Serviceability and strength criteria are discussed for each material to better understand how their performance criteria may relate to free-standing timber frame structures with knee braces.

- Chapter 3 describes the cyclic tests. Two timber frames that had been previously tested in a field demonstration were reconstructed and then tested under cyclic load to determine the hysteretic behavior and probable damage states. One of the two timber frames was also rehabilitated to determine one possible repair scenario where self-tapping screws are used

to strengthen damaged members in timber frames. The chapter includes a description of the frame preparation and assembly, instrumentation, cyclic loading sequence, rehabilitation approach, data reduction, and a discussion of the test results.

- Chapter 4 describes the durability tests. Two types of mortise and tenon connections were subjected to damp conditions for an extended period of time (6 months) and then tested under monotonic load to determine the effect of a slope cut and a weep hole cut on the tensile strength of the connection, and to determine damage states for performance assessment and life-cycle analysis. The chapter includes a description of the joint preparation, instrumentation, monotonic loading rate, data reduction, and a discussion of the test results.

- Chapter 5 describes the vibration tests. Timber frames at various locations in the United States were tested in the field under impulse loading to determine the fundamental period of vibration and to estimate damping. The field tests were conducted used a crowd-sourced approach: the Brigham Young University team and volunteers from the Timber Frame Engineering Council downloaded an app to their smartphone and use it to measure accelerations. The chapter includes a description of the testing sequence, data reduction, and a discussion of the test results.

- Chapter 6 describes the life-cycle analysis and presents component fragility curves. A life-cycle analysis was used to determine the embodied carbon and the damage states for knee-

brace connection. Component fragilities for performance assessment were established based on data from a survey of practicing timber framers.

- Chapter 7 contains a summary of the research project (cyclic tests, durability tests, vibration tests, and life-cycle analysis) and the implications of the main findings from the research. Areas for future research are also identified.

CHAPTER 2 LITERATURE REVIEW

This chapter contains a literature review. Performance criteria and limit states for steel structures, concrete structures, masonry structures and timber structures are briefly discussed. Serviceability and strength criteria are discussed for each material to better understand how their performance criteria may relate to free-standing timber frame structures with knee braces.

2.1 Serviceability Criteria for Steel

Serviceability criteria for steel buildings is covered in AISC 360-22 *Specification for structural steel buildings* (AISC 2022). Deflection in steel structures can result in separation, cracking, leakage onto exterior features, as well as damaging interior components of a building. Limiting values of deflection will vary depending on structure type, detailing and intended use. Limit states also vary on visually objectionable deformations repairable cracking, creep, settlement, and similar long-term effects.

Limits are instituted on lateral deflection to counteract any damage effects of wind on exterior cladding as well as non-structural walls and partitions. The defining parameter of this measurement is the total building drift or the story drift determined for each floor of the building.

Brittle cladding may result in smaller drift limits. Lateral drift may also be caused by rigid body rotation of cladding or partitions. The wind load used for drift limit checks will vary by designer, particularly at which yearly interval is selected.

Floor vibrations are an increasing focus for designers. Damping properties are diminished with long-span, flexible floor plans. Vibrations can be considered annoying or a disturbance to occupants depending on the usage of a building. Acceleration is the defining evaluation standard for this criterion.

Wind motions are often measured by the floor or roof accelerations. The human toleration of the effects of wind motions is subjective. AISC 360-22 describes this criterion as related to the perception of building motion from factors such as "maximum displacement, velocity, acceleration, and the range of change of acceleration" (AISC 360-22). Available dampening is often an important project control for this criterion.

Temperature effects such as creep, shrinkage, and expansion can become an increasing concern for buildings with masonry walls. Steel expansion may result in various patterns of cracking in concrete, depending on both cover thickness and reinforcement spacing (Browne 1980).

Slippage between standard connections is not accounted for in serviceability criteria, unless the connection is a special case or produces substantial rotation or deflection from relatively small bolt slip. Special provisions are made for slip-critical conditions in AISC 360-22 Section J3-8.

2.2 Strength Criteria for Steel

Strength criteria for steel buildings is also covered in AISC 360-16. For example, for tension members, the limit states include yielding in the gross section, rupture of the net section, and block shear. Compression members such as columns may either be governed by global buckling or local buckling depending on the slenderness of the element. For flexural members, the limit states include yielding (plastic moment), lateral torsional buckling, and local buckling, as well as other limit states. For deep and or thin webbed I-shaped members, shear yielding in the web or shear buckling may be significant limit states. Fatigue failure is also possible and can be a long-term strength limit state for steel members, particularly for members subject to vibrations within the structure or cyclic weight bearing (Ulewicz and Mazur 2013).

Since steel structures typically consist of thinly shaped cross sections, stability design is crucial for both individual elements and the surrounding structure. Thus, steel structures must be designed to consider all deformations (e.g., shear deformations), second order effects, geometric imperfections, inelastic stiffness effects, and uncertainty in both strengths and stiffnesses (AISC 360-22, Chap. C).

2.3 Serviceability Criteria for Concrete

Serviceability criteria for concrete structures is covered in ACI 318-19 Building Code Requirements for Structural Concrete (ACI 2019). Members in flexure are designed according to maximum permissible deflections as indicated in ACI 318 Table 24.2.2. Immediate and time-dependent deflections are considered in the ACI code by standard modulus of elasticity and

moment of inertia. Members prone to cracking and varying depth requiring a more complex analysis. Time-dependent deflections vary between prestressed and non-prestressed members. Prestressed flexural members with regards to serviceability are designated by three different classes: uncracked, cracked, or transitioning between cracked and uncracked. These classifications depend on the magnitude of stress in the pre-compressed tension zone. The difference between these classes will also affect which basis deflection is calculated on, whether in the gross section or the cracked section.

A well distributed array of flexural reinforcement is important to control cracking; in this case, it is optimal to have many finer cracks versus a few larger cracks in a reinforced concrete member for durability and appearance sake. Poor durability of the concrete itself and deterioration in reinforcement bars is one leading cause of corrosion in scenarios where reinforced concrete is subject to external chemicals and weathering (Vu and Stewart 2005). In order to circumvent corrosion, a designer may use reinforcement with a higher yield strength due to its higher chromium content and micro-composite alloy structure (Harries et al. 2012).

ACI 318 24.4 states that shrinkage and temperature effects on structural concrete slabs require the placement of reinforcement perpendicular to that of the principal reinforcement. In the event that other structural members restrain a slab from change in volume, additional reinforcement may be needed in order to negate tension effects. With rise or fall in temperature and difference in the coefficients of thermal expansion, thermal stresses can change and cause either tensile or compressive effects (Chen and Choi 2002).

Although ACI 318 Section 24.4 does not apply to slabs-on-ground, corrosion in these slabs may be also be eliminated with the substitution of Glass Fiber Reinforced Polymer (GFRP) rebar

over steel rebar (Chen and Choi 2002). However, this could result in lower tensile stresses, causing both larger crack-spacing and widths.

2.4 Strength Criteria for Concrete

The latest ACI code abides by the ultimate strength design method with safety reduction factors unique for specific structural elements and action taken on each member. The reduction factor may also vary depending on the strain distribution of the reinforced concrete member and whether this indicates that the member is compression controlled, tension controlled, or falls in the transition zone. Nominal strength capacity is calculated for parameters such as flexural strength, axial strength, one-way shear strength, two-way shear strength, torsional strength, bearing, and shear friction (ACI 2019).

2.5 Serviceability Criteria for Masonry

Masonry will crack due to a variety of external factors such as dimensional change, extreme loading, thermal change, reactive soil movement, interaction with other structural elements and internal factors such as long-term internal expansion from clay products. These conditions require masonry to have a series of design procedures in order to mitigate and chance of cracking. Mortar also plays a role in serviceability due to the ability to seal irregularities in masonry units as well as allow some movement between units (Hochwalt and Amrhein 2012).

2.6 Strength Criteria for Masonry

Both solid and hollow clay masonry units physically require a minimum compressive strength, maximum water absorption, and maximum saturation coefficient to be defined for each grade (Hochwalt and Amrhein 2012). Concrete masonry unit strength also relies on minimum compressive strength and maximum water absorption, along with oven-dry density of concrete used per each grade.

2.7 Limit States for Traditional Timber Frames

Timber frames have been observed in failure for both serviceability and strength limit states from various instances. In load-bearing cases, frame members may fail in strength from excessive bending or shear. However, under seismic activity, heavy timber frames must transfer significant forces through a small number of highly stressed connections (Kasal et al. 2004). These joint connections are assumed to carry no moment, with members in contact at joints modeled as beam-columns with the effects of shear (Bulleit et al. 1999). Mechanical failures at these connections can occur in either the fasteners or joints themselves. The preferred method of failure is yielding of the pegs, due to the ease of replacement and isolating pegs as a primary item of design for joint construction (Schmidt and Scholl 2000).

Among the first to research joint behavior in traditional timber frames was Brungraber (1985), who developed general test programs for mortise and tenon connections subject to gravity loads. His analysis succeeded in demonstrating prediction basic connection failure, specifically that the peg or mortise would fail prior to the tenon. A few years later, Wilkinson (1991) proceeded

to apply the European Yield Model developed by Johansen (1949) to establish the first relations between specific gravity and bolt diameter with bearing strength of dowels in timber connections. Although these tests were performed on metal nail and bolt connectors, this initial observation indicated that such relationships could potentially be applied to wooden dowels as well. That same year, Soltis (1991) stated that the NDS would adopt the EYM approach to determining lateral strength in single-fastener connections. Three failure modes and associated equations to establish yield strength were given with this change.

Schmidt and Mackay (1997) were among the first to truly apply the EYM to wooden-peg dowels in testing with traditional frame connections. Tests were performed in peg bending, shear, and dowel bearing in order to confirm that the existing yield model equations from the latest NDS were applicable to wooden pegs. Concluding results indicated that the EYM was applicable, as well as improving some areas of knowledge within this specific connection. One such example was the conclusion that tenon splitting/relishing could be prevented by ensuring an end distance from the peg center to tenon end of at least three times the peg diameter. However, at this point, researchers did not fully understand which failure mode was preferable for design recommendations.

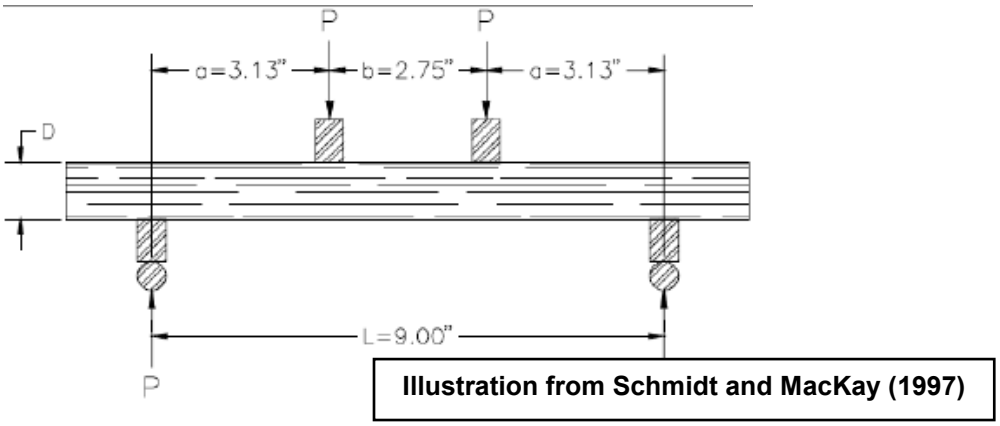

Fig. 2.1. Peg bending test.

Two years later, Schimdt and Daniels (1999) performed a variety of tests in order to better summarize failure modes, verify allowable stress values, and determine proper joint design recommendations. They determined that the preferred failure mode at these connections is peg failure, due to the ductile nature prior to ultimate failure within the dowel. Their findings indicated that there were in fact five possible failure modes for pegged mortise and tenon joinery. Bearing failure of the main and side members is specified, along with bearing failure of the peg. Both shear and bending failure are possible in such pegged connections. These connections are more likely to fail in shear when the base material of the peg has a relatively high bearing strength. Fig. 2.2 below shows the revised list of failure modes.

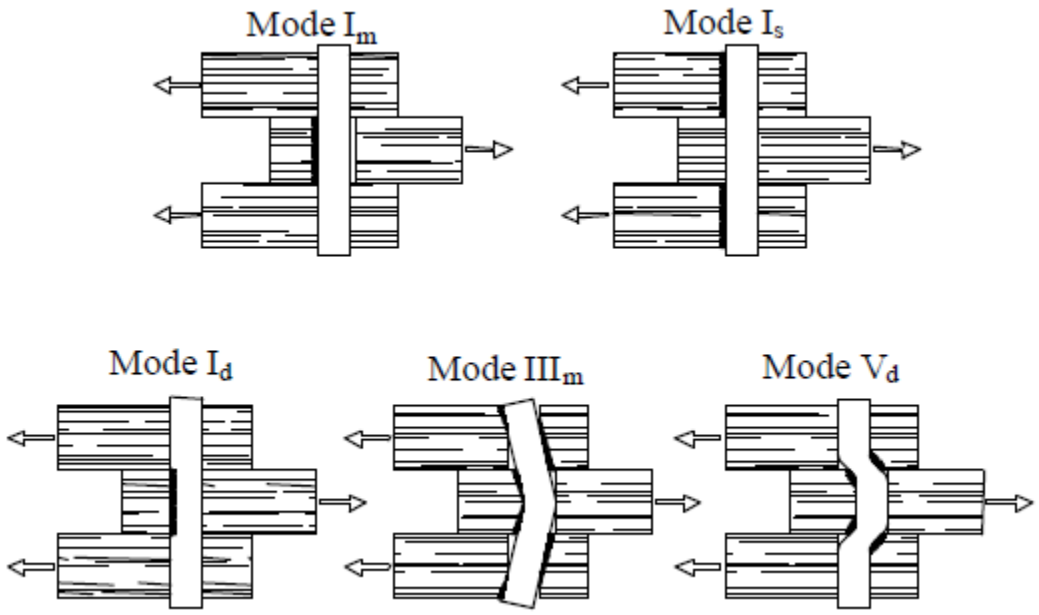

Fig. 2.2. Proposed failure modes for joints.

The same research performed by Schmidt and Daniels to summarize these failure methods also produced strength equations for four of the five failure modes based on factors such as the diameter and number of fasteners, as well as dowel shear capacity and bearing strength. However, an analysis of stiffness characteristics for pegged joints was not produced until Sandberg et. al (2000). They developed a linear model based on specific gravity of the joint members to estimate overall joint stiffness. From this, an empirical equation for joint stiffness based on peg and member flexibility was derived.

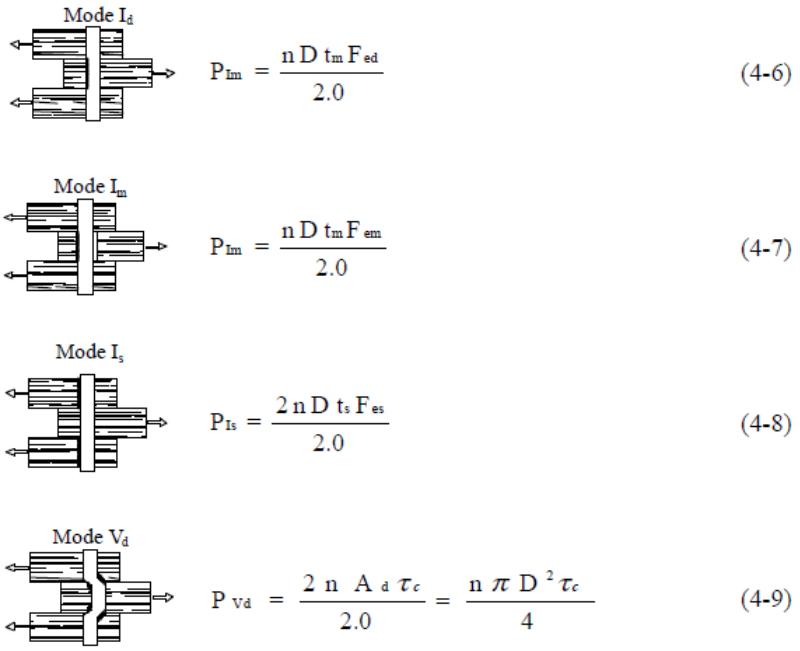

Fig. 2.3. Design strength equations for failure modes.

As mentioned in the introduction, Schmidt and Miller (2004) produced an analytical model for the shear wooden peg dowels loaded in tension within these joints. They produced an allowable shear equation based on the specific gravity of the joint and peg species. These studies also concluded that Yellow Poplar is a viable choice in timber framing, comparable to Douglas Fir. Hindaman (2017) determined a conservative estimate of dowel bearing strength Fyb by combining data from Schmidt and MacKay (1997) with a single-factor regression of additional test data done at Virginia Tech. The resulting equation was based solely on the specific gravity of the dowel base material, negating the effect of diameter.

Another form of joint failure in mortise and tenon frames can occur via splitting due to tension acting perpendicular to the grain (Schmidt and Miller 2004). The NDS recommends that "designs which induce tension stress perpendicular to grain shall be avoided whenever possible (AWC 2018)." For dowel-type fasteners loaded perpendicular to the grain at the edge, an edge distance factor of 4D (four times the diameter) is required. Van der Put (1999) developed design criteria for notches subject to perpendicular tension based on mechanics of crack propagation. This method of determining perpendicular tensile strength in timber notches is utilized in CSA 086, which was found by Hindaman (2016) to have the most accurate results in terms of predicting splitting resistance amongst other models. Hindaman's testing of different species of timber resulted in significant interaction of edge distance and specific gravity with the maximum load and stiffness. However, wood anatomy was found to not have an effect on the mechanical properties which played a role in resistance.

The grain orientation and angle of mortise in a joint were observed by Judd et al. (2012) in a test of different specimens. Results varied between failure modes, but ultimately showed a trend of decreasing stiffness with smaller angles of the mortise connection. Ring orientation did not

exhibit any specific trends in stiffness relative to the tested specimens. This study generated a theoretical tensile strength model for mortise and tenon connections and confirmed that orienting the tenon member radially to the mortise grain would result in higher strength.

Gaps in between the mortise and tenon of a joint appear to have a significant impact in the behavior of failure. When these members are fitted tight against each other with a zero-gap value, the shear strength of a dowel is found to result in up to 1.3 times increase from the initial value (Schmidt and Daniels 1999). Sandberg et al. (2000) recommends modifying the double shear test used to predict joint stiffness to include a maximum gap or reduction of mode V_d capacity in order to account for this behavior.

Research on seasoning and load duration of mortise and tenon joints has developed alongside the aforementioned articles. Wilkinson (1988) initially studied bolted joints under short-term and long-term durations. Results showed an increase of maximum strength in the specimens tested after 1 year under a constant load. Creep in the specimens under lower loads approached zero after a period of three months, while considerable creep had occurred in a specimen tested at a larger constant load. Limited scope from this test made it difficult to draw any firm conclusions on time-dependent effects. Schmidt and Scholl (2000) conducted tests on full-sized mortise and tenon joints to determine the seasoning and detailing effects, as well as effects of drawboring and peg diameter in a long-term study. Drawboring was concluded to have a more adverse effect on larger peg diameters, and increase overall creep deflection (at least in Douglas Fir specimens). Damage in the tenon from shrinkage was found to be independent of magnitude or direction of the load applied. Another product of this study was a table of minimum detailing distances for several species of timber, as shown in Table 2.1.

Table 2.1 Minimum detailing distances.

Species	End (D)*	Edge (D)
Douglas Fir	2	2.5
Eastern White Pine	4	4
Red/White Oak	3	2
Southern Yellow Pine	2	2

*Add 1D with Drawbore

Table from Schmidt and Daniels (1999)

Schmidt and Scholl also verified, along with evidence from previous researchers, that load duration has a negligible effect on the yield strength of mortise and tenon joints. They recommend the further study of moisture content on tenon splitting and determining an allowable maximum moisture content.

Prediction of joint failure can be demonstrated through the aforementioned equations and modes in strength analysis developed in various studies. Jiang et al. (2018) developed a novel index for structural stiffness identification in traditional Chinese mortise and tenon joints through accelerations outliers and effective stiffness. This model could be used to predict structural joint stiffness in the event of rehabilitation capability and repairs. Additional research is needed in order determine if this approach is valid for traditional frames with knee braces.

Deflection is a key serviceability factor for timber members in loading. The NDS has outlined deflection calculations for bending members and long-term loading when experienced (AWC 2018). Palka (1981) reviewed literature based on previously studied timber fasteners and summarized the criteria in which long term deflection is affected heavily by joint behavior, while short term deflection is usually governed by elements of the frame itself. Beerschoten et al. (2012) demonstrated that longitudinal post-tensioning in beams within timber frames can assist in satisfying deflection criteria.

The IBC outlines decay and termites as another failure mechanism for timber in service. Decay may take presence as a result of thermal, light, mechanical, or chemical effects (Stalker, 1971). As per section 2304.12.4, any frames in geographical areas of heavy termite hazards must be of a durable species or contain treated preservative as per approved methods. Epoxy injection and sealing is a common method for treating weathered timber in a structural application (Avent, 1985). In accelerated aging tests done on shear blocks, Avent recommends reducing the dry condition shear stress of Southern Pine by 1/3 following epoxy repair. Design criteria is needed in this area in order to determine the most optimal repair scheme for timber subject to decay, and whether epoxy is an efficient means for repair in the event of weathering.

2.8 Summary

Literature on performance criteria and limit states for steel structures, concrete structures, masonry structures, and timber structures were reviewed in this chapter. Previous research has examined the behavior and failure modes of traditional mortise and tenon timber frames. Several areas of timber frame performance criteria have not been fully addressed in prior research were identified. These areas are the focus of the next four chapters, starting with the strength and behavior of frames (as opposed to joints) under cyclic loads and rehabilitation of damaged frames (Chapter 3), strength and behavior of mortise and tenon joints due to weathering and decay (Chapter 4), elastic stiffness and fundamental period of free-standing timber frames (Chapter 5), and the carbon embodied in timber frames and component fragilities for performance seismic, wind, or other assessment of free-standing timber frames with knee-braces (Chapter 6).

CHAPTER 3 CYCLIC TESTS

This chapter describes the cyclic tests. Two timber frames that had been previously tested in a field demonstration were reconstructed and then tested under cyclic load to determine the hysteretic behavior and probable damage states. One of the two timber frames was also rehabilitated to determine one possible repair scenario where self-tapping screws are used to strengthen damaged members in timber frames. The chapter includes a description of the frame preparation and assembly, instrumentation, cyclic loading sequence, rehabilitation approach, data reduction, and a discussion of the test results.

3.1 Frame Specimen Preparation and Assembly

Prior to the tests mentioned in this report, the two timber frames were previously tested in a field demonstration under a cyclic load in order to determine (1) the hysteretic behavior and (2) the probable damage states. Fig. 3.1 shows a photo of the field demonstration. Both frames were retained their respective field tests and the braces which had failed originally were replaced with newly manufactured members.

Fig. 3.1. The 3-peg frame originally tested in the field under cyclic loading.

Fig. 3.2 shows an elevation view drawing of the frame. Each frame had two nominal 8x8 posts connected by an 8x12 beam. The posts and beam were Douglas Fir. White Oak was used for the 1-inch diameter pegs. 4x8 braces (also Douglas Fir) connected each post to the beam. One timber frame used 2-peg connections and 4x8 knee braces, and the other frame used 3-peg connections and 4x10 knee braces. The connection details for these braces were based on a previous study sponsored by the TFEC (Judd et al. 2018). Fig. 3.3 shows a rendering of the 3-peg connections. The original timber frames were constructed by Trillium Dell Timberworks.

An apparatus was designed in order to properly fit both the two-peg and three-peg frames for support and testing. The base of each post was connected to a pin support via metal plate connections fitted into the dado slot on the front of the leg. Both supports were welded to a wide flange beam which was anchored to the floor with a DYWIDAG bar system

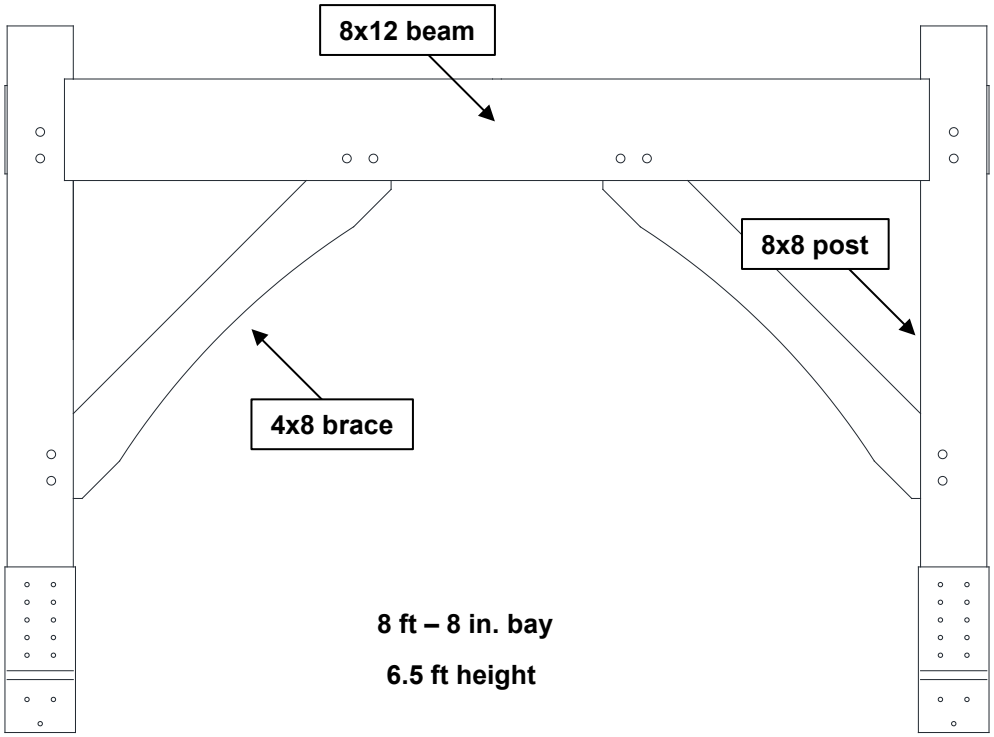

Fig. 3.2. Drawing of the 2-peg frame.

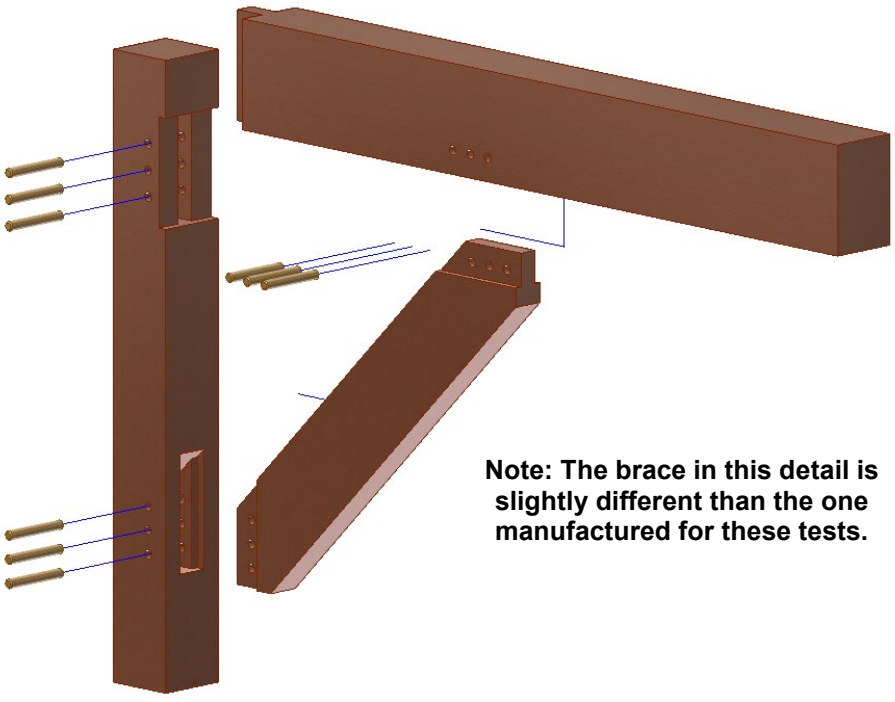

Fig. 3.3. Rendering of the 3-peg frame connection details.

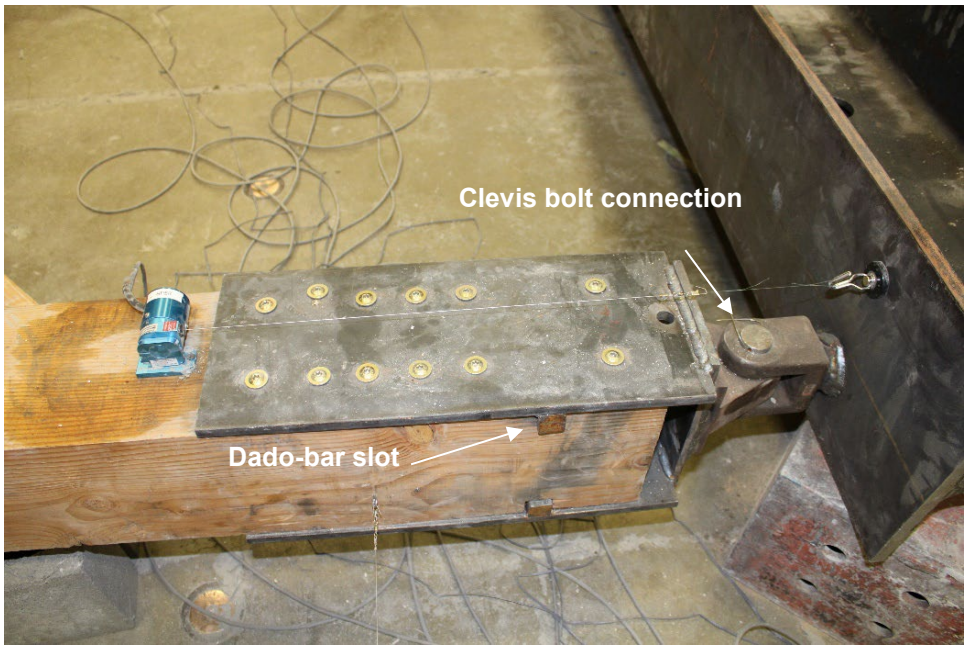

Fig. 3.4. A dado-slot plate connection to beam for the frame support system.

Fig. 3.5. DYWIDAG Anchors securing the support beam to the floor.

The top of the frame rested on two separate rollers that were supported by a wide-flange beam. The faces of each post were fixated between a spreader beam resting on top of the rollers at the same elevation as the frame. A hydraulic actuator was fastened to the face of the spreader beam as shown in Fig. 3.6. This provided the ability to cyclically load the frame according to the stroke of the actuator. The actuator was fastened in place by a DYWIDAG anchor system similar to that of the supports at the base of the frame (Fig. 3.7).

Fig. 3.6. DYWIDAG Anchor system securing actuator to the floor.

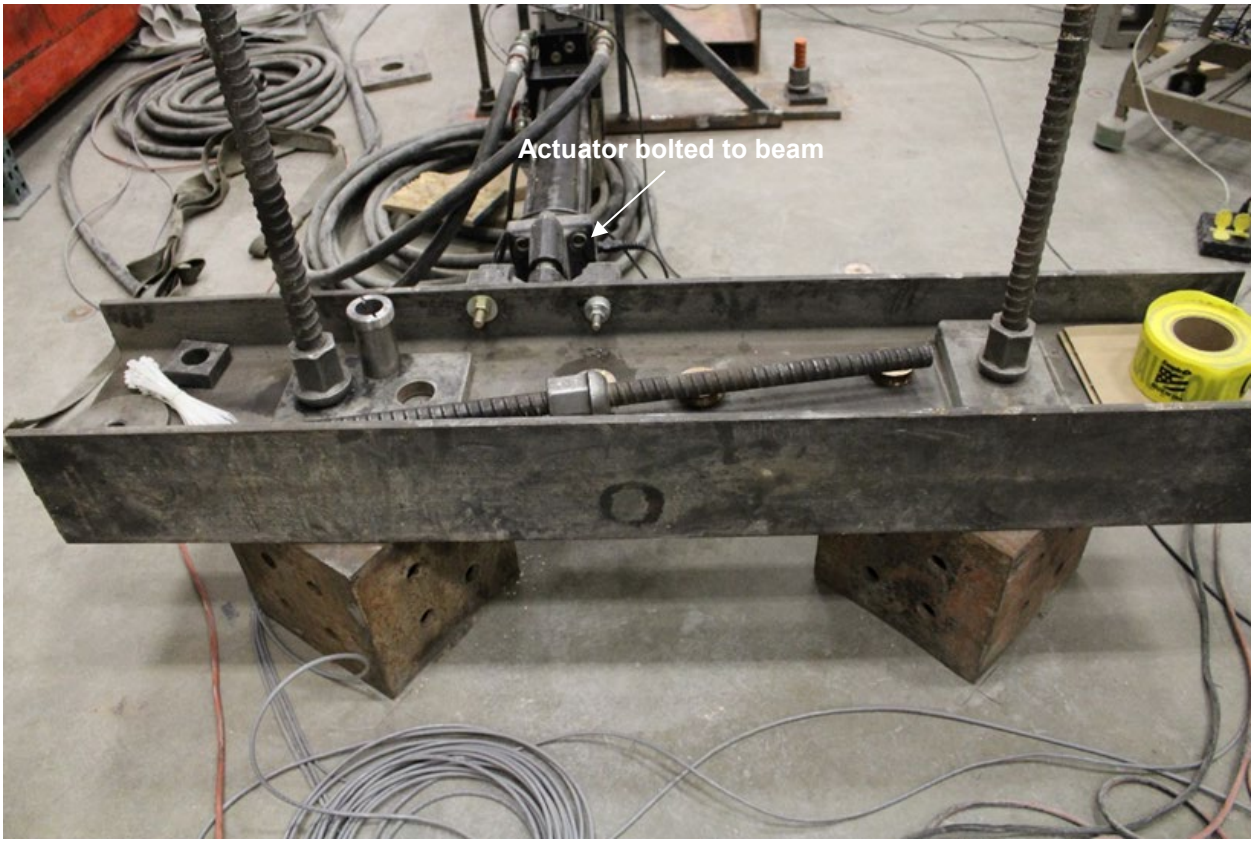

Fig. 3.7. DYWIDAG Anchor system securing actuator to the floor.

3.2 Instrumentation

String potentiometers were secured to the frame at different locations along adjoining members and connections to the supports. Two strain gauges were placed on each brace within the frame, totaling the instrumental count to 14 string pots and four strain gauges. Each of these instruments were calibrated prior to the tests and utilized during each cycle in order to show displacement within the frame. The four string pots at the base of the supports were utilized in order to account for slippage in the DYWIDAG anchors. This slippage was first experienced in a preliminary test and addressed prior to the remaining trials in order to minimize impact on instrument readings.

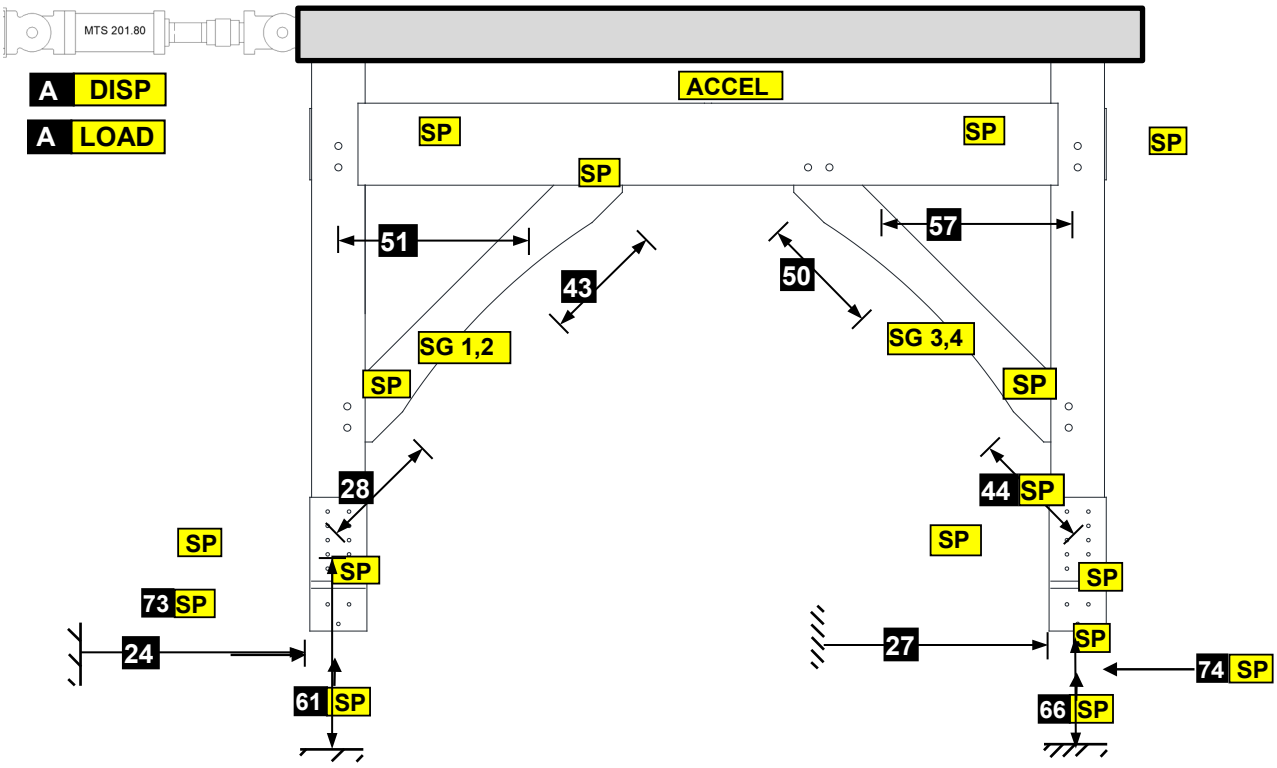

Fig. 3.8. Instrumentation plan showing position of string potentiometers and strain gauges.

Table 3.1. Instrumentation plan: label and purpose.

Label	**Purpose**
A1	Actuator load
A2	Actuator displacement
SP20	Frame drift
SP24, SP27	Left, right reaction displacement
SP28, SP43, SP44, SP50	Brace to post/beam connection separation
SP51, SP57	Beam to post separation
SP58, SP59	Frame uplift
SP73, SP74	Anchor support drift
ACCEL	Acceleration
SG 1,2 SG 3,4	Strain gages: top of left and right braces

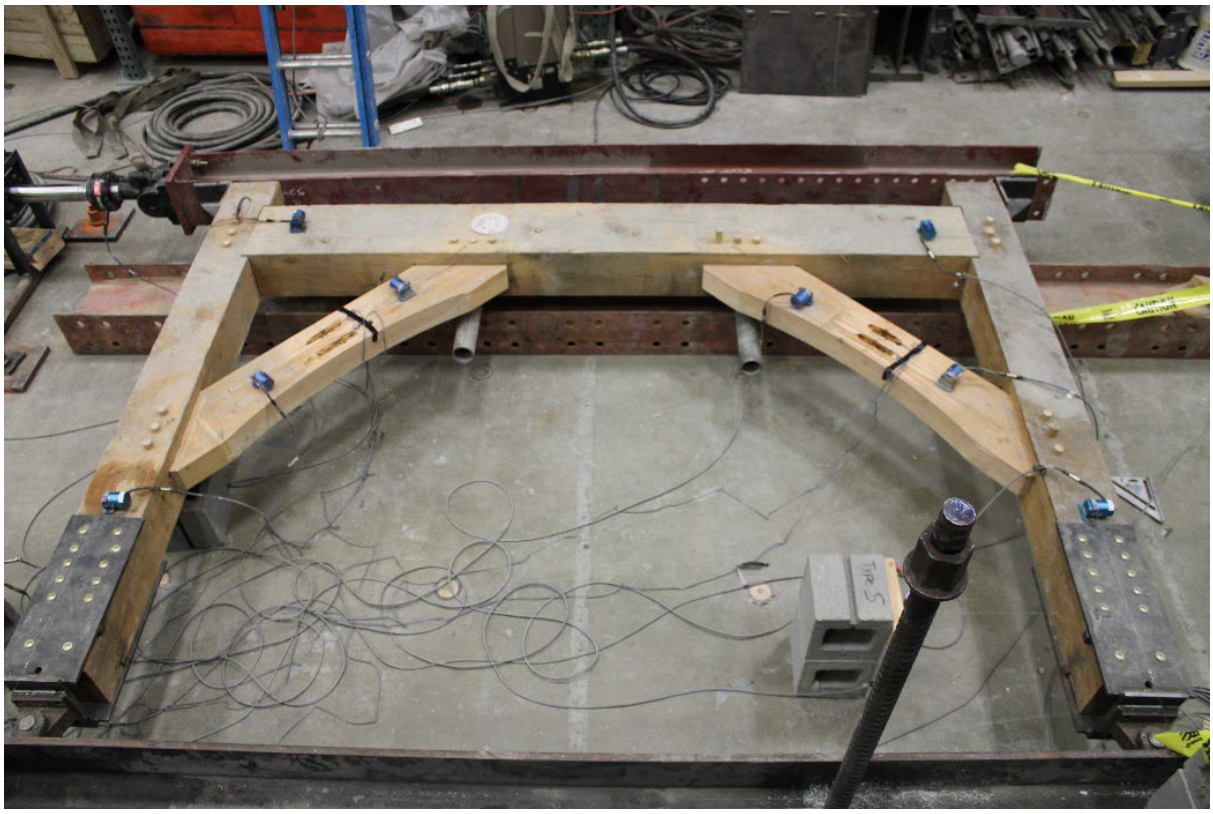

Fig. 3.9. Completed testing apparatus with 3-peg frame specimen.

3.3 Loading Sequence

Each frame was tested under the same fully-cyclic loading regime consisting of increased displacements from the actuator arm per every two intervals. The loading sequence was adapted from the AISC 341 (AISC 2022) loading sequence that is used for seismic qualification of steel buckling restrained braced frames. The approximate first yield was defined as $\Delta_y = 0.5$ inches, and story drift as $\Delta_m = 2.0$ inches actuator displacement. The rate of loading on the displacement control was 2.0 inches per minute. The load sequence is shown in Table 3.2.

As failure occurred within the frames, the test would be paused in order to observe the type of failure and overall condition of the frame before proceeding. When the frame was rendered incapable of sustaining more load, the test was ended and the frame reverted to its starting position.

The first test was run up to the 2.0-inch displacement mark and then paused due to noticeable slippage in the anchors near the footings. This was due to the washer used to fasten the DYWIDAG anchors through the slab giving every time the actuator reached max displacement. In addition, a lag-screw was inserted through the spreader beam flange into the top of the post (Fig. 3.10) in order to keep the spreader from drifting off the frame. After pausing and making proper adjustments, including the string pots used to measure the anchor slippage, the test was re-run on the 3-peg frame.

Table 3.2. Loading sequence for the cyclic loading tests.

Δ_y, Δ_m	Displacement (in.)	Time of Cycles (min.)	Total Elapsed Time (min.)
$0.5\Delta_y$	0.25	1	1
$1.0\Delta_y$	0.50	2	3
$1.5\Delta_y$	0.75	3	6
$2.0\Delta_y$	1.00	4	10
$2.5\Delta_y$	1.25	5	15
$3.0\Delta_y$	1.50	6	21
$3.5\Delta_y$	1.75	7	28
$1.0\Delta_m$	2.0	8	36
$1.5\Delta_m$	3.0	12	48
Additional 2 cycles at incremental deformation of $0.5\Delta_m$ = 1 inches until failure			

3.4 Test Results

The full trial of the 3-peg frame test was run up to 3Δ (6 inches) before ending the test. At around 4 kips of force applied to the frame, noticeable crack propagation was present between the top-right post and beam connection. Following this observation, there was slight rupture within the right brace during the next cycle and the connection became loose. Fig. 3.11 demonstrates the

aftermath of the increased load on the brace connection. The increasing tension pulled the brace tenon further out of the beam as the actuator reached 4.5 kips as observed in the SP50 data. While this brace continued to give, the left brace to left post tenon gradually started to fail and had demonstrated full failure at the loading point of 6 kips. The dado slot at the bottom of the right post began to fail during the last couple cycles and was followed with connection failure between the footing plate screws and the post. At this point the test was stopped and the displacement returned to zero.

Due to the tearout failure between the plate screws and post as seen in Fig. 3.13, the plate footing was unable to re-attach to the right post of the frame. This rendered the 3-peg frame useless to rehabilitate, and the 2-peg frame was inserted next into the testing apparatus.

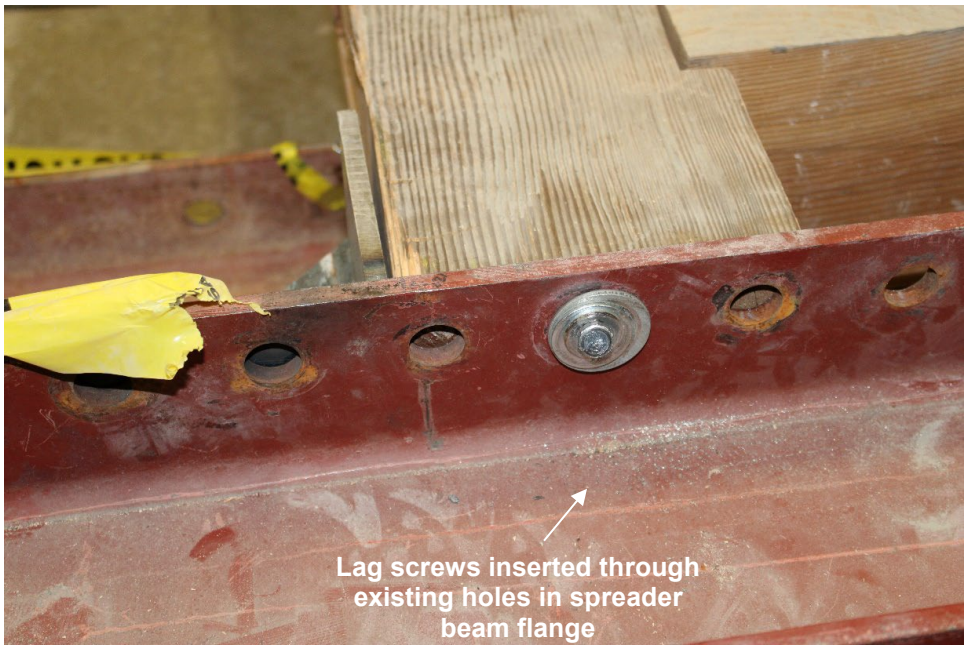

Fig. 3.10. Lag screw inserted into post to secure spreader beam.

Fig. 3.11. Tenon failure in the right brace-beam connection.

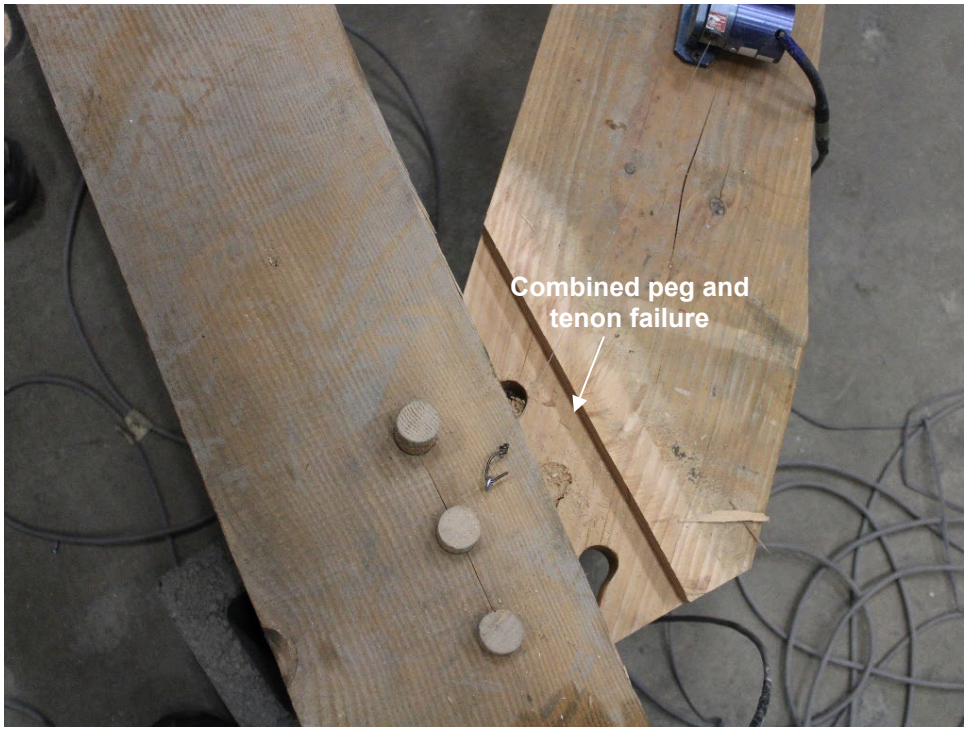

Fig. 3.12. Tenon failure in the right brace-beam connection.

The 2-peg frame was tested and resulted in a different behavior throughout the loading regime. At 4.5 kips of load, the top beam-to-post connection had a rupture within the tenon and resulted in crack propagation from the connection on the left side of the beam. On the following cycle, the crack began to move through the beam to the center as observed in Fig.s 3.14 and 3.15. At this point, the test was stopped and the frame was reverted to zero displacement. Partial tenon failure in the right brace was visible as the final rupture through the beam occurred.

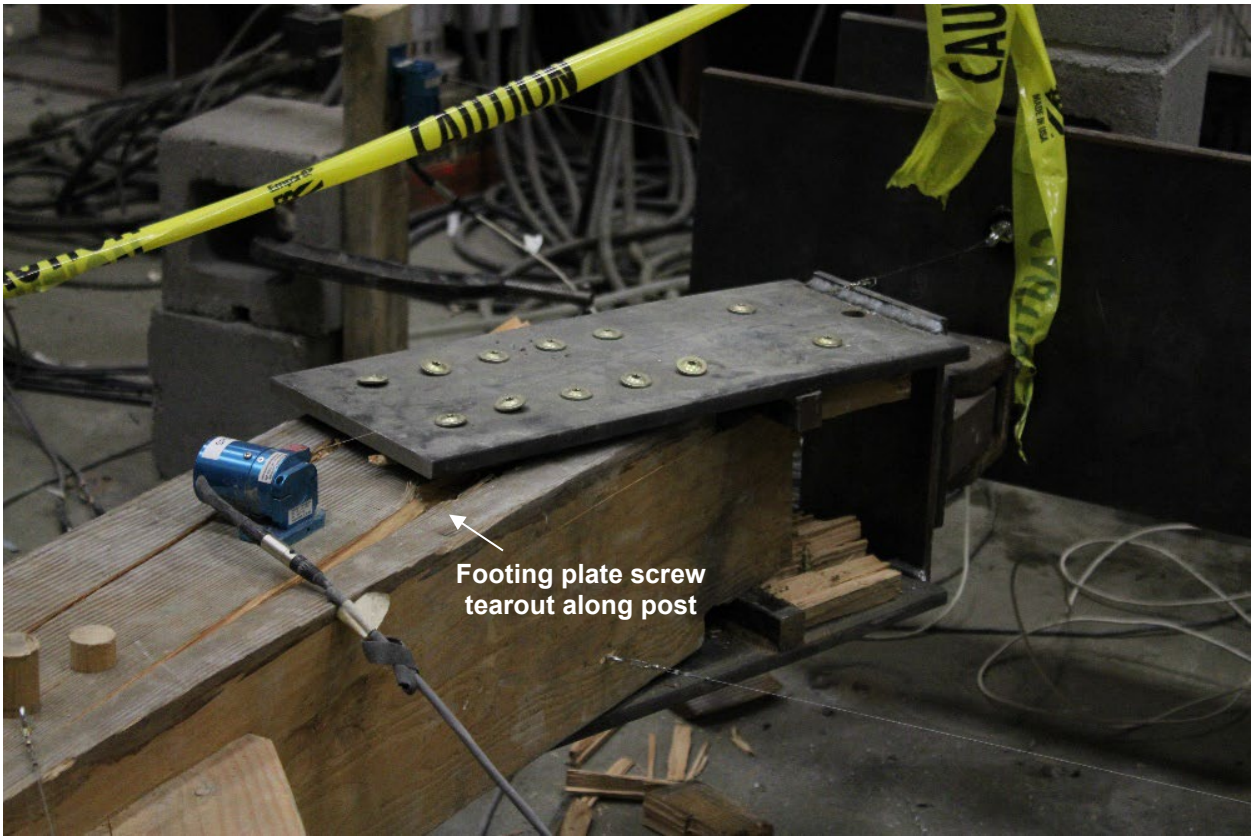

Fig. 3.13. Failure in the footing connection (tearout of screws and dado bearing).

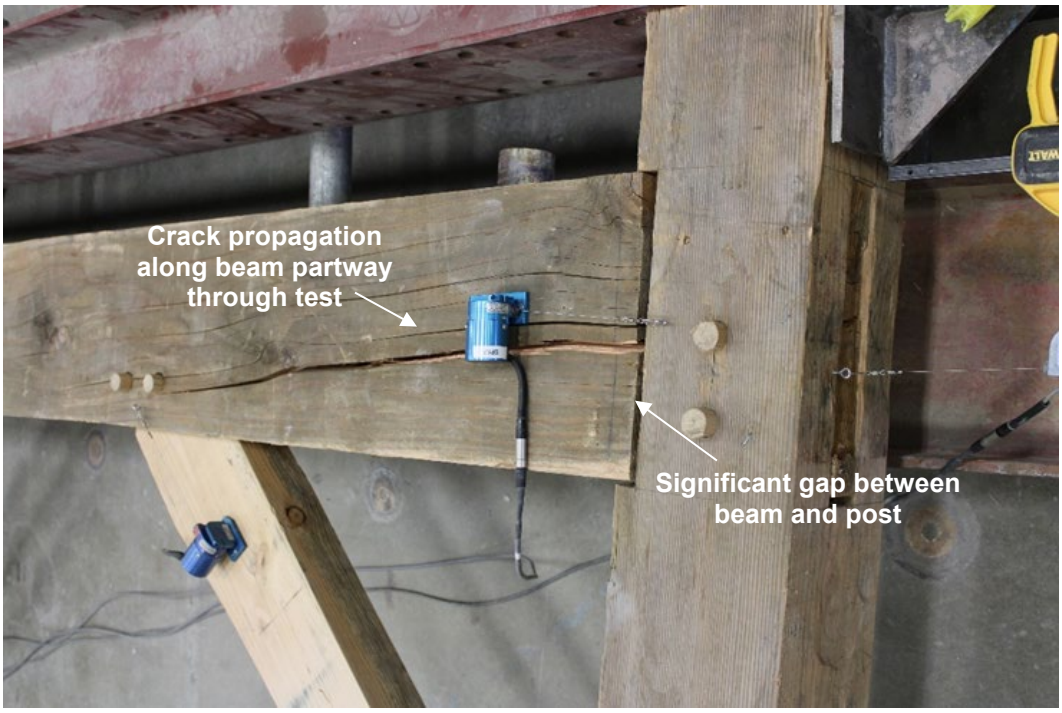

Fig. 3.14. Initial crack propagation in the right beam-to-post face.

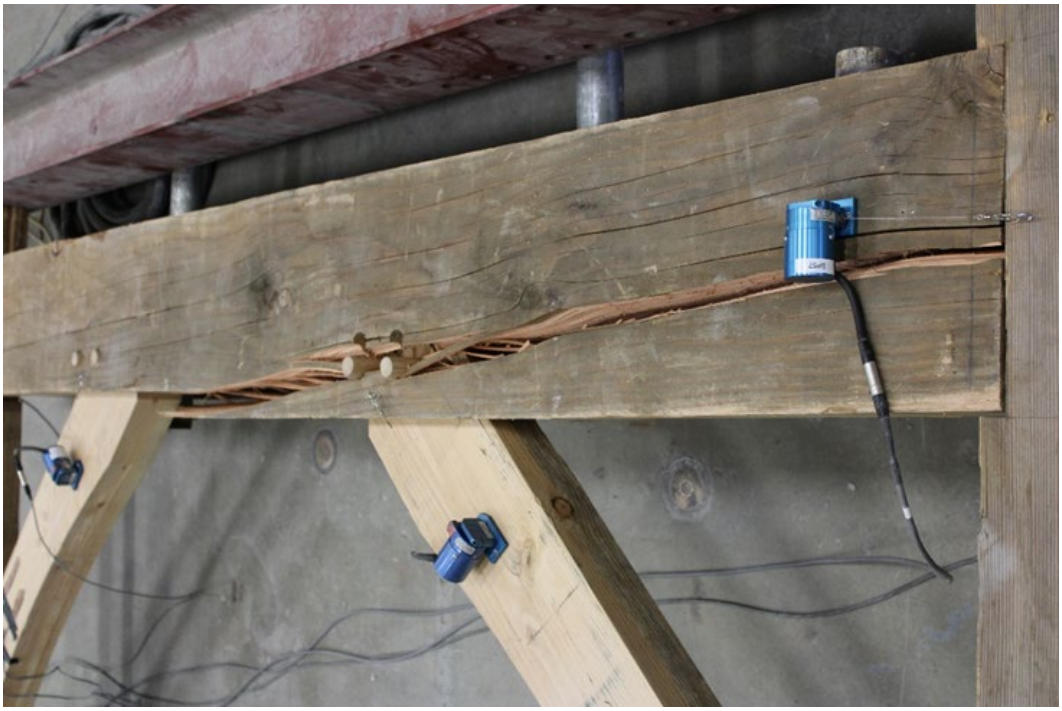

Fig. 3.15. Further cracking through the beam towards the right brace.

3.5 Rehabilitation Approach

The condition of the 2-peg frame following the completion of the initial test was sufficient enough to warrant a rehabilitation involving self-tapping screws to reinforce the beam. CYL 5/16x11-7/8 in. self-tapping screws were selected based on length needed to reinforce the depth of the beam with sustained cracking. Screws were inserted at an embedment angle of roughly 60º. Twelve screws were inserted from the top of the beam to the right of the brace, while another ten were inserted on the bottom of the beam to the left of the brace (Fig. 3.16). This was done due to the position of the crack as it moved from the right connection towards the center demonstrated in Fig. 3.15. The finished result of the lag screw installment is shown in Fig. 3.17 and Fig. 3.18.

Prior to starting the test, a C-shape member was also welded to the side of the left footing plates due to noticeable movement of the post during the original test. The right brace to beam connection was partially ruptured from the original test, but still had enough surface area between the tenon and beam joint to provide resistance when under compression.

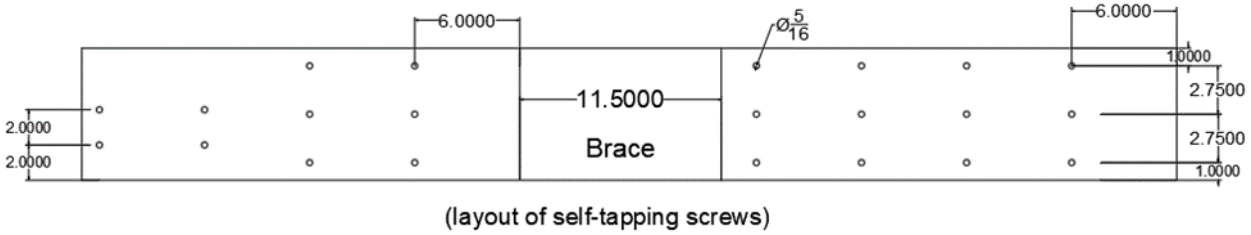

Fig. 3.16. Lag screw rehabilitation array.

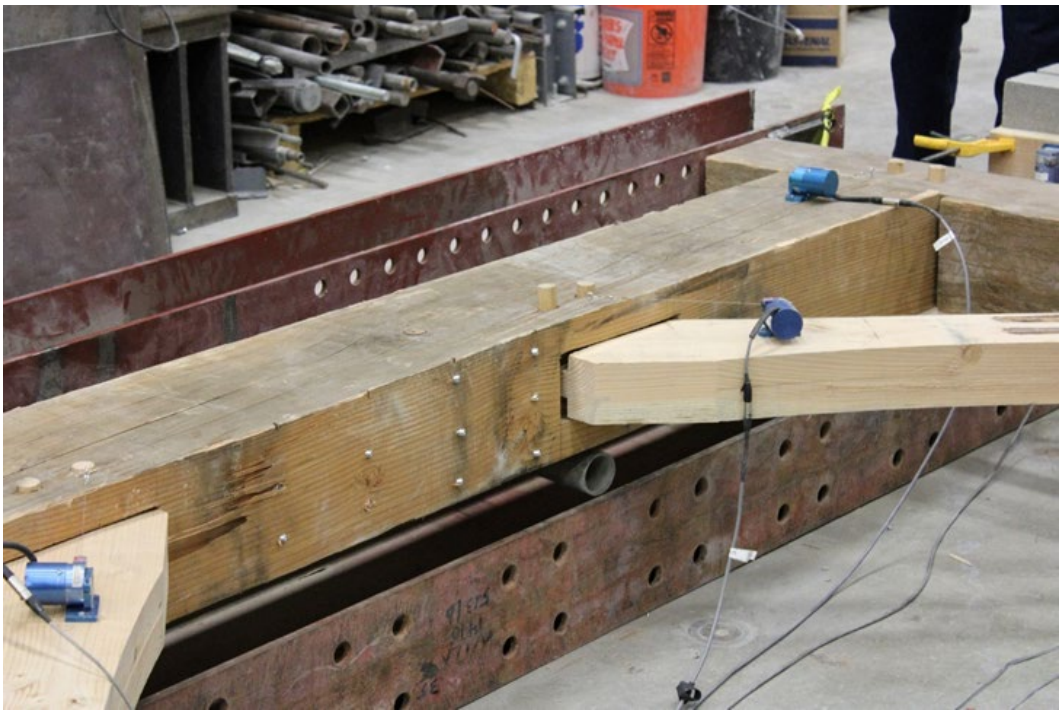

Fig. 3.17. Lag screws inserted in the bottom beam face.

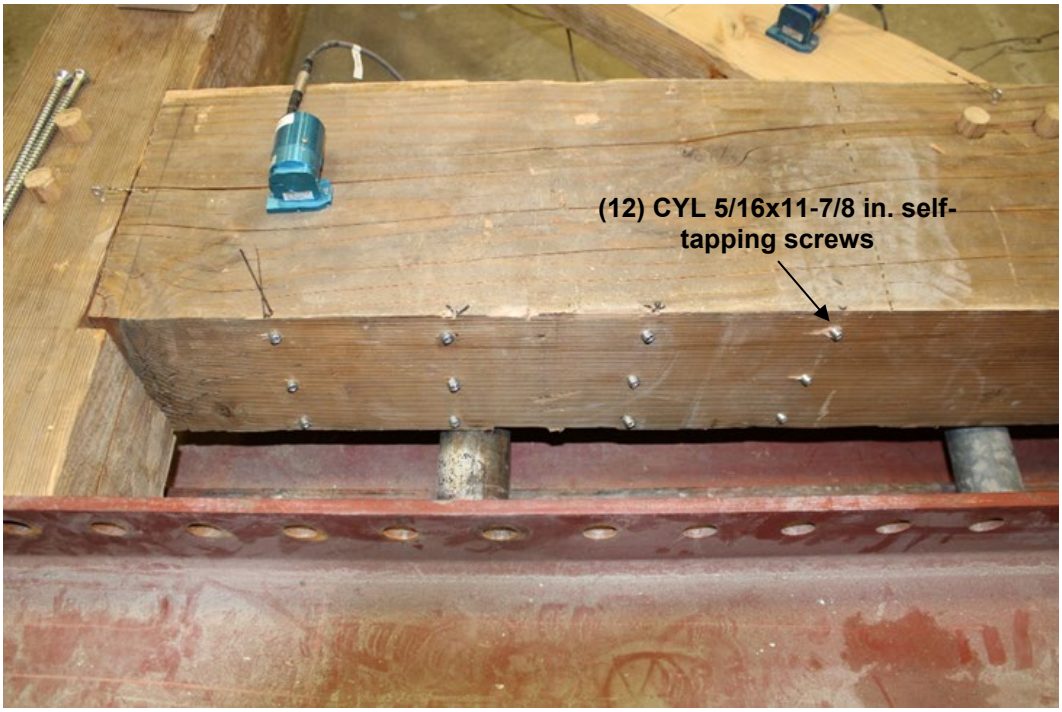

Fig. 3.18. Lag screws inserted in the top beam face to the right of the brace.

Despite part of the tenon joint being ruptured, the frame proceeded to transfer load throughout the system in a behavior similar to the original test. The tenon joint failed completely at 5 kips, yet continued to provide compressive strength to the frame when positive displacement from the actuator occurred. The beam did not experience cracking again until nearly 7 kips of applied force, in which the joint between the beam and right post also began to give as shown in Fig. 3.16. This crack continued through the base of the beam while the right brace-to-beam joint failed completely. Through the last cycle, both footings experienced bending within the plate connections (Fig. 3.21).

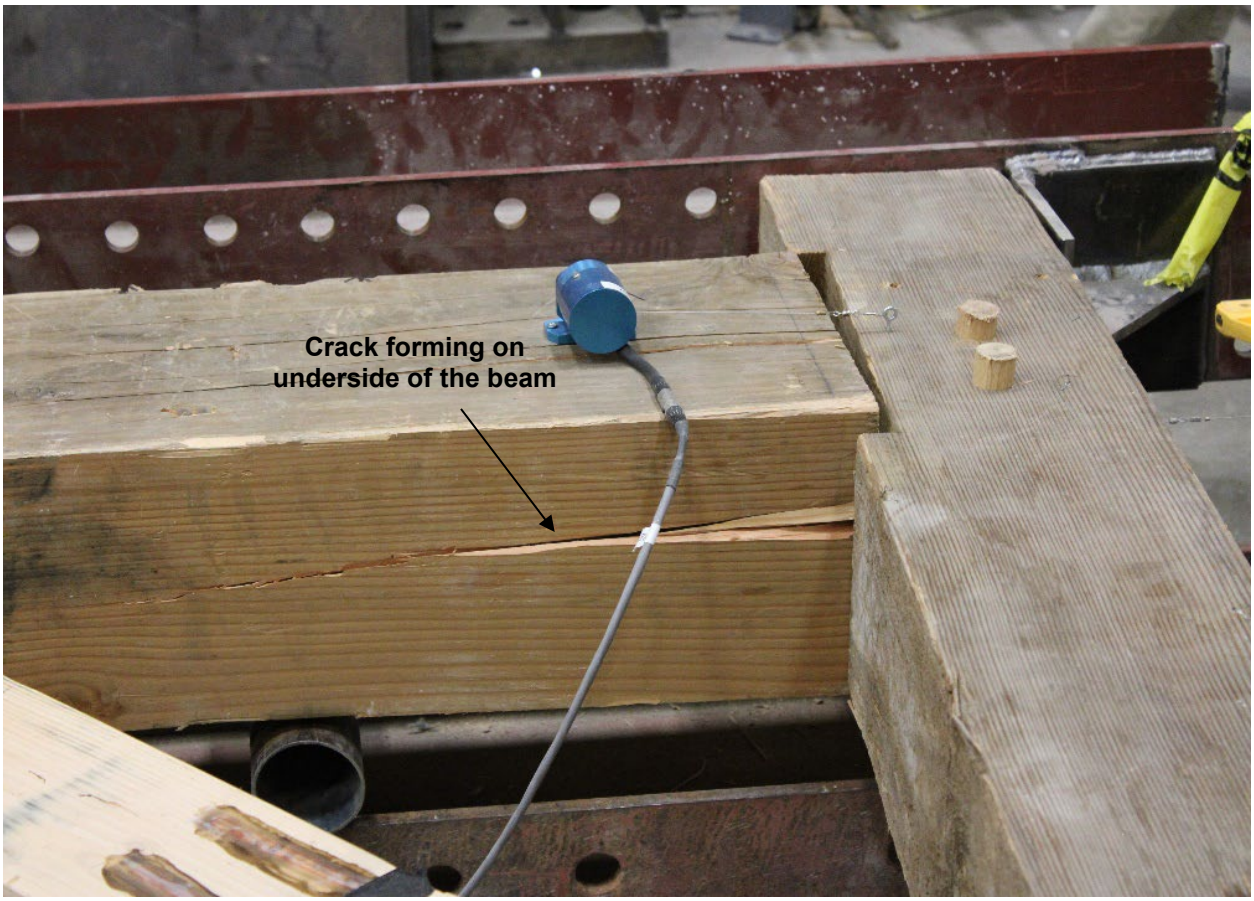

Fig. 3.19. Crack forming in the rehabilitated beam.

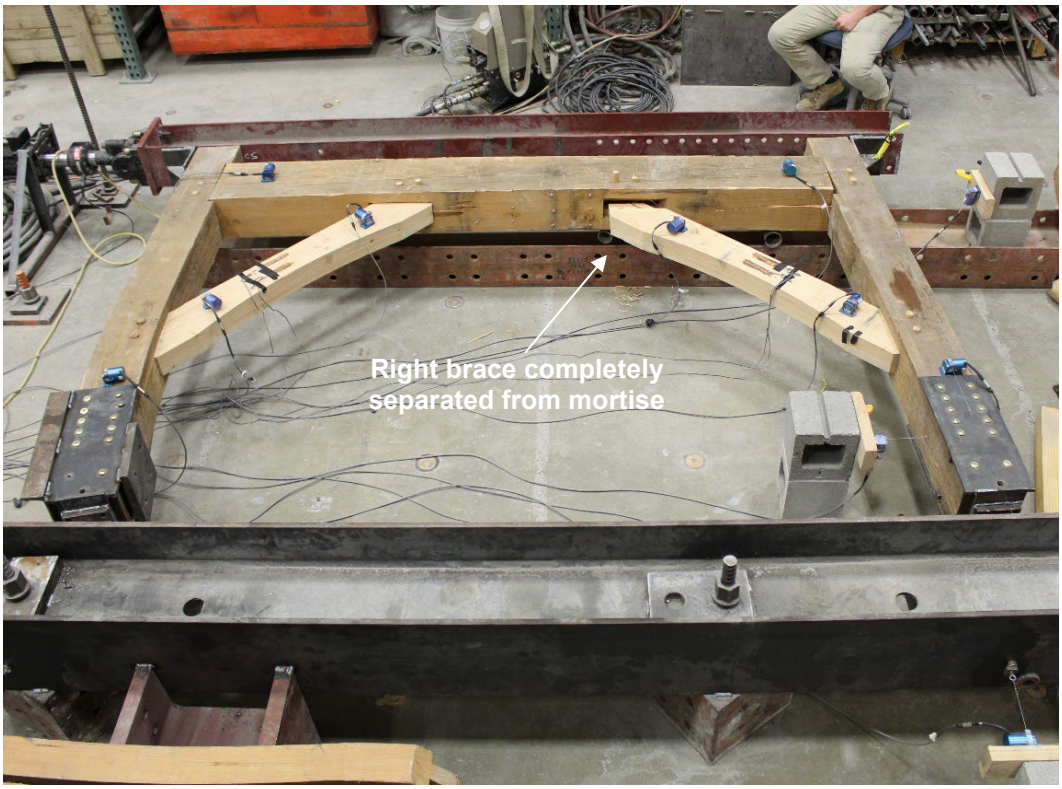

Fig. 3.20. View of the frame at the highest displacement cycle before stopping.

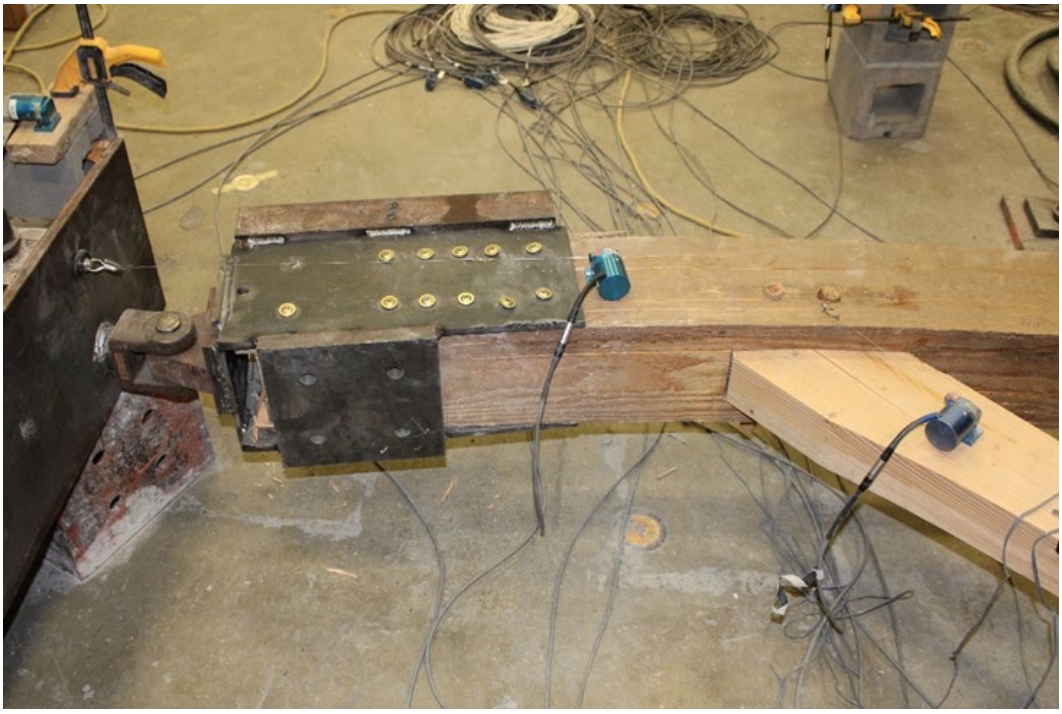

Fig. 3.21. Detail of left post footing experiencing flexure during the test.

3.6 Measured Response

3.6.1 Results for 3-Peg Frame

When remove from the testing apparatus, the 3-peg frame was observed to have tenon joint failure in both braces. As multiple cracks were heard during the test procedure, the right brace-to-beam failed in tearout at roughly 4.5 kips and the left brace-to-post failed in both tearout and peg shear when the load neared 6 kips. This was confirmed by the hysteresis graphs of force versus connection displacement in the right brace (Fig. 3.22) and force in the left brace versus connection displacement (Fig. 3.23). Following both of these cracks, the frame failed to transfer any more load. Fig. 3.24 shows the normalized lateral strength versus story drift ratio. The ultimate strength was 6.0 kips, compared to the expected nominal strength of 6.4 kips. The frame ductility was 2.2.

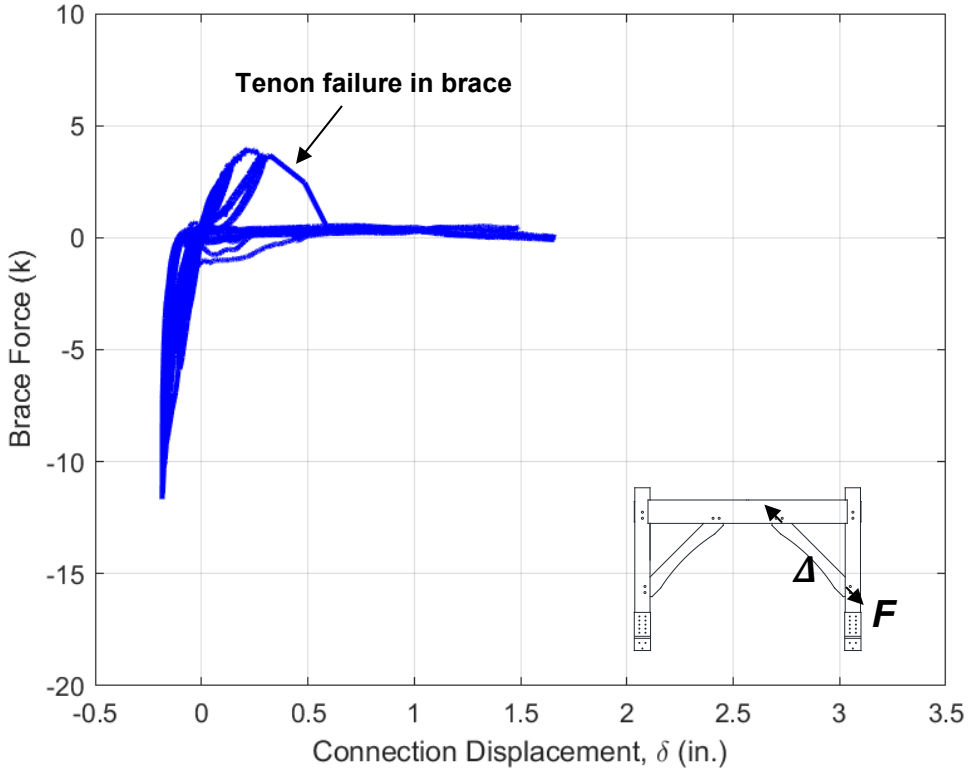

Fig. 3.22. Right brace force versus connection displacement for 3-peg frame.

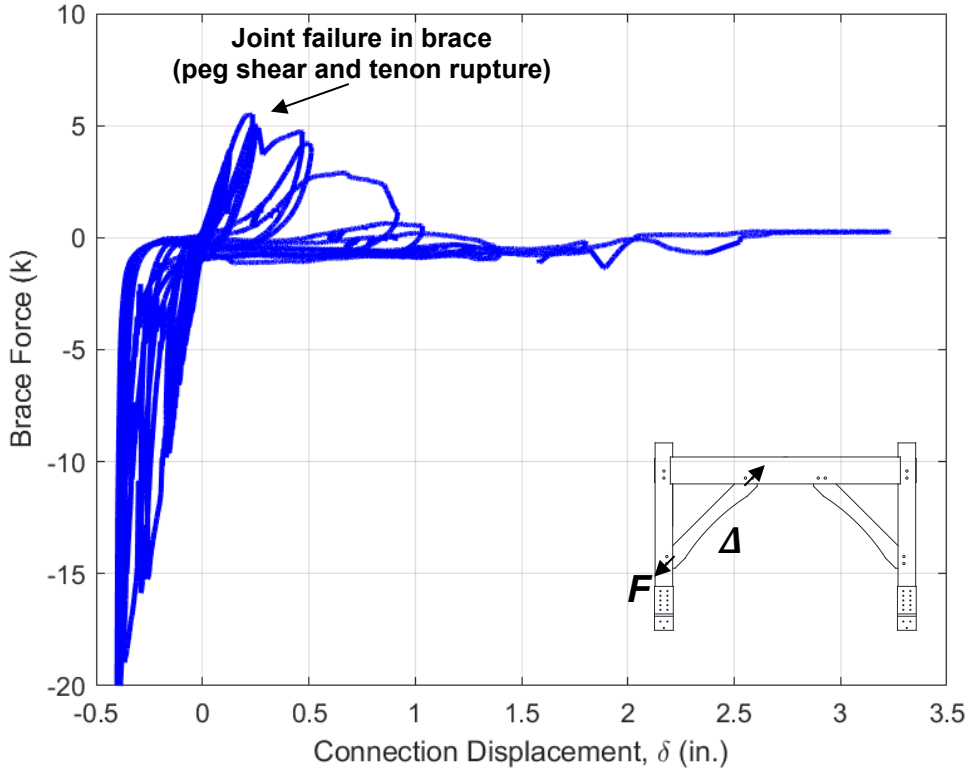

Fig. 3.23. Left brace force versus connection displacement for 3-peg frame.

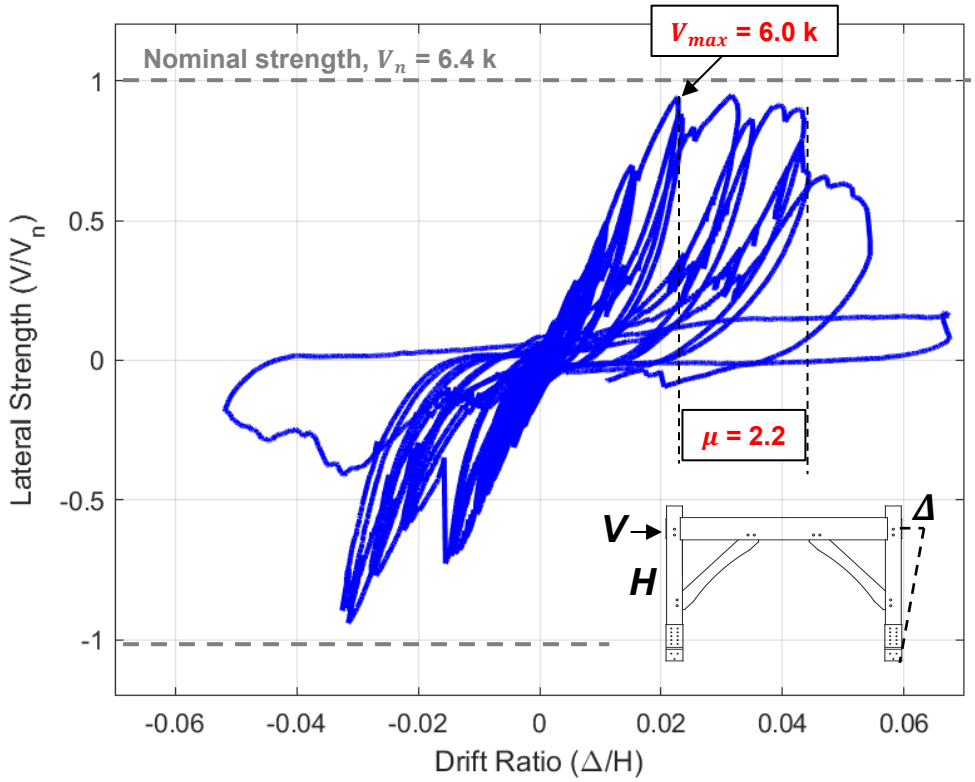

Fig. 3.24. Normalized lateral strength versus story drift ratio for 3-peg frame.

3.6.2 Results for 2-Peg Frame

The 2-peg frame exhibited lateral cracking in the beam prior to any total failure of the brace connections demonstrated in the 3-peg test. Fig. 3.25 shows the force versus connection displacement recorded in the right brace, with the force only reaching 4.7 kips before splitting in the beam occurred. It should be noted the connection displacement was significantly less than the 3-peg frame trial, due to the early tenon failure that occurred in the 3-peg test. Fig. 3.26 shows the left brace response. Fig. 3.27 shows the normalized lateral strength versus story drift ratio. The ultimate strength was 4.7 kips, compared to the expected nominal strength of 4.3 kips. The frame ductility was 1.2.

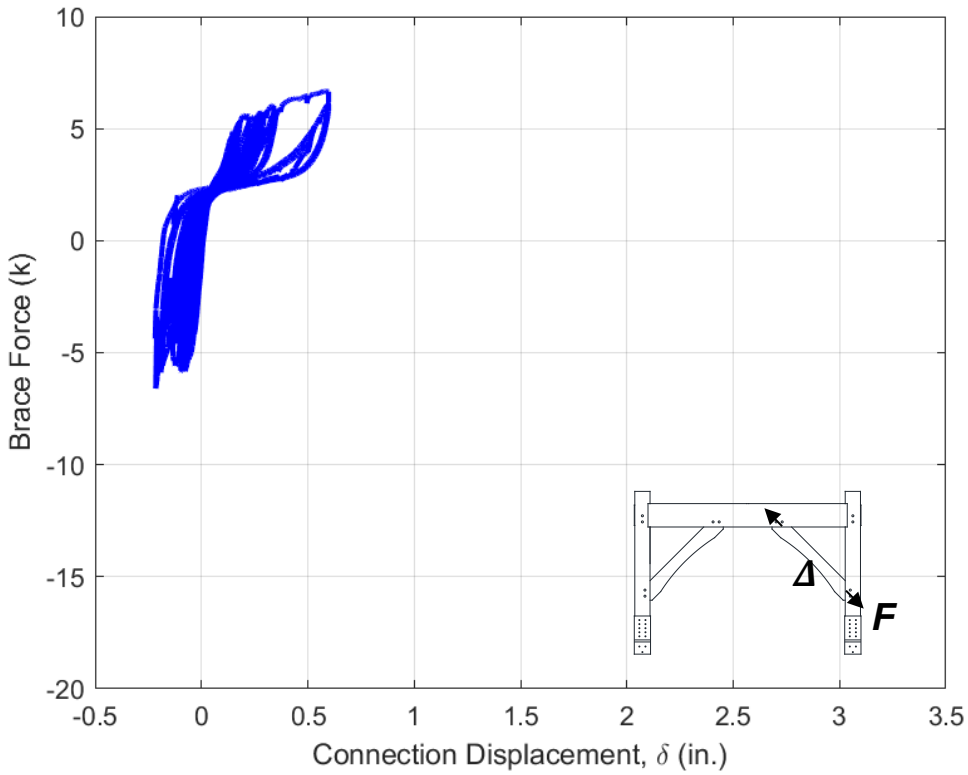

Fig. 3.25. Right brace force versus connection displacement for 2-peg frame.

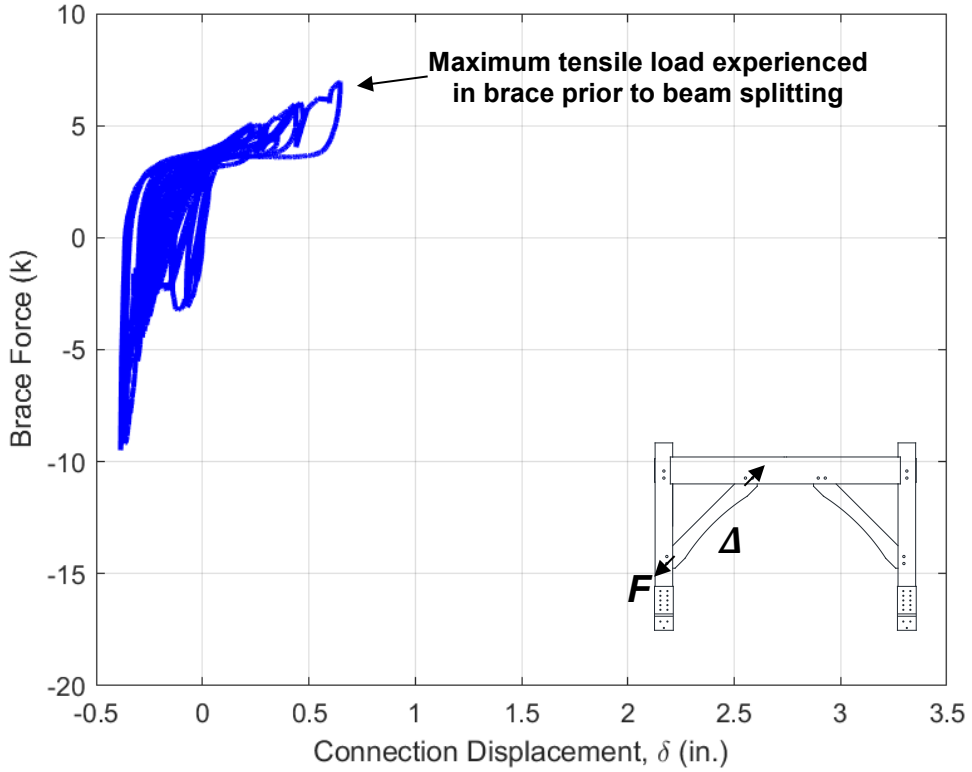

Fig. 3.26. Left brace force versus connection displacement for 2-peg frame.

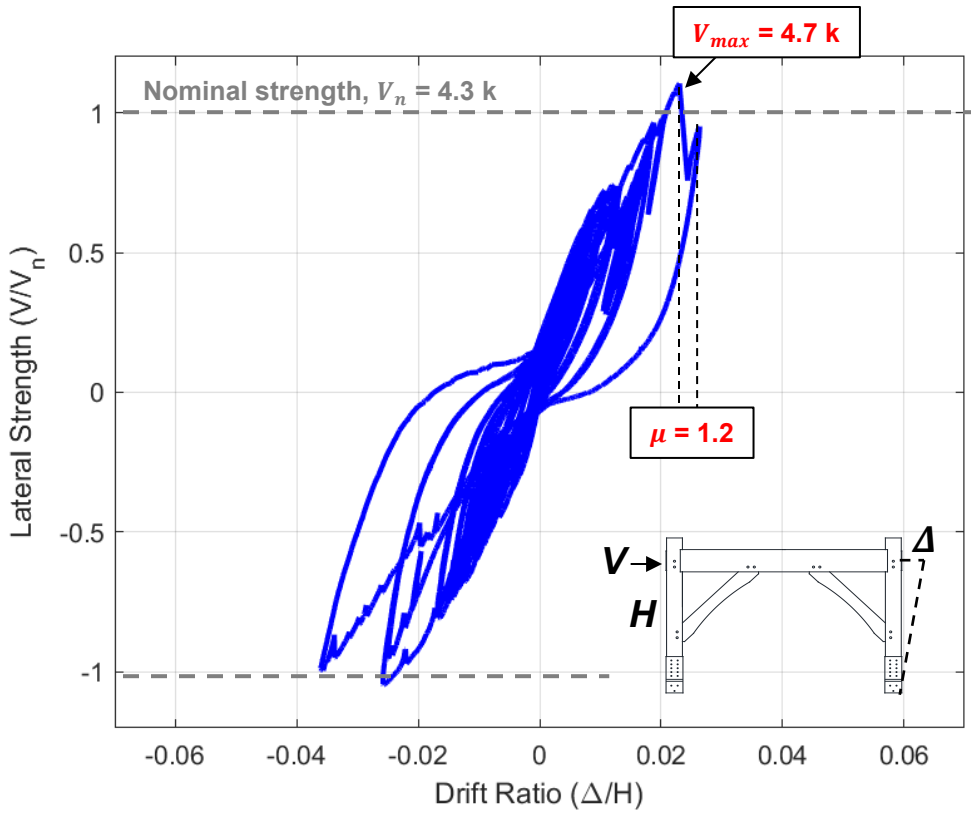

Fig. 3.27. Normalized lateral strength versus story drift ratio for 2-peg frame.

3.6.3 Results for Rehabilitated 2-Peg Frame

Results from testing the rehabilitated 2-peg frame showed an increase in strength of the frame. Though the right brace tenon was compromised from the partial failure experienced in the first test (limited transfer of load visible in Fig. 3.28), the frame was able to transfer load for a significantly longer duration of the testing protocol. The left brace response is shown in Fig. 3.29. Fig. 3.30 shows the normalized lateral strength versus story drift ratio. The ultimate strength was 7.0 kips, significantly above the 4.3-kip nominal strength of the 2-peg frame. The frame ductility was 2.7. Fig. 3.31. shows the beam tenon and Fig. 3.32 shows the peg shear failure inside the post mortise.

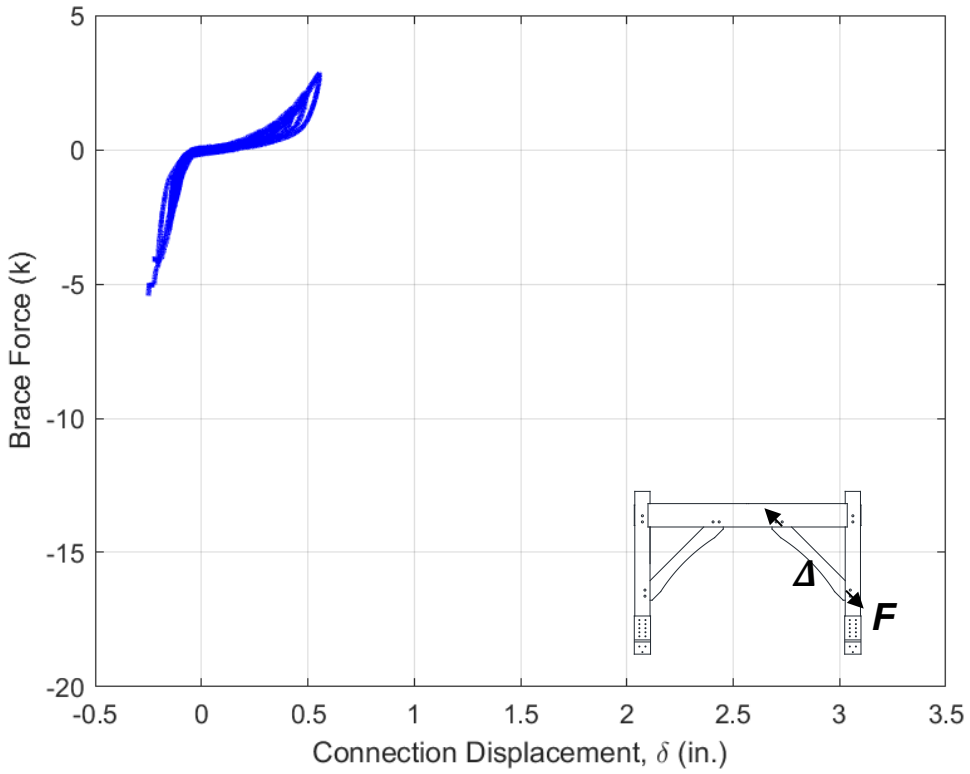

Fig. 3.28. Right brace force versus connection displacement for rehabilitated 2-peg frame.

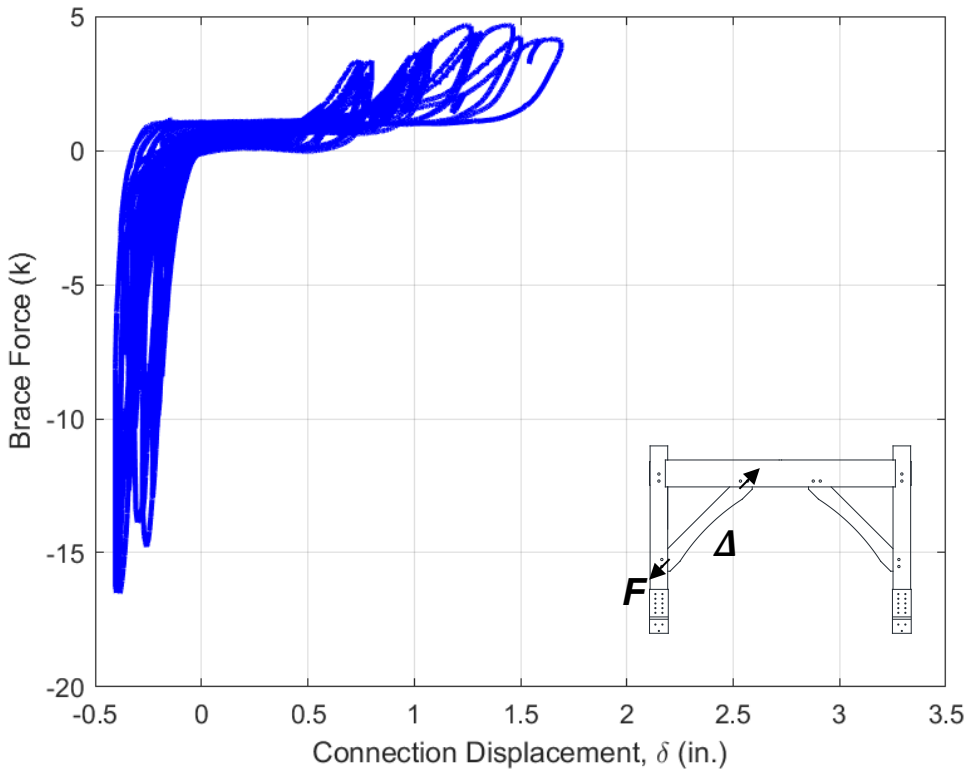

Fig. 3.29. Left brace force versus connection displacement for rehabilitated 2-peg frame.

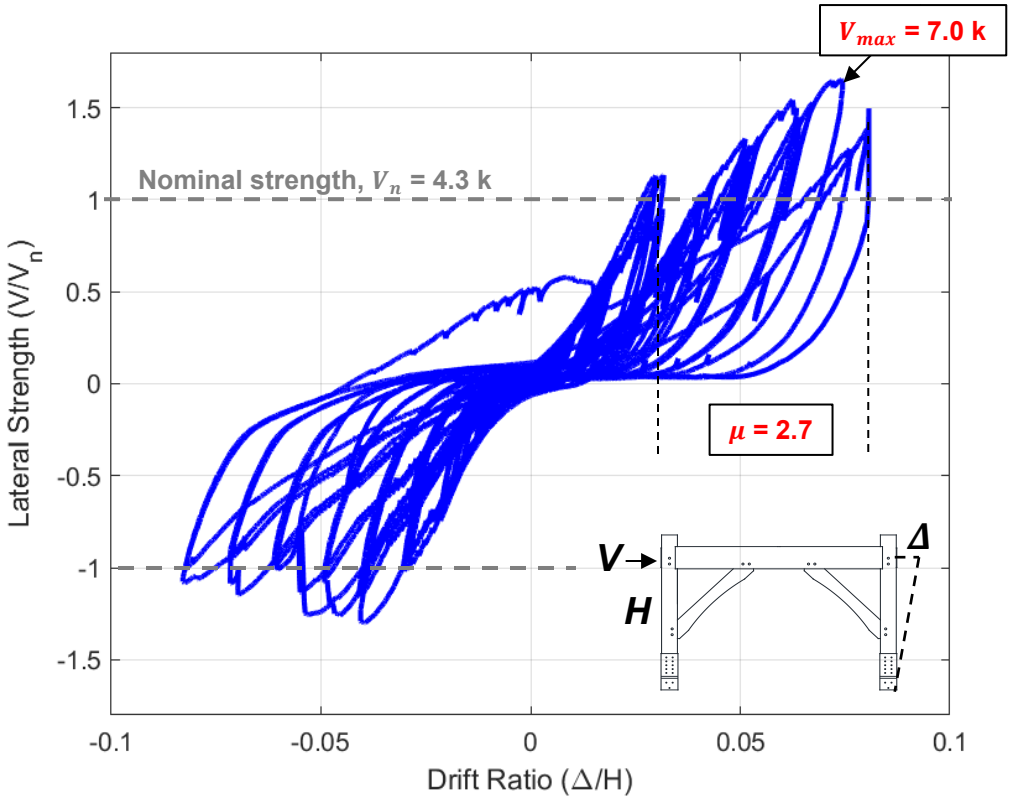

Fig. 3.30. Normalized lateral strength versus story drift ratio for rehabilitated 2-peg frame.

Fig. 3.31. Beam tenon from rehabilitated 2-peg frame displaying mode III_m failure.

Fig. 3.32. Peg shear failure inside of post mortise from rehabilitated 2-peg frame.

3.7 Summary

Two types of free-standing timber frames with knee braces were tested under cyclic loading. The hysteretic behavior of the 2-peg and 3-peg frames confirmed the behavior observed in the subassemblage tests tested in a prior research study (Judd et al. 2018). Three damage states for were identified: (1) peg shear and (2) tenon tearout at approximately 0.02 rad. joint rotation, and (3) splitting of the post or beam at approximately 0.05 rad. joint rotation. The damage states are employed in the component fragilities discussed in Chapter 6.

The post base connection of the 3-peg frame was destroyed, so the 3-peg frame was not rehabilitated. The beam in the 2-peg frame split, so the 2-peg frame was rehabilitated. The frame was rehabilitated by installing an array of twelve CYL 5/16 diameter by 11-7/8 in. long self-tapping screws. The self-tapping screws were driven perpendicular to the split plane of the beam. The test results showed that the self-tapping screws restored the strength of the 2-peg timber frame with the damaged beam, but the stiffness of the 2-peg frame was only partially restored. The effect of moisture content on the monotonic (tensile) strength of the brace to beam/post connection is discussed in Chapter 4.

CHAPTER 4 DURABILITY TESTS

This chapter describes the durability tests. Two types of mortise and tenon connections were subjected to damp conditions for an extended period of time (6 months) and then tested under monotonic load to determine the effect of a slope cut and a weep hole cut on the tensile strength of the connection, and to determine damage states for performance assessment and life-cycle analysis. The chapter includes a description of the joint preparation, instrumentation, monotonic loading rate, data reduction, and a discussion of the test results.

4.1 Joint Specimen Preparation and Assembly

Test specimens for the durability criteria tests were built after both frames were dismantled following the cyclic loading procedures. While the existing braces were rendered un-usable due to tenon failure, each mortise connection from the three-peg frame was still intact and therefore able to be utilized to create a knee brace connection. The two-peg frame was rendered un-usable due to the condition of the posts and beam. New three-hole braces were once again manufactured to be used in conjunction with the existing connections.

Each of the two mortise connections from the beam were cut out in roughly even-sized chunks using a circular saw shown in Fig. 4.1. The mortise connections sourced from the frame posts were also cut in this manner. Both newly manufactured braces were cut evenly down the center, as shown in Fig. 4.2, to create knee brace connection specimens.

With four connection specimens available, two of the mortises were modified with the goal to allow easier drainage of moisture from the connection when place under damp conditions for an extended period of time (6 months) and then tested under monotonic load. Limited literature exists on traditional mortise and tenon drainage behavior; therefore, the connection details were altered based on engineering judgement.

Fig. 4.1. Mortise specimens sourced from previously tested 3-peg frame.

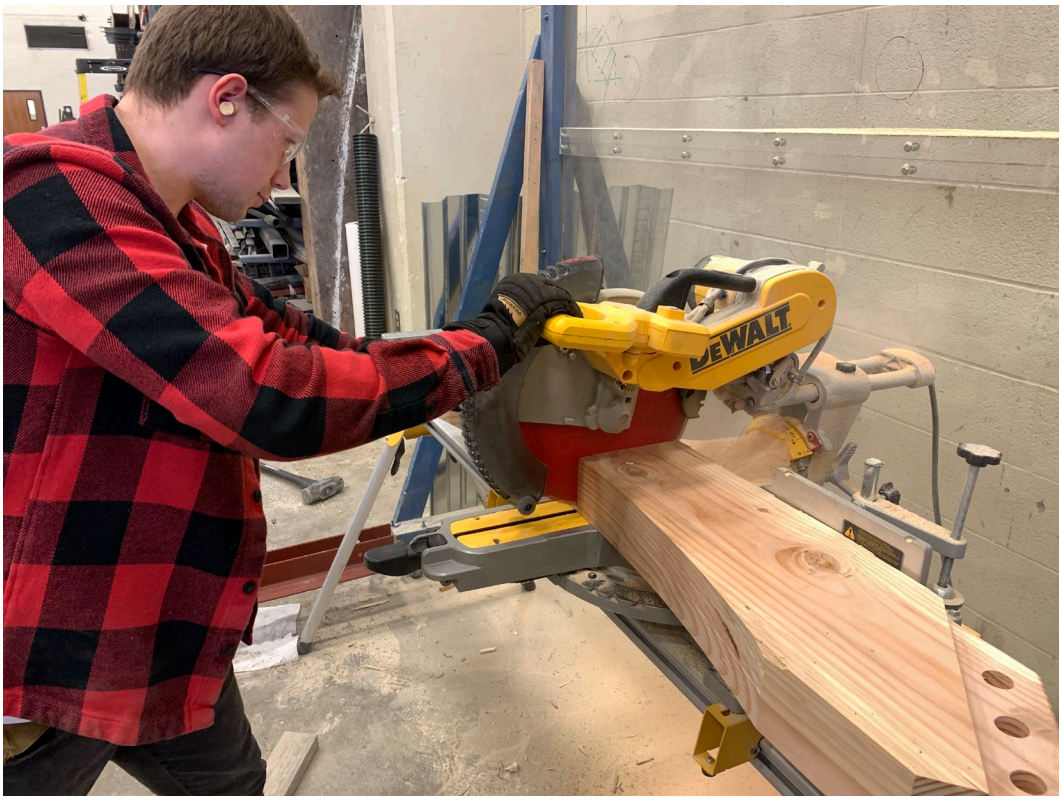

Fig. 4.2. Dividing newly manufactured brace for connection specimens.

Two of the connections were first beveled-out through part of the tenon bearing surface. A 15-degree bevel was first cut through the center-slot of the bearing. A ½" boring bit was used to drill a weep-hole through the beveled surface at a 20-degree angle, penetrating the rear face of the post. This connection detail modification was performed on one of the mortises cut from the beam, and one of the mortises cut from the post of the three-peg frame. Test specimens would be labeled one through four, with either a drained ("D") or un-drained ("U") condition, shown in Fig. 4.3.

The mortise and tenon specimens were assembled with the 1-inch diameter pegs and each placed on concrete masonry units in order to ensure no excessive moisture entrapment occurred at the base of the posts. Each specimen was placed in a curing and storage room ("fog" room) with constant vapor to maintain high humidity. The specimens were stored in the fog room for six months. Fig. 4.4 shows the specimens before and after the six-month period.

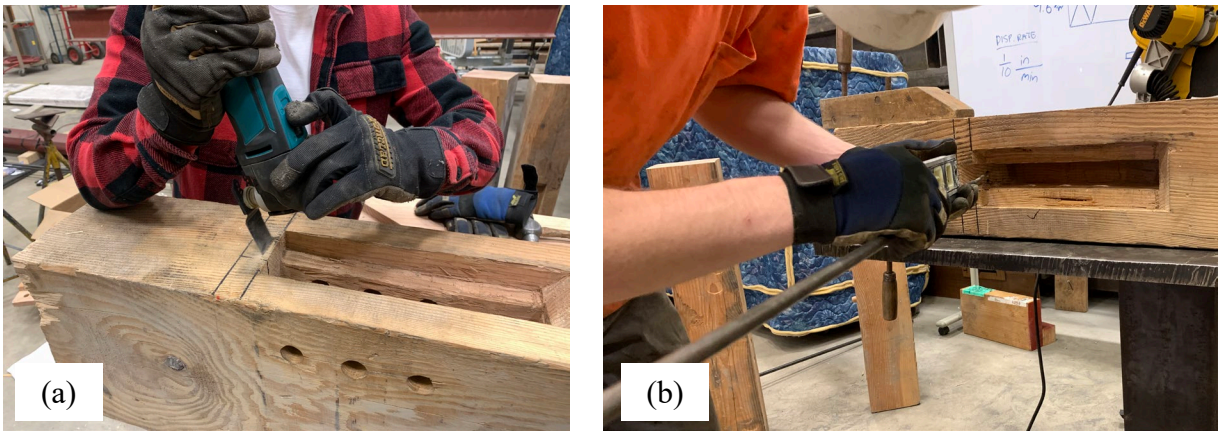

Fig. 4.3. Modification of connection details: (a) beveling out, and (b) boring bit insertion.

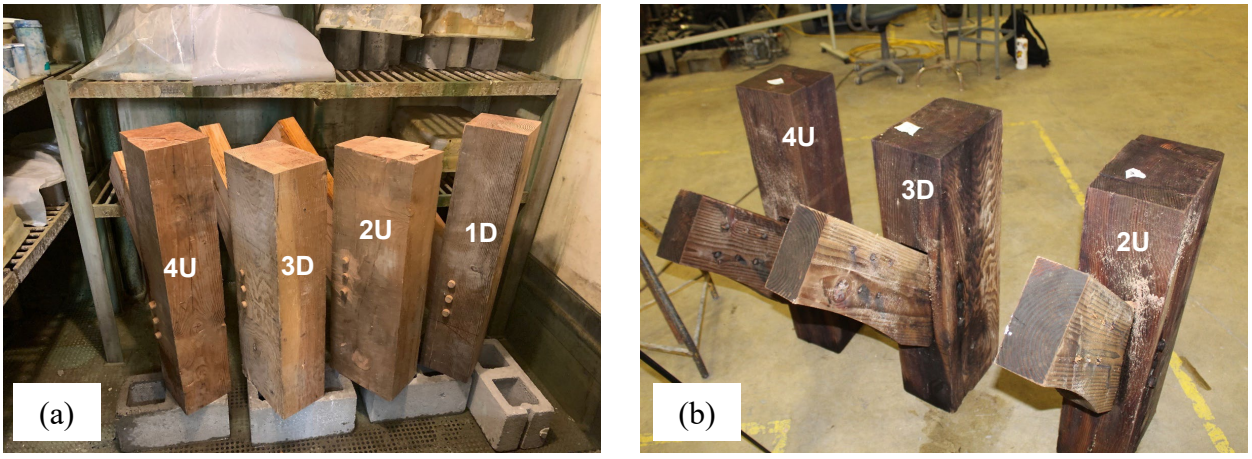

Fig. 4.4. Joint specimens: (a) at start of 6-month period, and (b) after 6-month period.

While the specimens were under damp conditions, a testing setup was developed in order to perform the monotonic loading tests. Each connection would undergo a tension test regime within a Baldwin Universal Testing machine. The test specimens would each be placed on a 45-degree channel, which is supported on top of a wide-flange beam (Fig. 4.5a). The posts were clamped down onto the channel in two locations with angle-shapes connected to all-threads (Fig. 4.5c).

A brace-plate connection was made using C-shape members welded at the top to a steel plate (Fig. 4.5b). Six holes were drilled into each end of the brace members on each specimen to connect to the plates (Fig. 4.5d). The holes were designed according to NDS section 12.5 (AWC 2018), including end distance, edge distance, and spacing requirements for fasteners in a row. NDS Table 12G was used to determine bolt design values. The nominal capacity of the brace determined to be 14,160 lbs. This exceeded the 9.5-kip nominal capacity of the tenon connection, indicating that the plate and fastener connection would be safe. Six ½-inch hex-head bolts were fastened through the plates and the brace members, allowing the plate connection to attach to the top of the Baldwin machine via a large bolt and nut at the top. The same bolted connection was welded onto the bottom of the wide-flange beam to fasten the bottom of the test apparatus to the lower part of the Baldwin.

General				
Type	=	Double shear		
Gap between side & main	g =	0.125	in.	

Fastener				
Type	=	1/2" x 6-1/8" bolt		
Diameter		D	0.5	in.
Root diameter		Dr	0.5	in.
Length		L	6.125	in.
Unthreaded length		S	0	in.
Tip length		E	0.000	in.
Dowel Bending Strength		Fyb,5%	45,000	psi

Side Member				
Type	=	1/4" plate A36		
Angle of load relative to grain	theta =	0	deg	
Thickness	ts =	0.25	in.	
Specific Gravity	Gs =	7.85		
Dowel diameter	Ds =	0.5	in.	
Bearing length	ls =	0.25	in.	
Dowel-bearing resistance				
Parallel to grain	Fe‖ =	87,000	psi	
Perp. to grain	FePerp =	87,000	psi	
Dowel-Bearing Strength	Fes,5% =	87,000	psi	
Dowel-Bearing Resistance	qs,5% =	43,500	lb/in.	
Dowel Moment Resistance	Ms,5% =	938	in.*lb	

Main Member					
Type	=	4x4 DF-L			
Angle of load relative to grain	theta =	0	deg		
Thickness	tm =	3.5	in.		
Specific Gravity	Gm =	0.50			
Dowel diameter	Dm =	0.5	in.		
Bearing length	lm =	3.500	in.		
Min. embedment length	pmin =	0.000	in.	OK	
Dowel-bearing resistance					
Parallel to grain	Fe‖ =	5,600	psi		
Perp. to grain	FePerp =	3,158	psi		
Dowel-Bearing Strength	Fem,5% =	5,600	psi		
Dowel-Bearing Resistance	qm,5% =	2,800	lb/in.		
Dowel Moment Resistance	Mm,5% =	938	in.*lb		

Yield Limits							
						Ktheta =	1.000
		Constants					
	Mode	A	B	C	Z,5% (lb)	Rd	Z (lb)
	Is				21,750	4.00	5,438
	Im				9,800	4.00	2,450
	II	9.5E-05	2	-9,255	3,903	3.60	
	IIIs	0.000184	0.25	-1,617	4,721	3.20	1,475
	IIIm	0.000101	1.875	-9,513	4,148	3.20	
	IV	0.00019	0.125	-1,875	5,658	3.20	1,768
						Min. =	**1,475** lb

$$F_{vn} = 6 \times (1.6)(1{,}475\ lb) = 14{,}160 lbs \quad (4.1)$$

# of fasteners C_D $Z_\parallel$

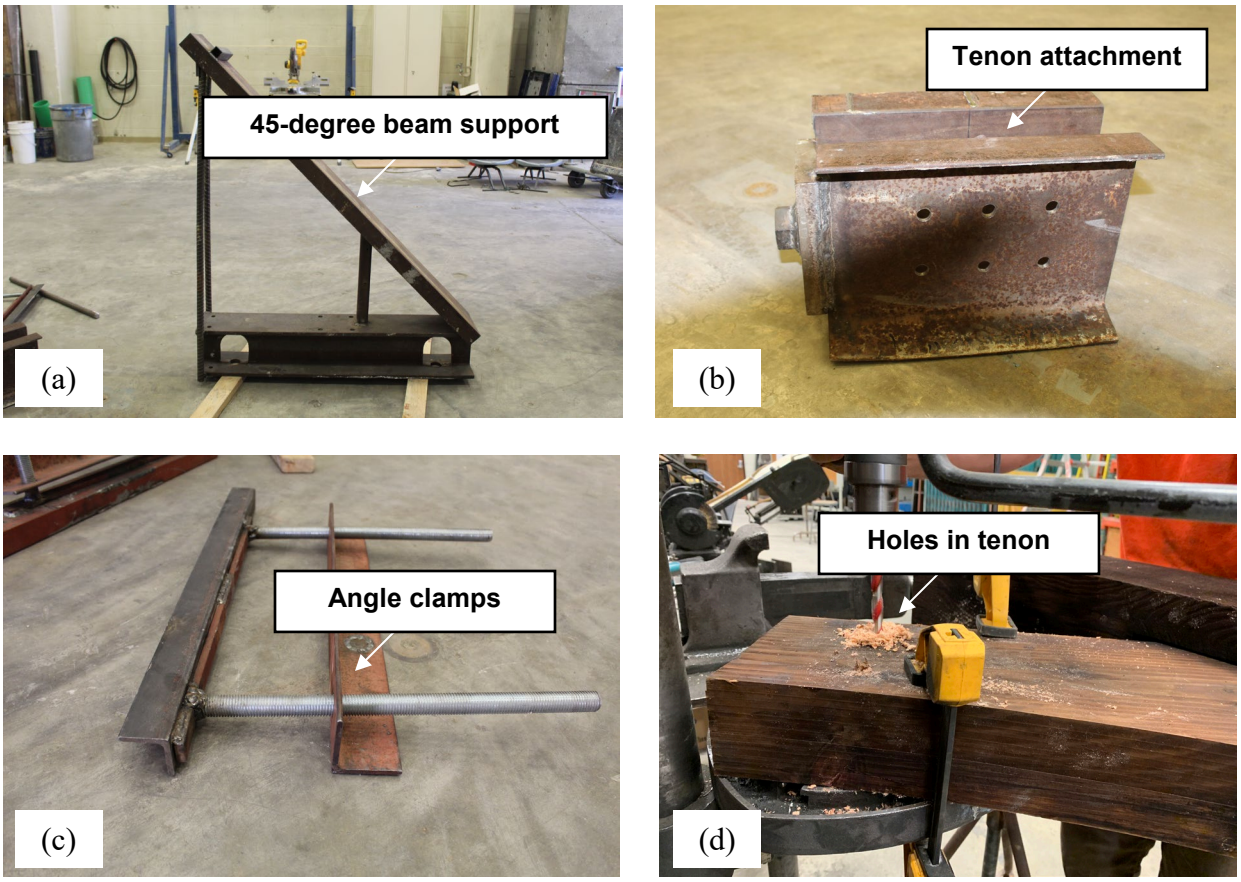

Fig. 4.5. Test apparatus and specimen prep: (a) beam, (b) tenon, (c) clamps, and (d) holes.

4.2 Tension Tests

Each specimen was loaded onto the beam setup and fastened to the Baldwin machine. A steel tube member was welded to the top of the 45-degree channel so that shims could be inserted to keep the specimen from sliding up during the tests. The monotonic tests were performed by the Baldwin machine lowering its bottom end attached to the wide-flange beam at 0.1 in./min. A string pot was also attached to the post and pinned to the plates before every test to measure displacement of the brace from the connection.

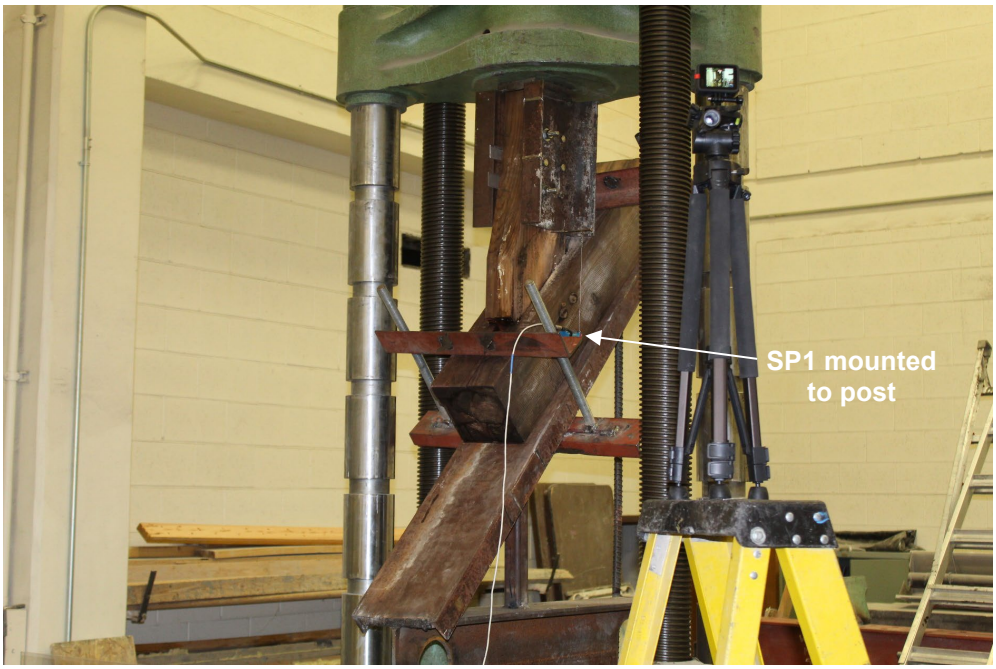

Fig. 4.6. The first specimen undergoing testing in the Baldwin machine.

Each test yielded similar behavior amongst the connection specimens. Audible cracking was heard during the intervals of 6 kips to 7 kips of load from the machine. Evidence of this can be seen on each test curve in Fig. 4.8. Ultimate failure was usually accompanied with splitting in the post through the peg holes as visible in Fig. 4.7a and 4.7b.

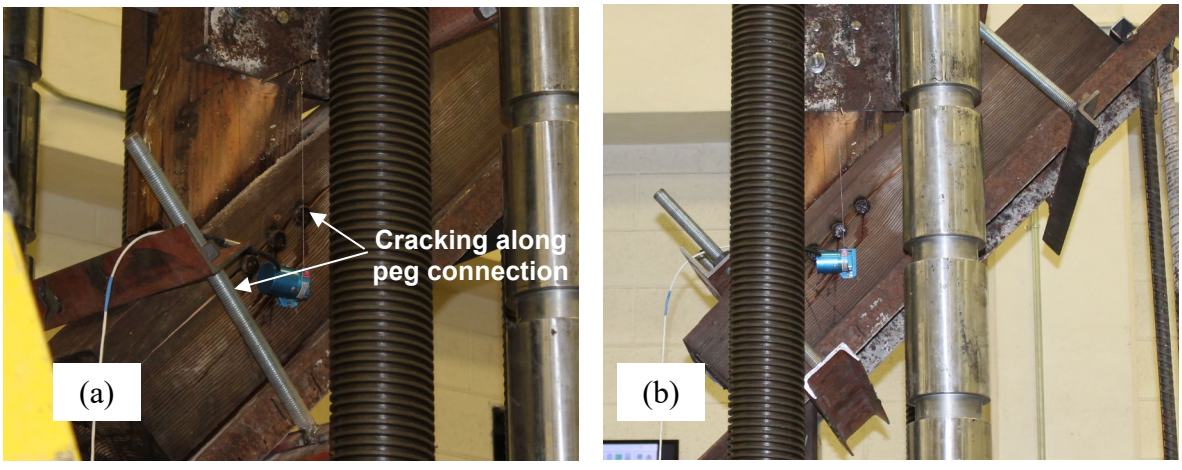

Fig. 4.7. Test specimens after tension load failure: (a) corner and (b) side views.

4.3 Test Results

Moisture content readings were taken from multiple locations on each specimen directly after being removed from the testing apparatus. Fig. 4.8 displays those results as measured. The findings indicate that there was not much overall variability in moisture content between drained and undrained specimens. The average moisture content in the drained specimens was 27%, whereas the average moisture content in the undrained specimens was 28%.

The collection of data from all tests indicated that the undrained specimens actually performed better than the drained specimens in terms of maximum load sustained. Specimens 2U and 4U failed at 8.41 kips and 8.09 kips respectively, while specimens 1D and 3D failed at 7.65 kips and 7.03 kips (Fig. 4.9). It is worth noting that the drained specimens did withstand a higher displacement before ultimate failure.

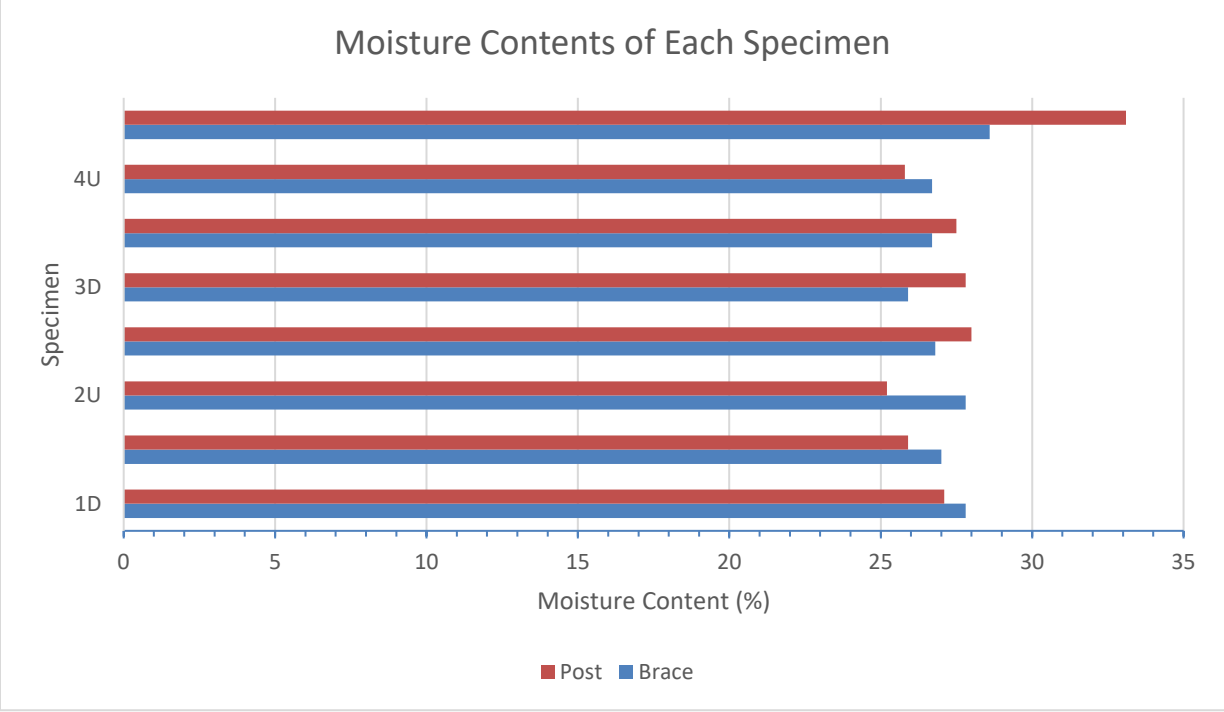

Fig. 4.8. Moisture content of durability test specimens.

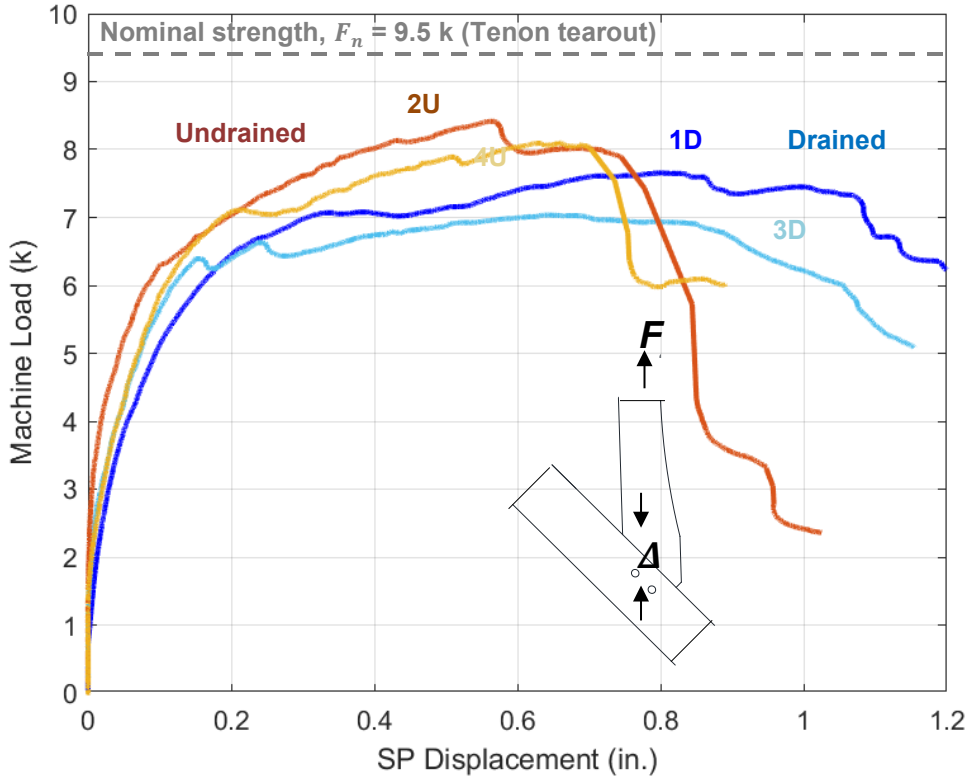

Fig. 4.9. Tensile load versus connection displacement for durability specimens.

Upon taking apart all specimens, the joint failure behavior was observed in each specimen. The tenon failure and peg-bending behavior was generally uniform across all specimens. Some tenons showed more excessive shear than others, as observed in Fig. 4.10 to Fig. 4.13.

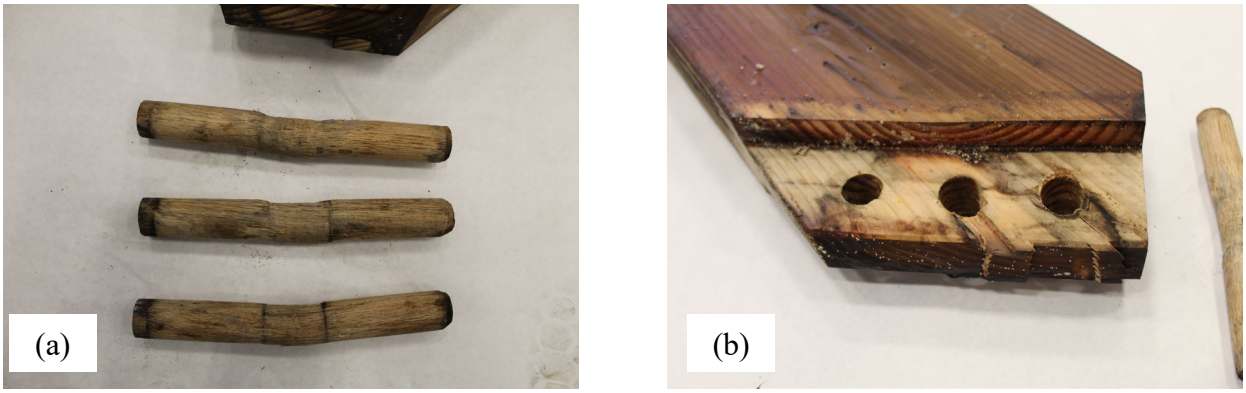

Fig. 4.10. Durability test specimen 1D: (a) peg bending, and (b) tenon failure.

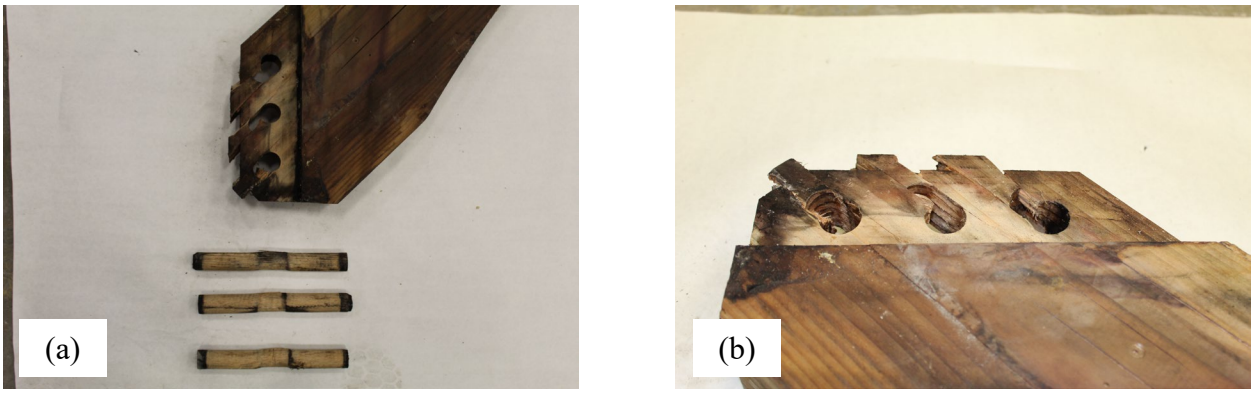

Fig. 4.11. Durability test specimen 2U: (a) peg bending, and (b) tenon failure.

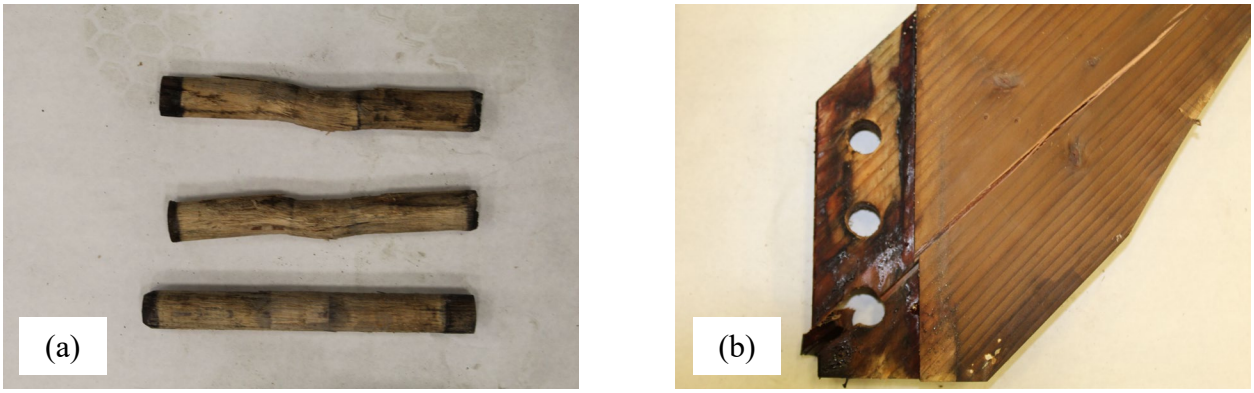

Fig. 4.12. Durability test specimen 3D: (a) peg bending, and (b) tenon failure.

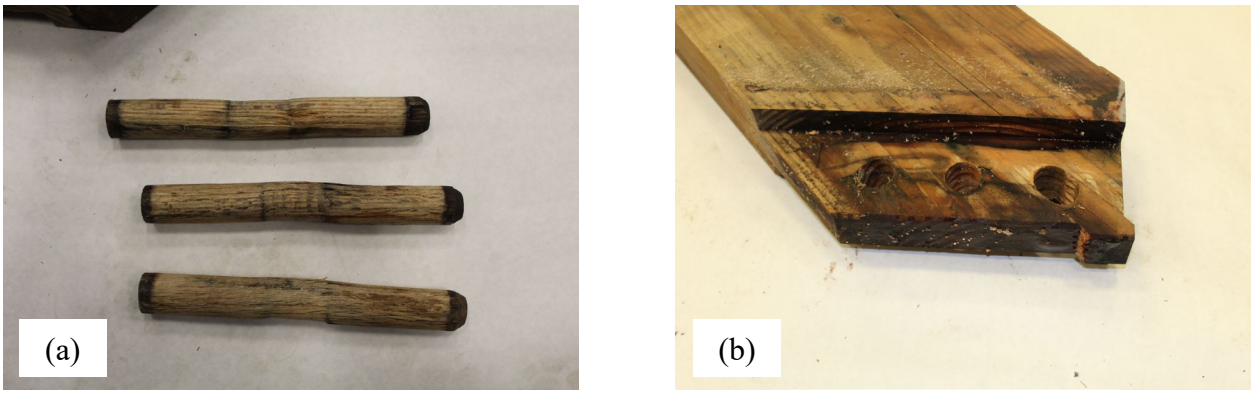

Fig. 4.13. Durability test specimen 3D: (a) peg bending, and (b) tenon failure.

4.4 Summary

Two types of mortise and tenon connections were subjected to damp conditions in a fog room for six months, removed from the fog room, and then tested under monotonic (tensile) load. One type of connection, a "conventional" connection, was considered "undrained" because the detailing was expected to allow moisture to collect and remain in the joint. The other type of connection, a modified connection, had a slope cut at the front of the post/beam and a weep hole at the opposite side to drain water. This modified connection was considered "drained." The monotonic behavior of the joints confirmed the failure modes (peg shear and tenon tearout) that were observed in the cyclic tests discussed in Chapter 3. Interestingly, the test results indicated that the drained connection did not enhance or diminish the strength or stiffness of the brace connection. The results from the durability tests were used to inform the component fragilities that are discussed in Chapter 6. Before discussing the fragilities, vibration tests of timber frames are discussed in the next chapter.

CHAPTER 5 VIBRATION TESTS

This chapter describes the vibration tests. Timber frames at various locations in the United States were tested in the field under impulse loading to determine the fundamental period of vibration and to estimate damping. The field tests were conducted used a crowd-sourced approach: the Brigham Young University team and volunteers from the Timber Frame Engineering Council downloaded an app to their smartphone and use it to measure accelerations. The chapter includes a description of the testing sequence, data reduction, and a discussion of the test results.

5.1 Methodology

Timber frames were tested in the field under impulse loading to determine the fundamental period of vibration and to estimate damping. Tests were conducted used a "crowd-sourced" approach. In this approach, the Brigham Young University team tested timber frames in Utah. Volunteers from the Timber Frame Engineering Council tested timber frames outside of Utah. To measure acceleration, the team member (or the volunteer) downloaded an app their smartphone. This study used the "Physics Toolbox Sensor Suite" app (https://www.vieyrasoftware.net/). Fig. 5.1 shows the app.

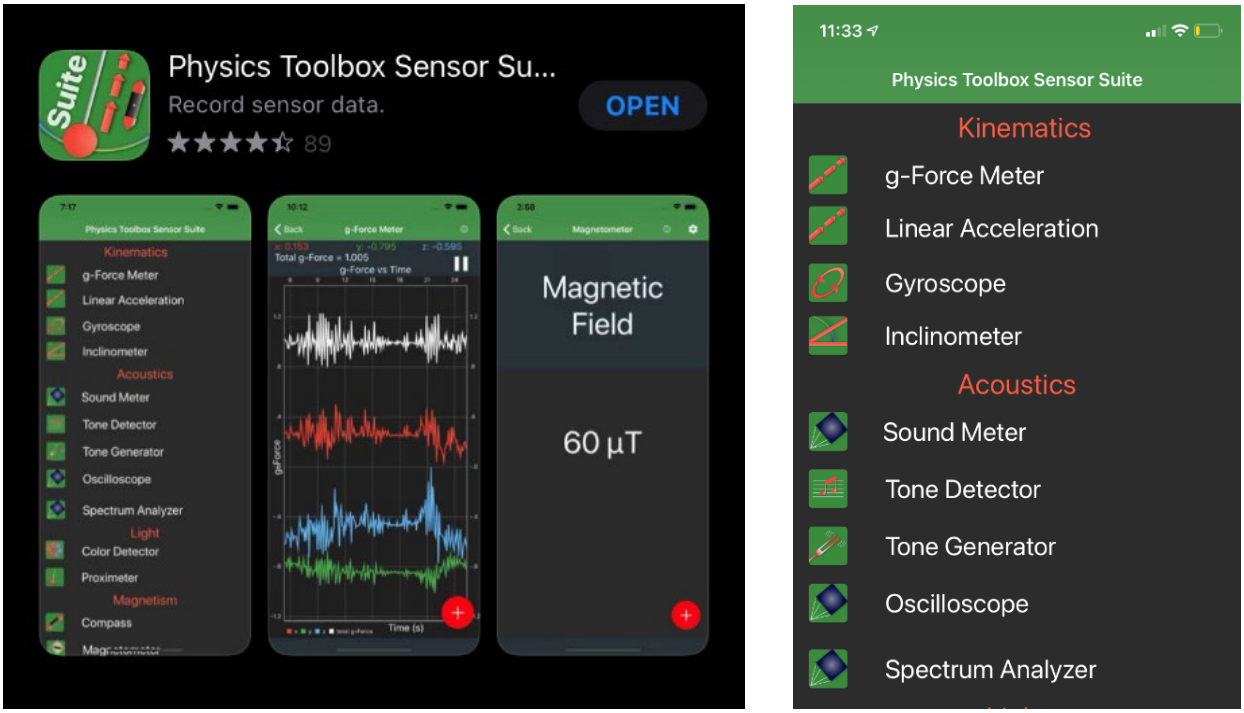

Fig. 5.1. Physics Toolbox Sensor Suite" app used to measure accelerations.

The app uses internal piezoresistive cantilever sensors or capacitative sensors, depending on the smartphone, to measure accelerations. In a smartphone with a piezoresistive cantilever sensor, a silicon cantilever bends as the smartphone accelerates. The change in resistance of the silicon correlates to acceleration. In a smartphone with a capacitative sensor, three masses are attached to springs (one spring in each principal direction). As the masses move, they change the electric potential across capacitor plates that are positioned between the masses (https://www.vieyrasoftware.net/sensors-sensor-modes).

5.1.1 Field Test Procedure

A vibration test procedure was developed so that the tests could be done independently of the Brigham Young University team. In the procedure, free-standing timber frames with knee

braces were identified. If possible, the testing was done without interruption. For each timber frame photos, drawings, and other information was collected if available.

Each frame was tested in each principal direction. Testing personnel would set up a ladder and place the smartphone on one of the spandrel beams in the transverse direction of the frame (Position ‘A’). They would then begin to record data on the app. The frame was tested by striking the post with a rubber mallet. Fig. 5.2 shows a typical placement of the smartphone and mallet strike. The intent was that the acceleration due to the impulse would be approximately 1 m/s2. The strike was repeated every six seconds for five-six intervals. The test was repeated in each principal direction with the smartphone oriented parallel and perpendicular to the beam, for a total of four tests. For the second direction, the personnel would then move the smartphone to a spandrel in the longitudinal direction of the frame and impart the same impulses (Position ‘B’). Fig. 5.3 shows the orientation of the smartphone relative to the principal directions of the timber frame. The test data was recorded to a .csv file measuring the time, x,y and z accelerations. Fig. 5.4 shows a sample acceleration recording in the app.

Fig. 5.2. Vibration test: (1) placement of smartphone, and (b) mallet strike.

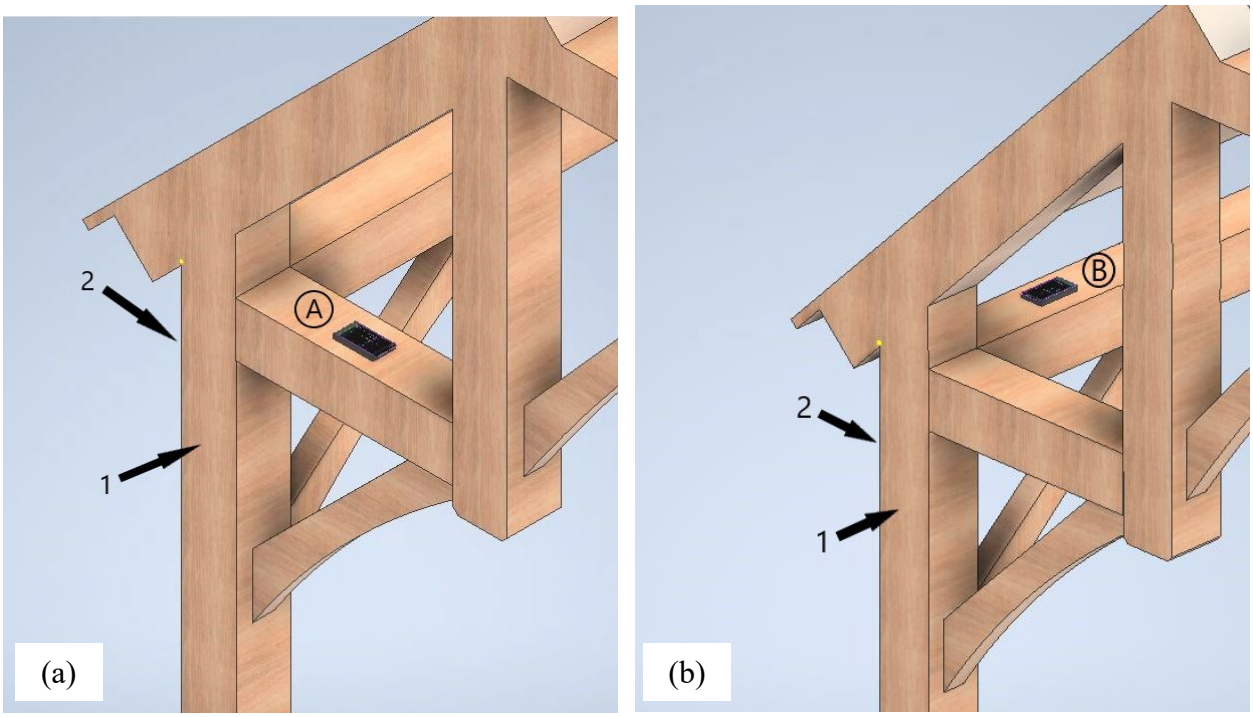

Fig. 5.3. Orientation of smartphone: (a) transverse and (b) longitudinal directions.

5.1.2 Fundamental Period of Vibration

The data was post processed using MATLAB (2021). If necessary, the acceleration record was clipped (or zero padding was added) to eliminate edge effects in the frequency analysis. Fig. 5.5 shows an example of a clipped acceleration record.

The fundamental period of vibration was determined using a frequency analysis of the test data. The acceleration record was then converted to the frequency domain using a fast Fourier transform (FFT) algorithm in MATLAB (2022) based on software developed by Frigo and Johnson (1998). The single-sided amplitude spectrum of period-content was used to identify the fundamental period of vibration in each principal direction.

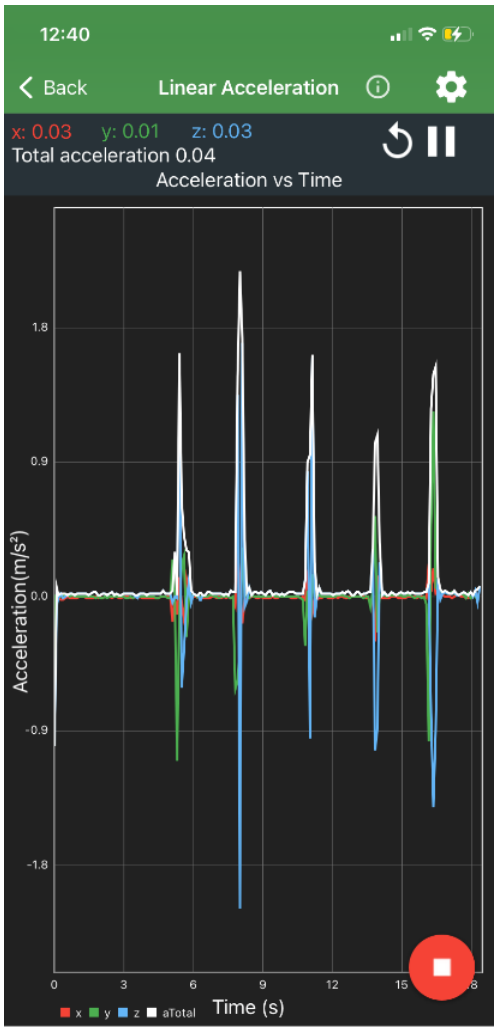

Fig. 5.4. Sample acceleration reading in the app.

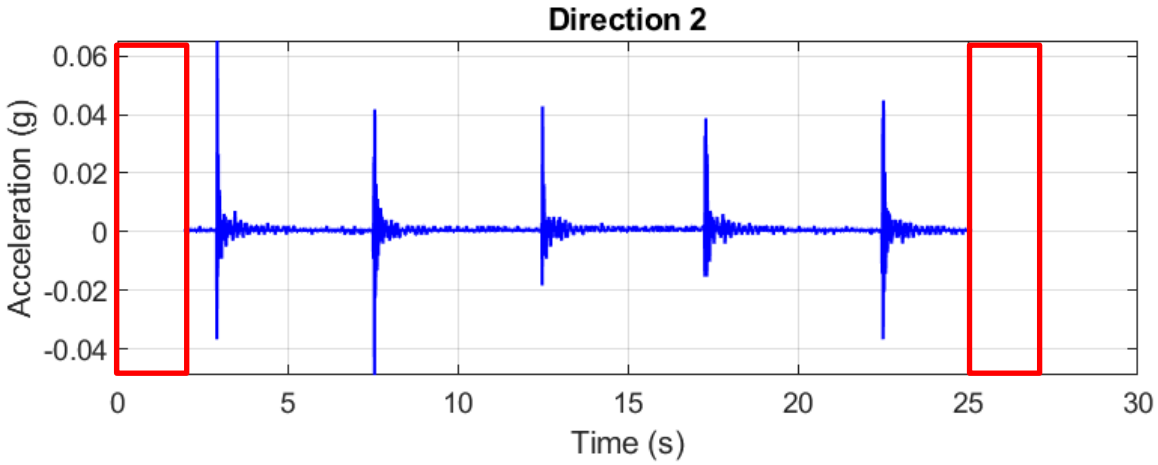

Fig. 5.5. Sample clipped acceleration record.

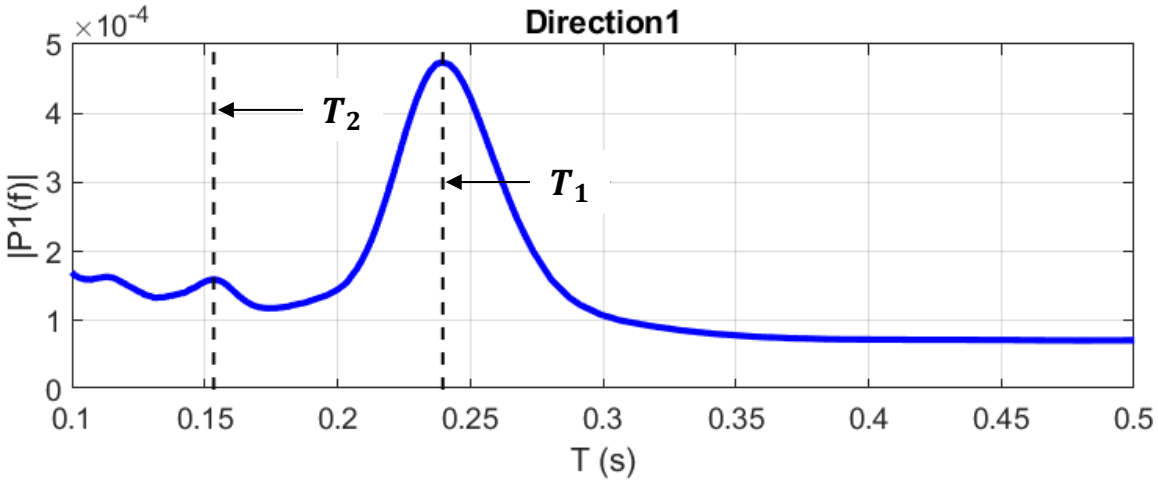

Fig. 5.6. Single-sided amplitude spectrum of period-content.

5.1.3 Modal Damping

The modal damping ratio was determined using a wavelet demodulation. The demodulation was based on the procedure developed by Dien (2008). In this study, a continuous wavelet transformation (CWT) of the acceleration record was completed using the default Morse wavelet in MATLAB. Fig. 5.7 shows the amplitude and frequency content of the Morse wavelet. The Morse wavelet had a symmetry parameter (β) equal to 3 and a time-bandwidth product (P^2) equal to 60.

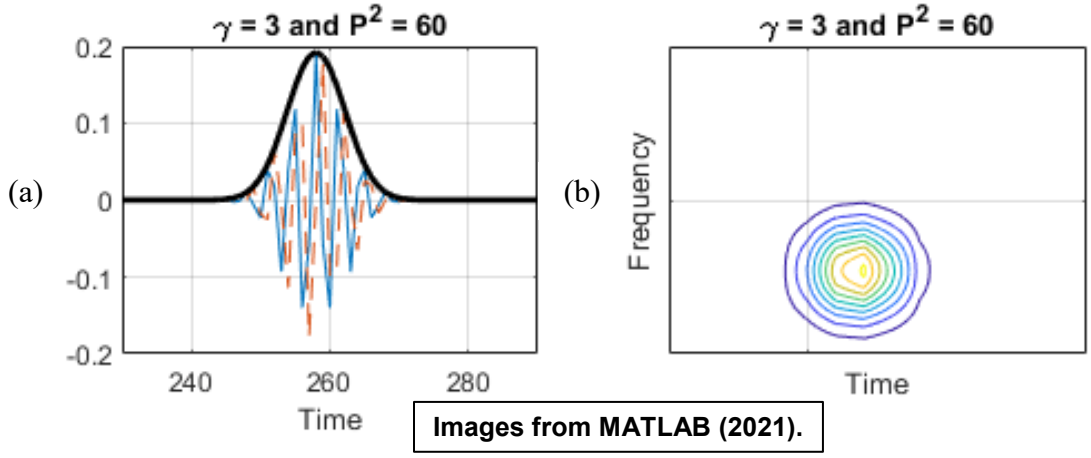

Fig. 5.7. Morse wavelet: (a) time domain and (b) frequency content versus time.

The continuous wavelet transformation was used to determine the frequency content of the data versus time. Fig. 5.8 shows an example of the frequency content from a CWT that resulted from a typical vibration test data. Since the focus of this study was on the fundamental period of vibration, period content is plotted in the scaleogram in lieu of frequency content. In this plot, a two-dimensional magnitude scaleogram is used to indicate the time-varying content (color is the magnitude of the signal). However, it can also be helpful to visualize the time-varying frequency content through a three-dimensional plot, as shown in Fig. 5.9.

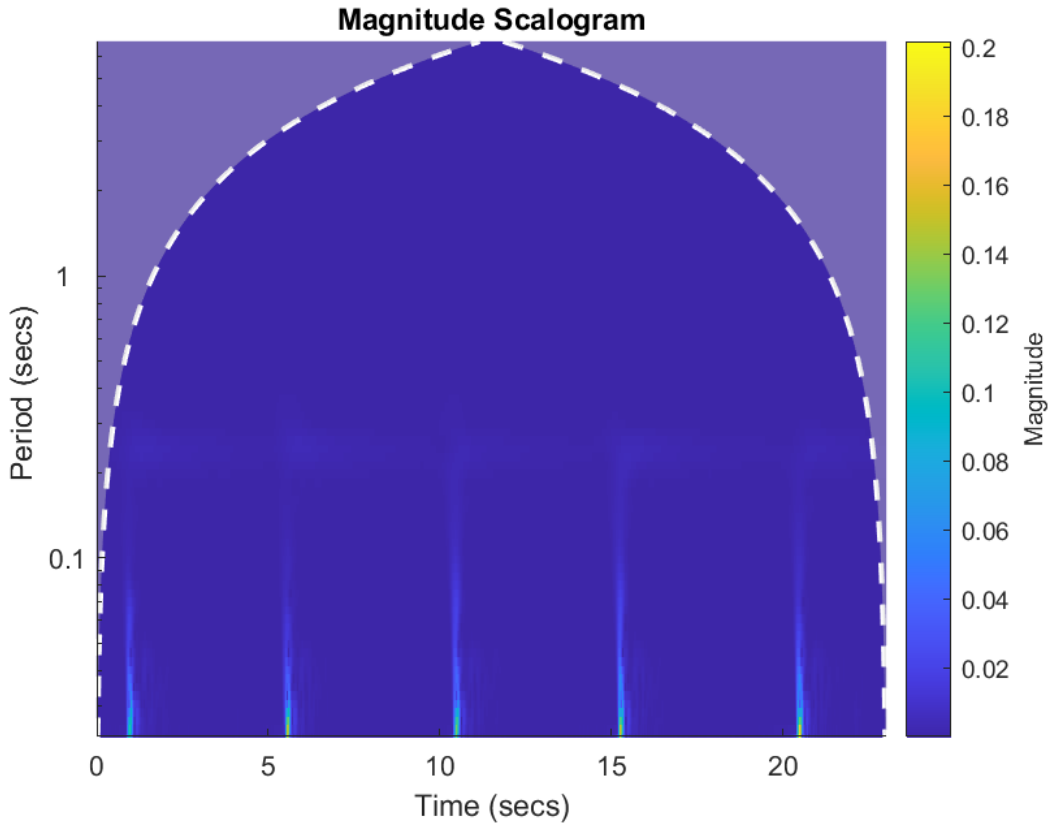

Fig. 5.8. Two-dimensional plot of frequency content (period of vibration) versus time.

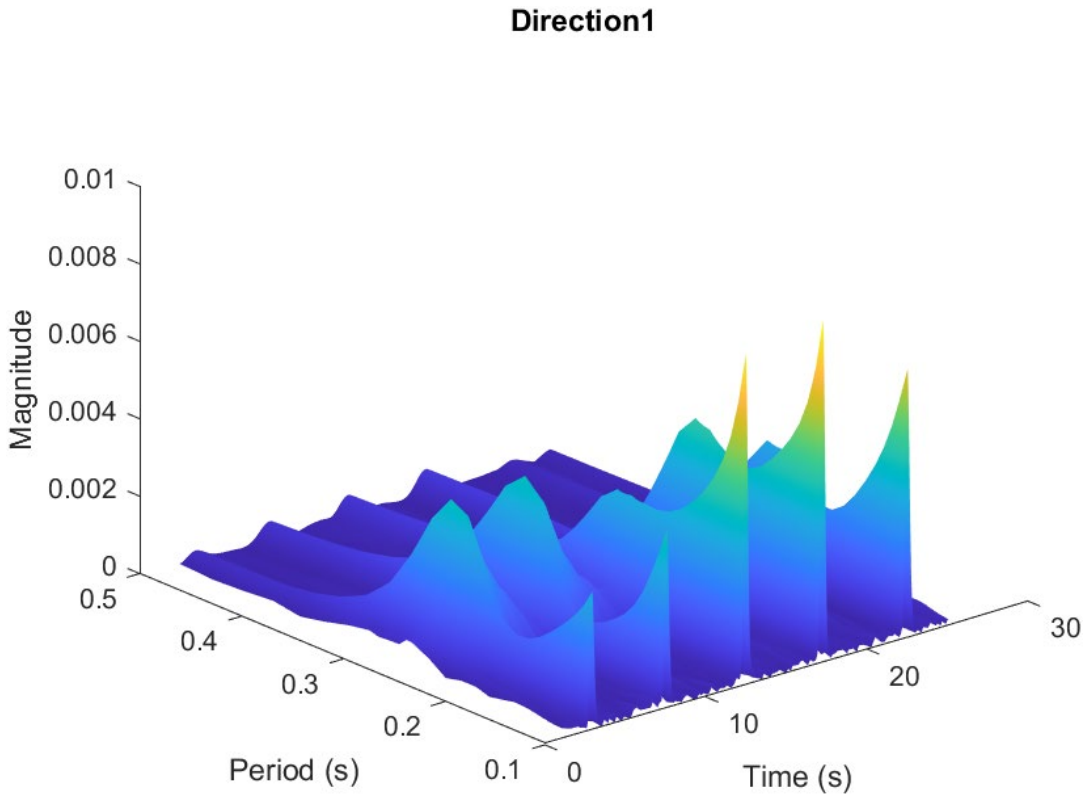

Fig. 5.9. Three-dimensional plot of frequency content (period of vibration) versus time.

The wavelet demodulation process used to determine modal damping is illustrated in Fig. 5.10. Since the scaleogram contains the frequency content versus time for the entire range of frequency (or periods), therefore the scaleogram was "sliced" at sliced at fundamental period of vibration. Therefore, this slice is the wavelet amplitude for a given mode.

The logarithmic decrement (decay) of the wavelet amplitude was used to determine modal damping. The approach is based on the solution to the equation of motion for displacement of an underdamped single-degree-of-freedom system is

$$x(t) = \exp(-\varsigma\omega_n t)\left\{x_0 \cos\omega_d t + \frac{v_0 + \varsigma\omega_n x_n}{\omega_d}\sin\omega_d t\right\}$$

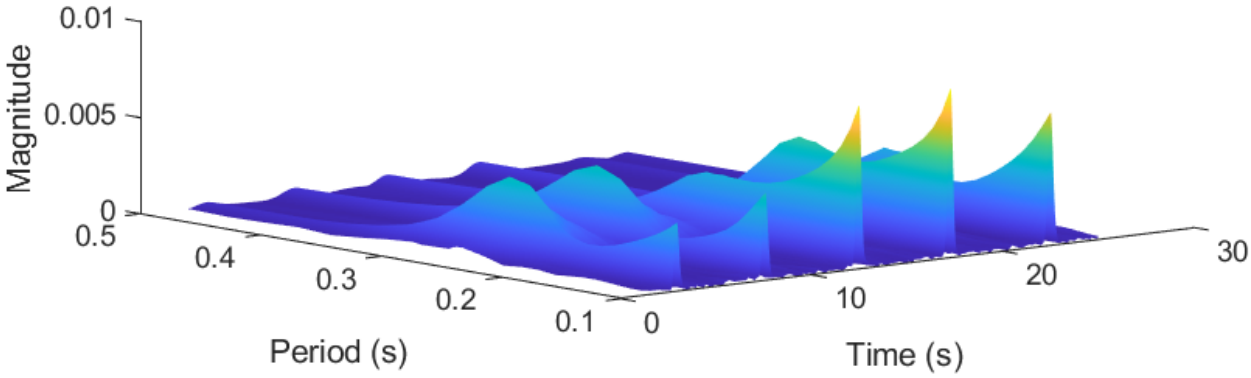

(a) Entire range of frequency content versus time.

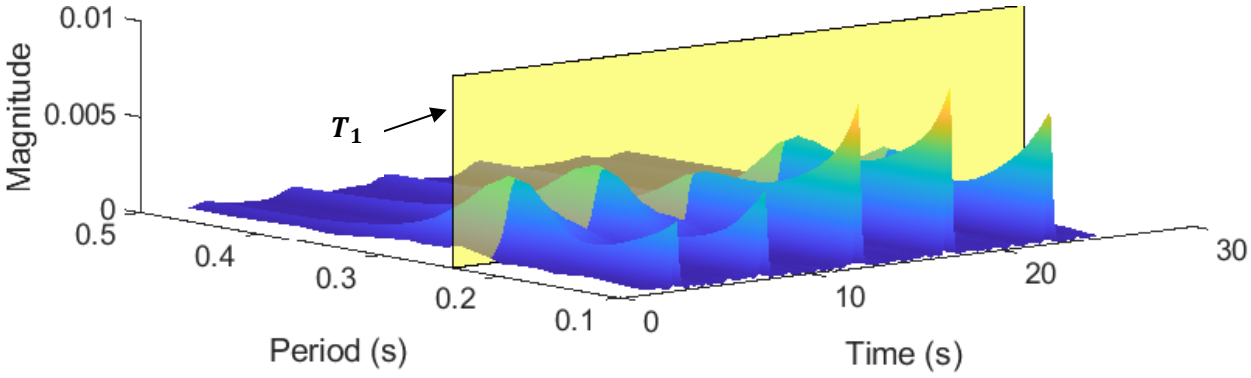

(b) Slice of frequency content (wavelet amplitude) at fundamental period of vibration.

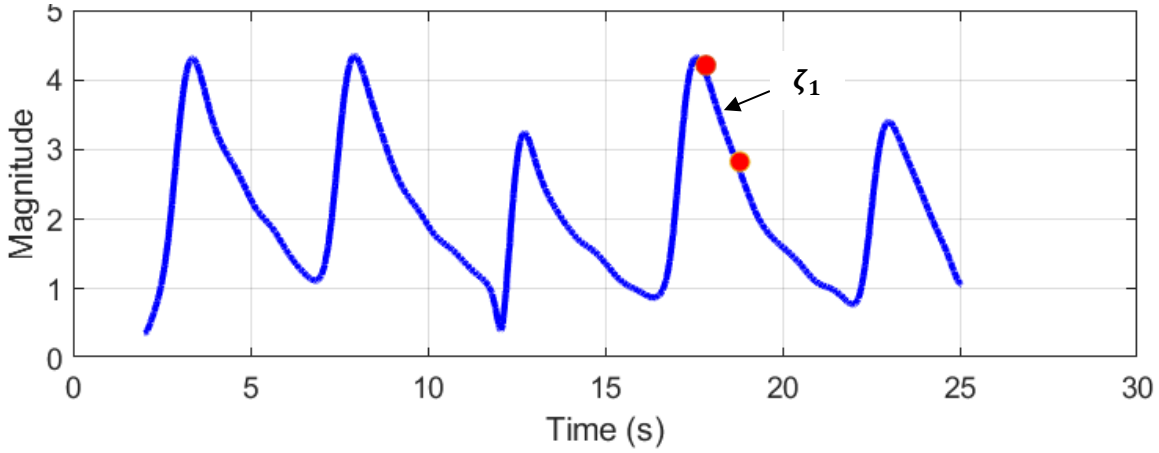

(c) Logarithmic decrement of wavelet amplitude at fundamental period of vibration.

Fig. 5.10. Illustration of wavelet demodulation process used to determine modal damping.

where $\omega_d = \omega_n \sqrt{1-\varsigma^2}$ is the damped frequency, $T = \frac{2\pi}{\omega_d} = \frac{2\pi}{\omega_n \sqrt{1-\varsigma^2}}$ is the period of vibration, and ζ is the damping ratio.

Fig. 5.11 shows how to do log decrement analysis based on a damped free vibration response. The logarithmic decrement in terms of displacement is $\delta = \log\left(\frac{x(t_n)}{x(t_{n+1})}\right)$

The time corresponding to each peak is $t_{n+1} = t_n + T$ Therefore,

$$\delta = \log \frac{\exp(-\varsigma\omega_n t_n)\left\{x_0 \cos\omega_d t_n + \frac{v_0 + \varsigma\omega_n x_n}{\omega_d} \sin\omega_d t_n\right\}}{\exp(-\varsigma\omega_n (t_n + T))\left\{x_0 \cos\omega_d (t_n + T) + \frac{v_0 + \varsigma\omega_n x_n}{\omega_d} \sin\omega_d (t_n + T)\right\}}$$

Writing the equation for logarithmic decrement in terms of the period of vibration and the damping ratio (ratio of critical damping) produces the following simplified equation: $\delta = \frac{2\pi\varsigma}{\sqrt{1-\varsigma^2}}$ Solving for the damping ratio gives $\varsigma = \frac{\delta}{\sqrt{4\pi^2 + \delta^2}}$

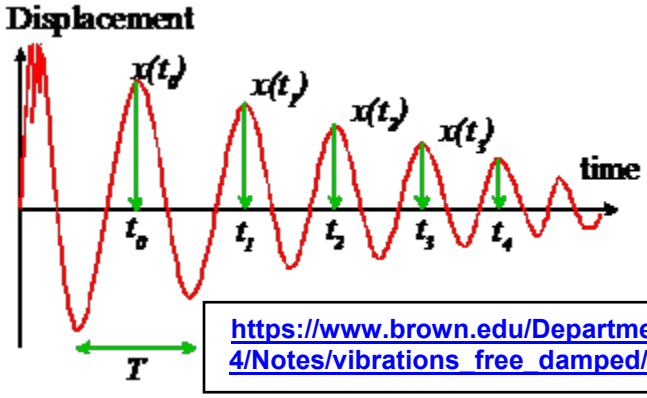

Fig. 5.11. Logarithmic decrement of free vibration with viscous damping.

5.2 Verification

Two tests were used to verify the research approach. First, a vibration test of a simply-supported beam was used to check the smartphone app. Second, the accuracy of the wavelet demodulation and log decrement method to determine damping was checked against the closed-form solution for free vibration of a single-degree-of-freedom system with viscous damping.

5.2.1 Acceleration App

To check the accuracy of the smartphone app, the smartphone was placed on a simply-supported steel HSS beam. Fig. 5.12 shows the beam. The beam was also instrumented with an accelerometer (Fig. 5.13). The beam was then struck to measure vibration data on both the phone and accelerometer. The FFT was used to determine the fundamental period of frequency of vibration and compared to the theoretical frequency. The results are shown in Fig. 5.14.

Fig. 5.12. Simply supported HSS beam for a vibration test.

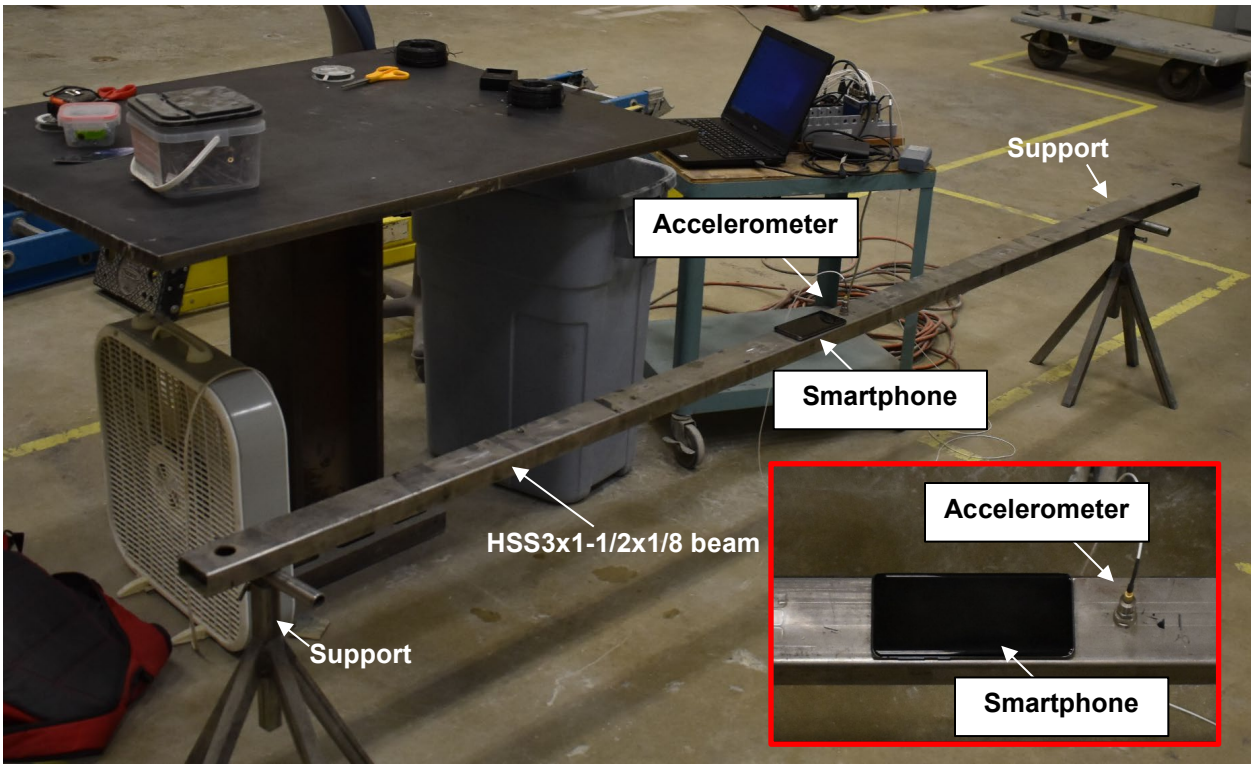

Fig. 5.13. Smartphone placed next to accelerometer on simply supported HSS beam.

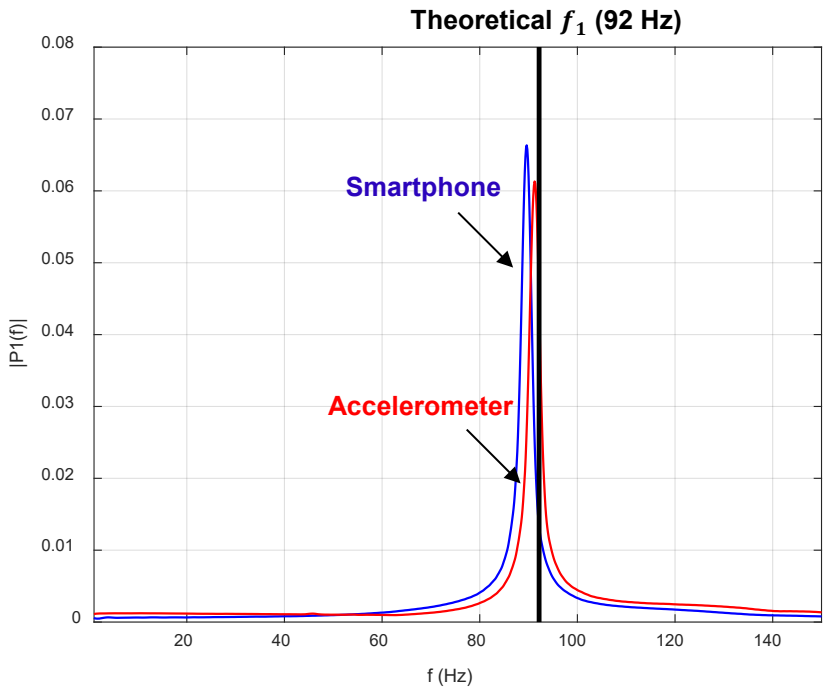

Fig. 5.14. Single-sided amplitude spectrum from HSS3x1-1/2x1/8 beam test.

5.2.2 Wavelet Demodulation Approach

To check the accuracy of the wavelet demodulation and log decrement method used to determine modal damping, the method was applied to two data sets: (1) the data from the simply-supported steel HSS beam test, and (2) data from the closed-form solution for free vibration of a single-degree-of-freedom system with a period of vibration of 2.81 seconds, and 10% viscous damping. Fig. 5.15 shows the results for the simply-supported beam (0.2% damping), and Fig. 5.16 shows the results for the single-degree-of-freedom system (9.6% damping).

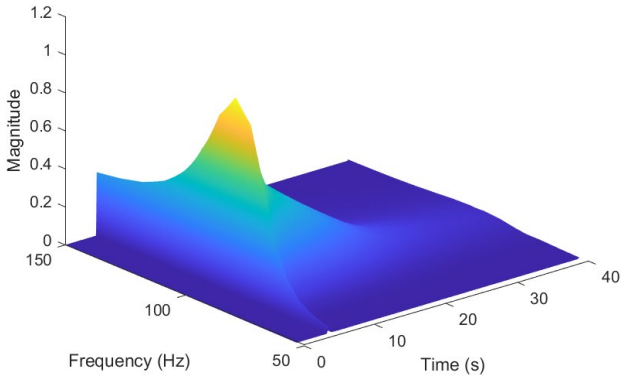

(a) Frequency content versus time.

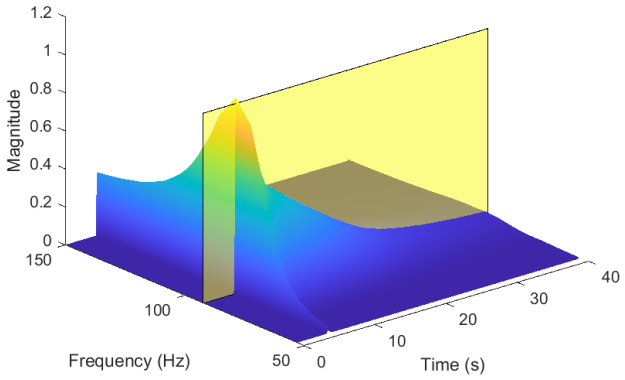

(b) Wavelet amplitude slice.

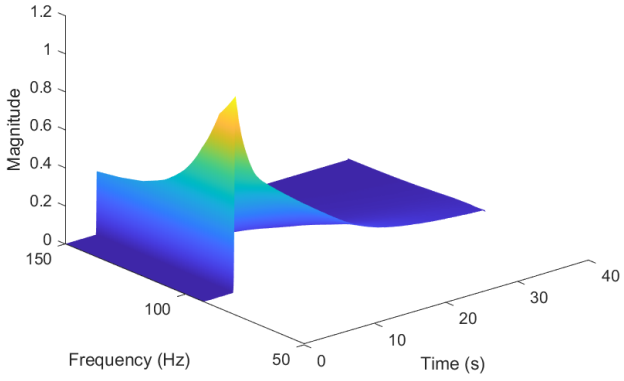

(c) Wavelet amplitude.

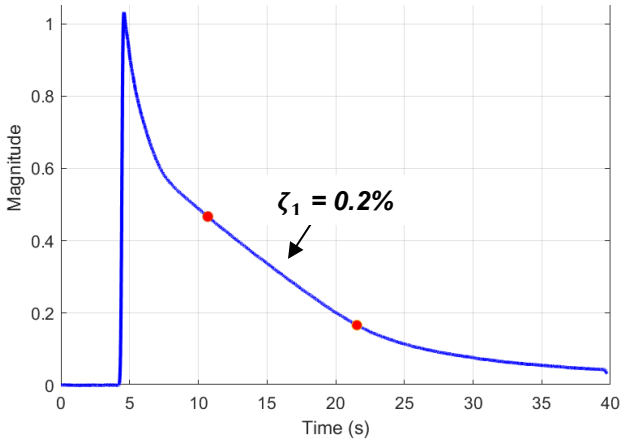

(b) Logarithmic decrement.

Fig. 5.15. Modal damping for the simply-supported steel HSS beam test.

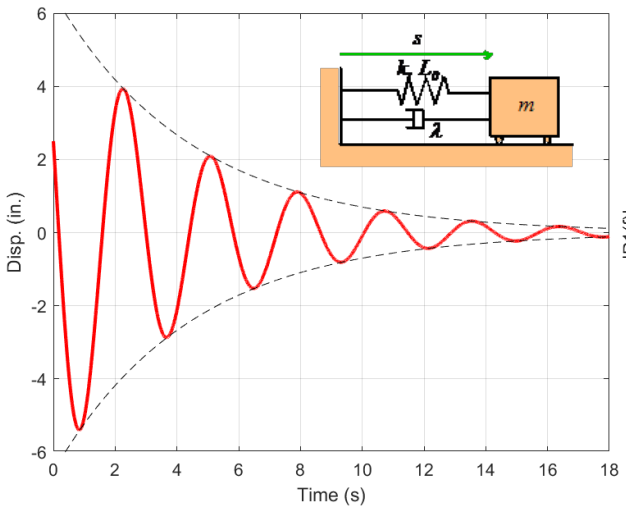

(a) Displacement versus time.

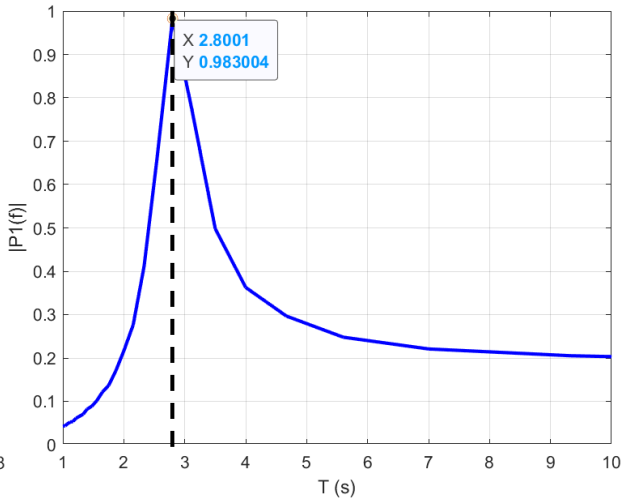

(b) Single-sided amplitude spectrum.

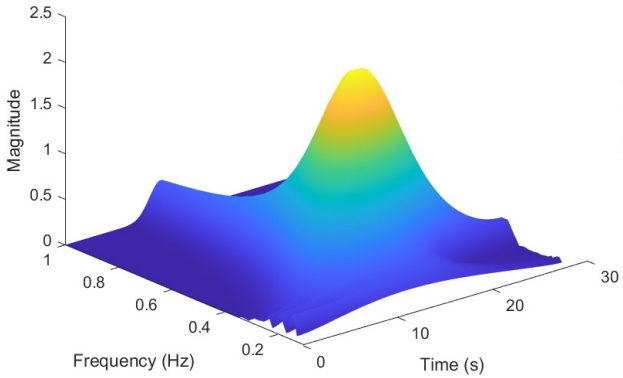

(c) Frequency content versus time.

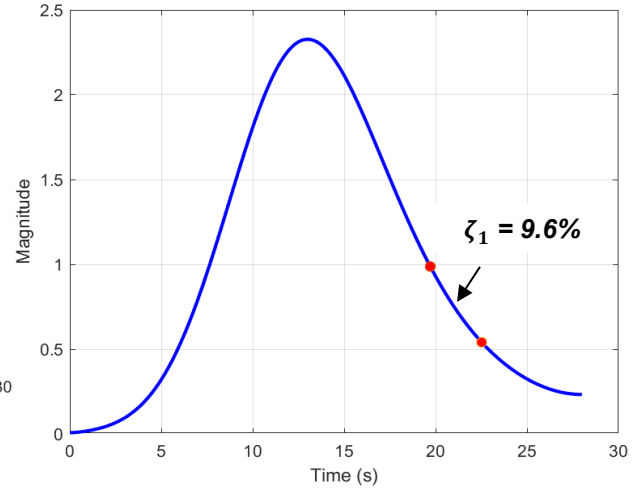

(d) Logarithmic decrement.

Fig. 5.16. Modal damping for free vibration of the single-degree-of-freedom system.

5.3 Vibration tests

Twelve free-standing timber frames with knee braces, located at various sites in the United States, were tested in the field between 2021 and 2022. The locations of the timber frames are shown in Fig. 5.17. Five timber frames were located along the Wasatch Front in Utah, three timber frames were located along the Front Range in Colorado, three frames were located in the Midwest (one in Minnesota and two in Michigan), and two frames were located in Virginia.

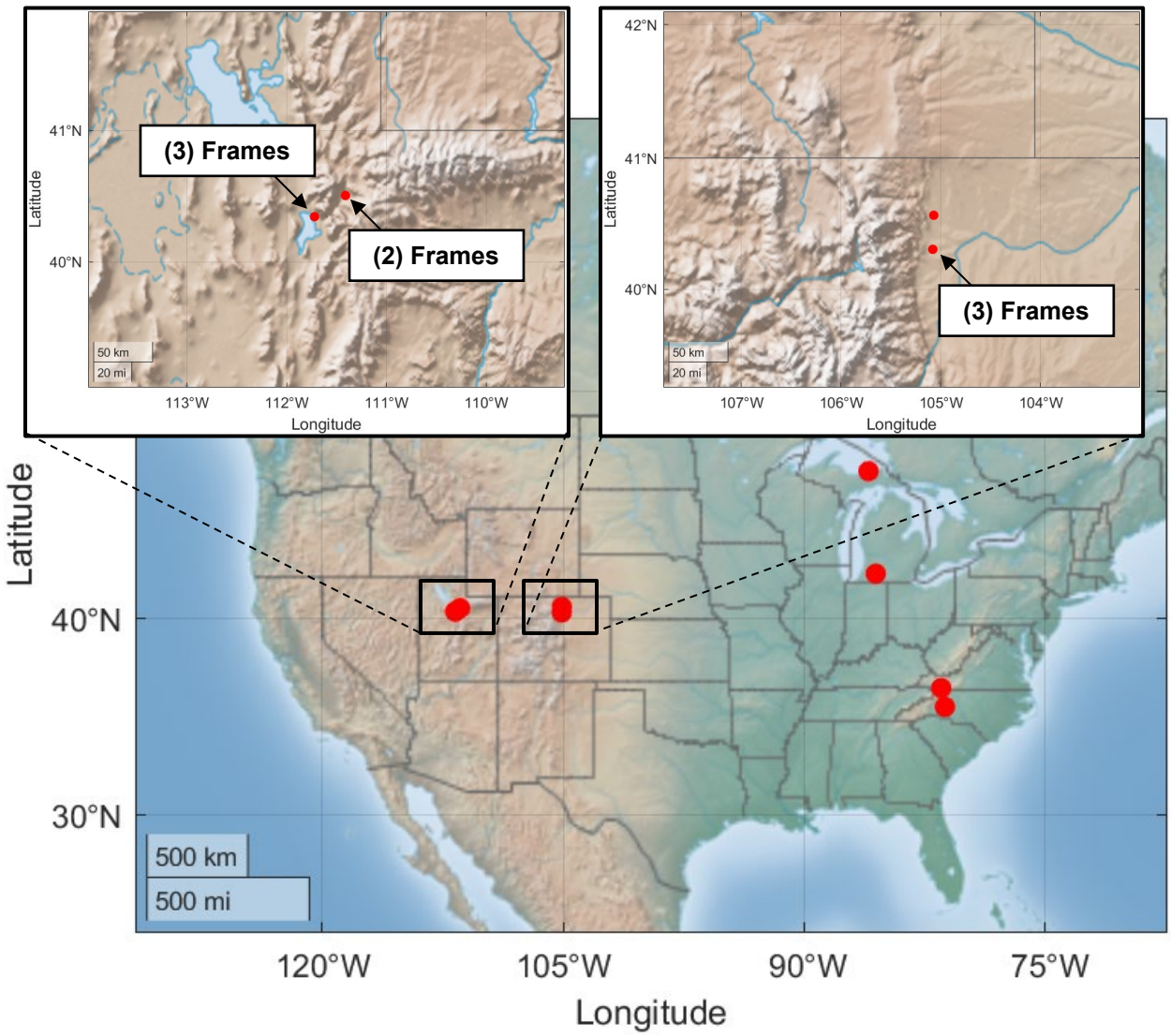

Fig. 5.17. Locations of timber frames in the vibration tests.

5.3.1 Hollow Park pavilion (Lindon, Utah)

The Hollow Park pavilion is a 25 ft wide by 35 ft long free-standing timber frame in a public park in Lindon, Utah. The frame is shown in Fig. 5.18. The beams span four posts in the longitudinal direction. The frame is supported by a concrete slab on grade. The mean roof height is approximately 12 ft. Fig. 5.19 shows example results from the frequency and wavelet analyses. The vibration test was conducted in May, 2021. The fundamental periods of vibration were 0.25 sec. and 0.31 sec. and the modal damping was approximately 1% to 2%.

Fig. 5.18. Hollow Park pavilion.

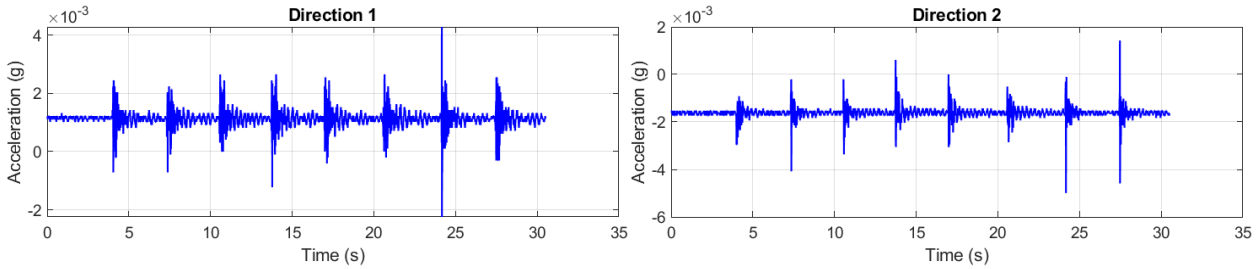

(a) Acceleration history

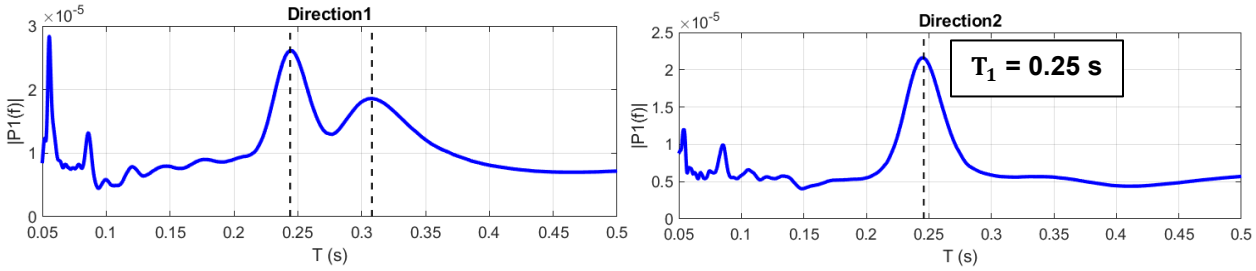

(b) Single-sided amplitude spectrum of period-content.

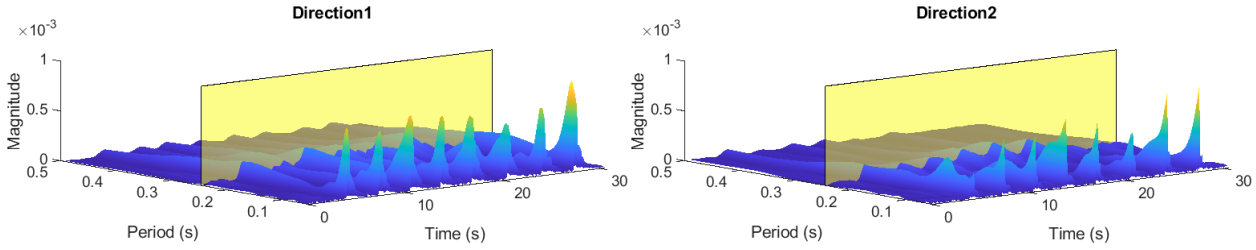

(c) Amplitude of period content versus time.

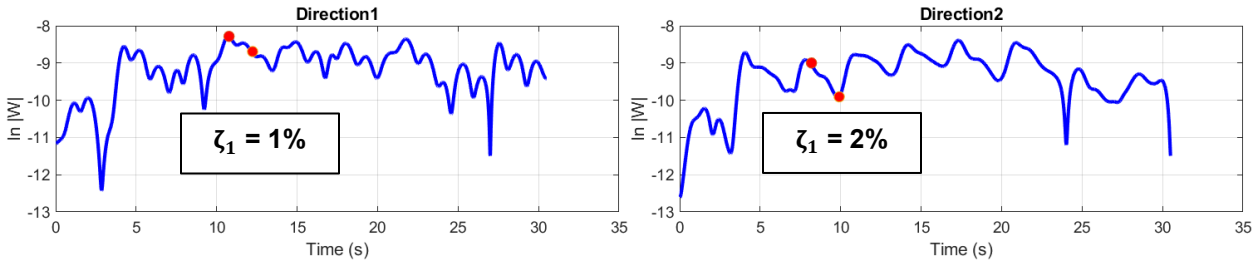

(d) Wavelet amplitude at fundamental period of vibration.

Fig. 5.19. Example frequency analysis of Hollow Park pavilion.

5.3.2 Lindon City Park pavilion (Lindon, Utah)

The Lindon City Park pavilion is a 72 ft long by 29.5 ft wide free-standing timber frame in a public park in Lindon, Utah (Fig. 5.20). It is supported on a concrete slab on grade. The beams span six posts longitudinally. The mean roof height is approximately 12 ft. The vibration test was conducted in May, 2021. The fundamental period of vibration was 0.32 sec. and the corresponding model damping was approximately 3% (see Fig. 5.21).

Fig. 5.20. Lindon City Park pavilion.

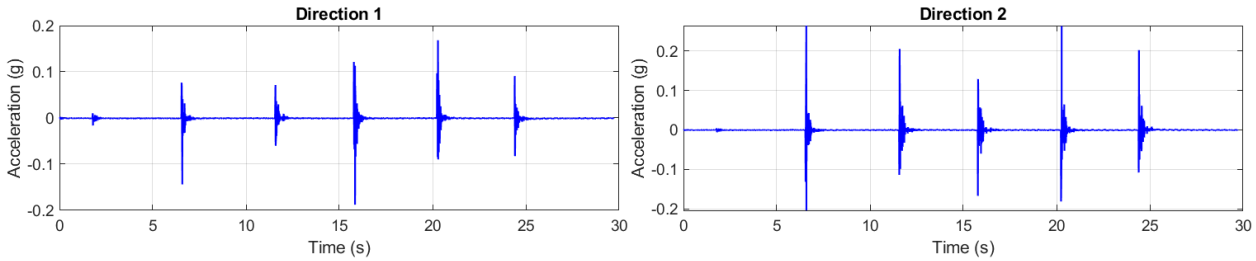

(a) Acceleration history

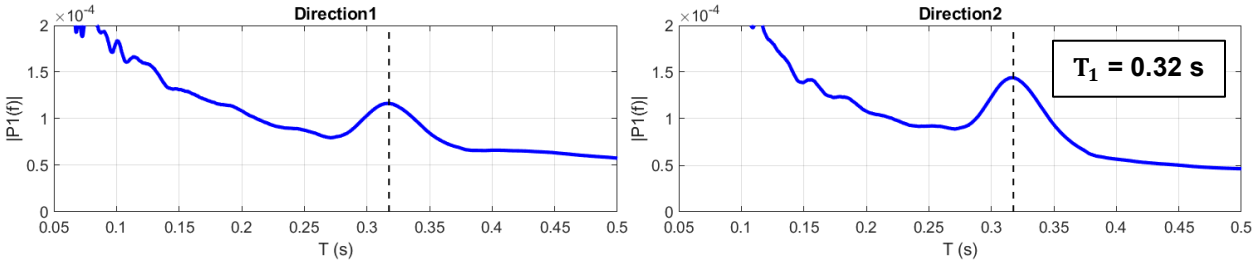

(b) Single-sided amplitude spectrum of period-content.

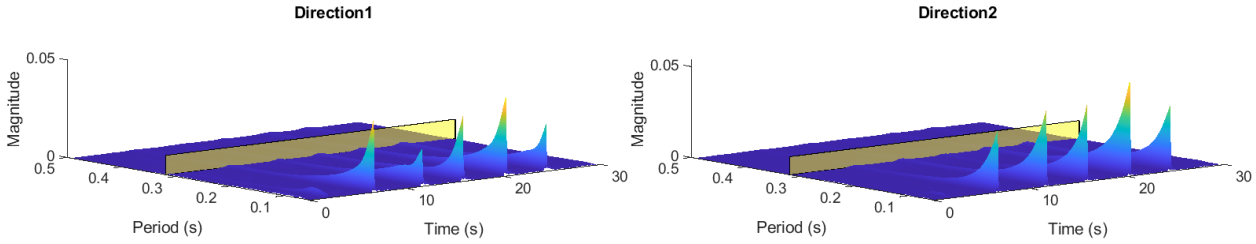

(c) Amplitude of period content versus time.

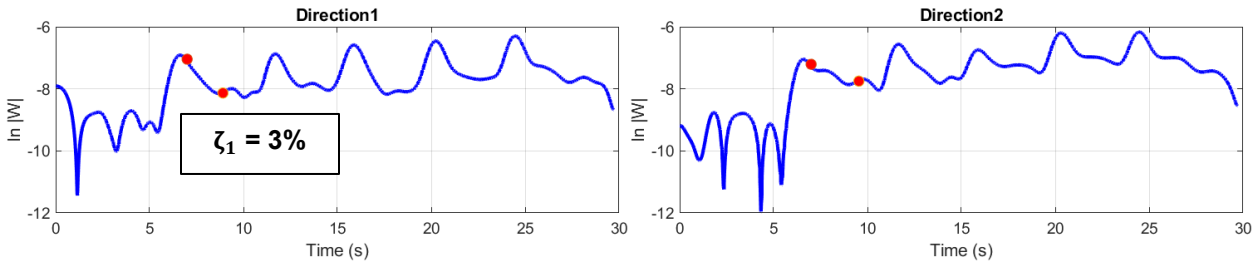

(d) Wavelet amplitude at fundamental period of vibration.

Fig. 5.21. Example frequency analysis of Lindon City Park frame.

5.3.3 Pioneer Park pavilion (Lindon, Utah)

The Pioneer Park pavilion is a 35 ft long by 25 ft wide free-standing timber frame in a public park in Lindon, Utah (Fig. 5.22). The posts are supported on a concrete slab on grade. The base of the post is on a steel plate. The beams span four posts longitudinally. The mean roof height is approximately 12 ft. The vibration test was conducted in May, 2021. The fundamental period of vibration was 0.25 sec. and the corresponding modal damping was 1% or less (see Fig. 5.23).

Fig. 5.22. Pioneer Park pavilion in Lindon, Utah.

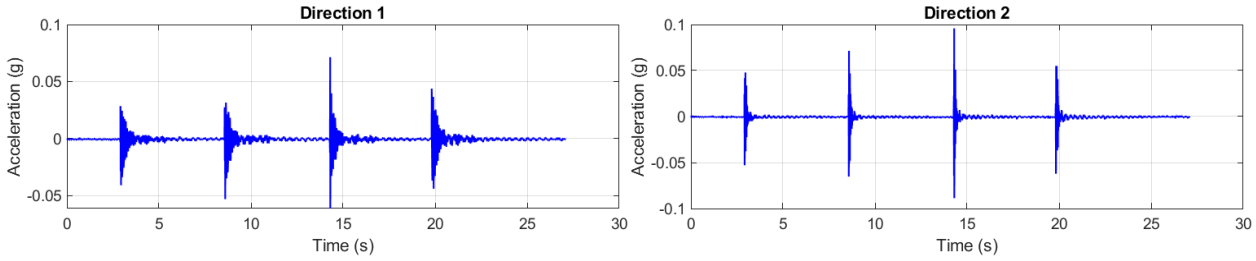

(a) Acceleration history

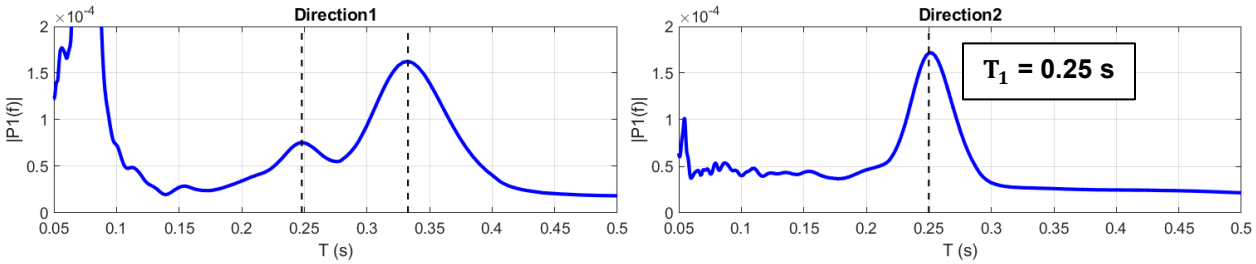

(b) Single-sided amplitude spectrum of period-content.

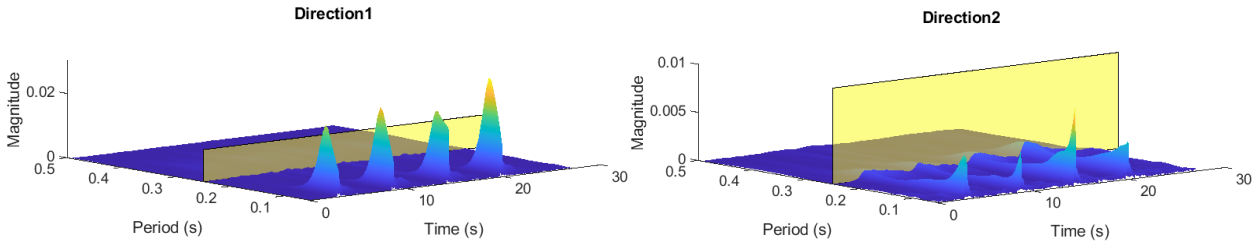

(c) Amplitude of period content versus time.

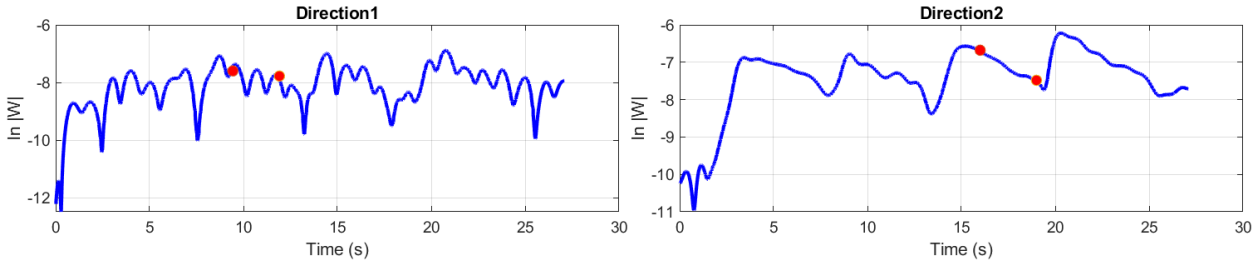

(d) Wavelet amplitude at fundamental period of vibration.

Fig. 5.23. Example vibration analysis results from the Pioneer Park pavilion.

5.3.4 River Bottoms Ranch pavilion (Midway, Utah)

The River Bottoms Ranch pavilion is a free-standing timber frame at a private event venue in Midway, Utah (Fig. 5.24). The frame is supported on a concrete slab on grade and spans five posts longitudinally. The mean roof height is approximately 12 ft. The vibration test was conducted in March, 2022. The fundamental periods of vibration were 0.20 sec. and 0.27 sec. and the modal damping was approximately 1% (see Fig. 5.25).

Fig. 5.24. River Bottoms Ranch pavilion in Midway, Utah.

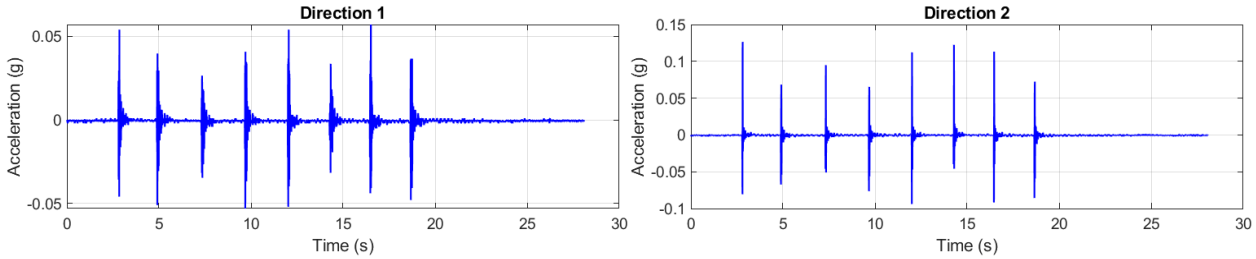

(a) Acceleration history

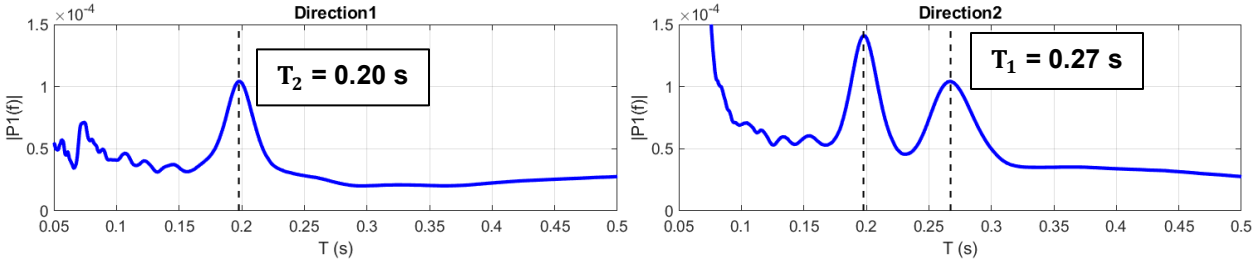

(b) Single-sided amplitude spectrum of period-content.

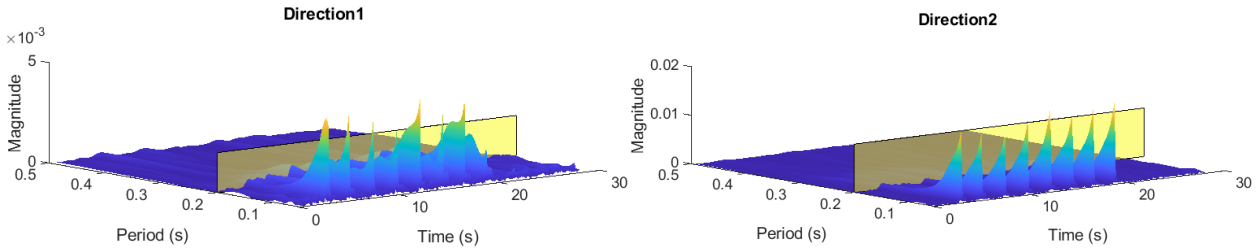

(c) Amplitude of period content versus time.

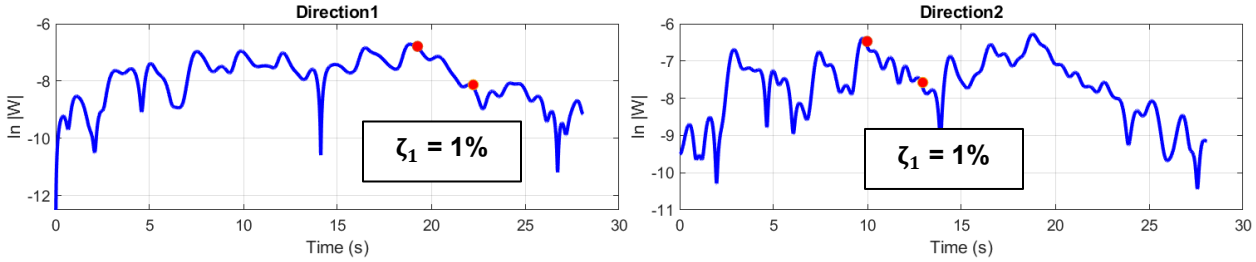

(d) Wavelet amplitude at fundamental period of vibration.

Fig. 5.25. Example frequency analysis of River Bottoms Ranch pavilion.

5.3.5 Legacy Bridge (Midway, Utah)

The Legacy Bridge is a covered bridge between Heber City and Midway, Utah (Fig. 5.26). The bridge is about 120-ft long—the longest covered bridge in Utah. The mean roof height is approximately 12 ft. The vibration test was conducted in March, 2022. The fundamental periods of vibration were 0.33 sec. and 0.2 sec. and the first-mode damping was approximately 1% (see Fig. 5.27).

Fig. 5.26. Legacy covered bridge in Midway, Utah.

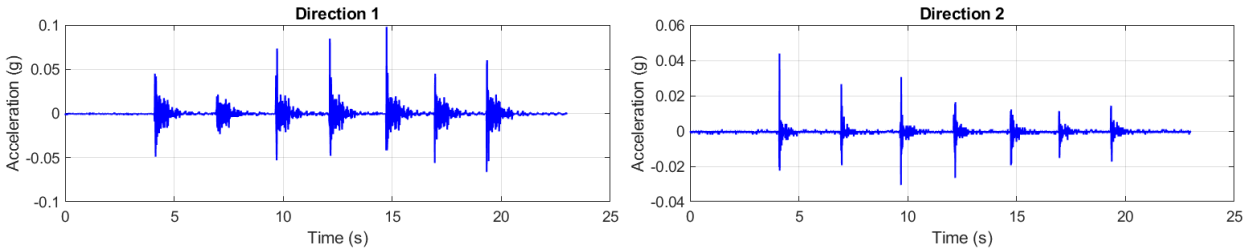

(a) Acceleration history

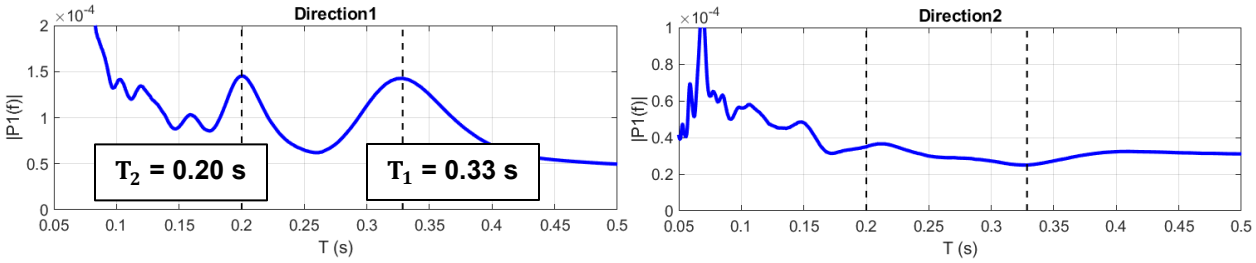

(b) Single-sided amplitude spectrum of period-content.

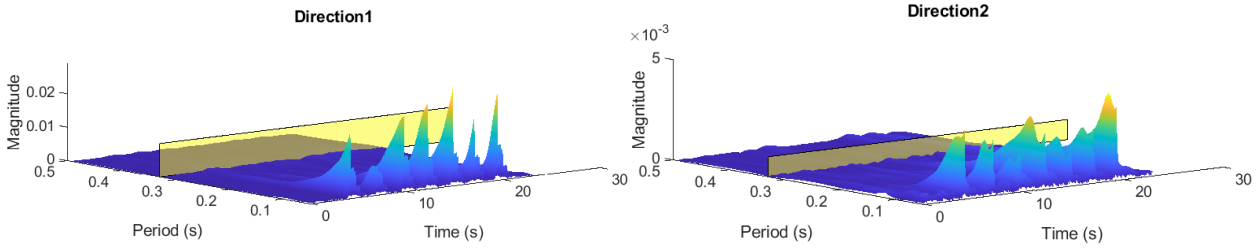

(c) Amplitude of period content versus time.

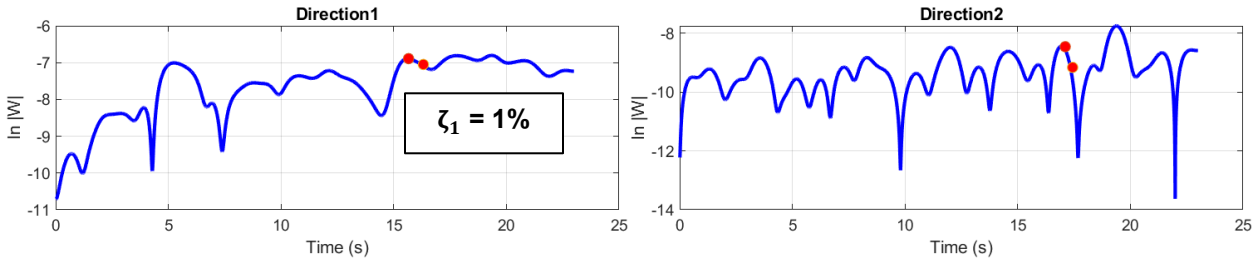

(d) Wavelet amplitude at fundamental period of vibration.

Fig. 5.27. Example frequency analysis of Legacy covered bridge.

5.3.6 Bag Corral pavilion (Berthoud, Colorado)

The Bag Corral pavilion is a 14.5 ft long by 10.5 ft wide free-standing timber frame at a golf center in Berthoud, Colorado (Fig. 5.28). It is a single-span frame in both directions. The posts are wrapped with masonry. There is a gap between the posts and the masonry. Each post on the frame is 5.5 ft high from the top of the pier to the spandrel beam. The mean roof height is 11.5 ft. The vibration test was conducted in March, 2022. The first period of vibration was 0.24 sec. and the corresponding damping was 2%. The second period of vibration was 0.16 sec. and the corresponding damping was 5% (see Fig. 5.29).

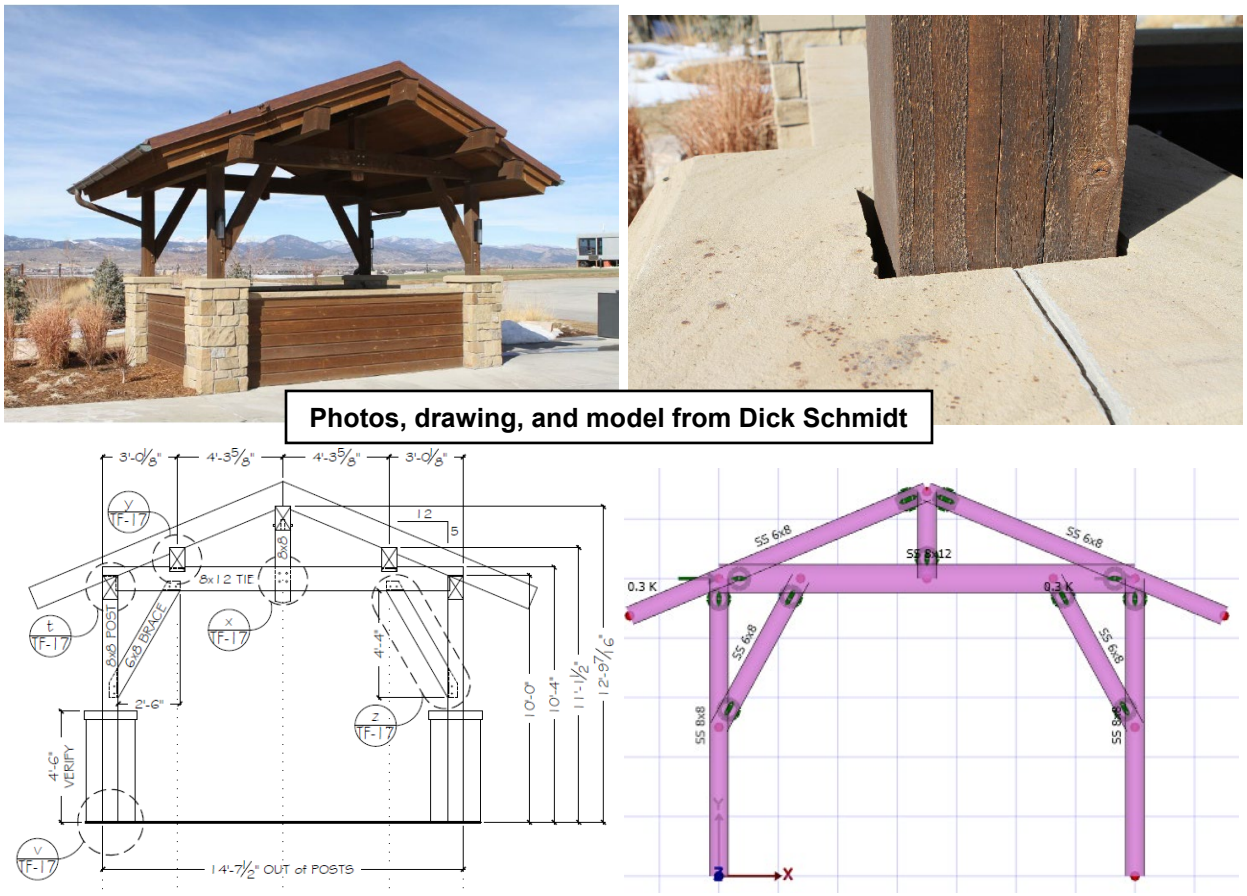

Fig. 5.28. Bag Corral pavilion in Berthoud, Colorado.

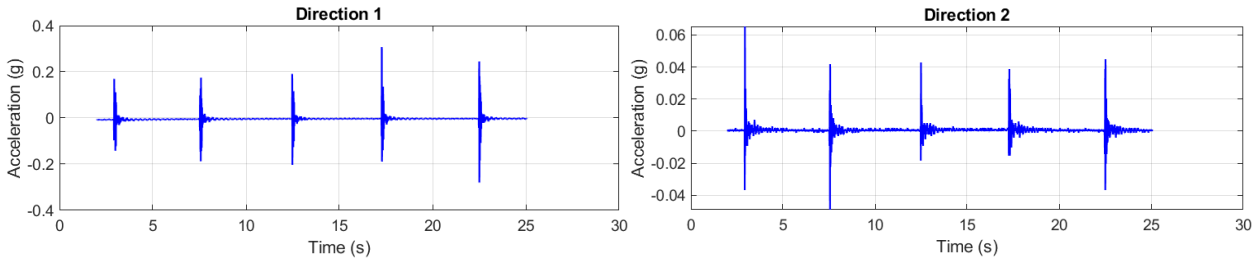

(a) Acceleration history

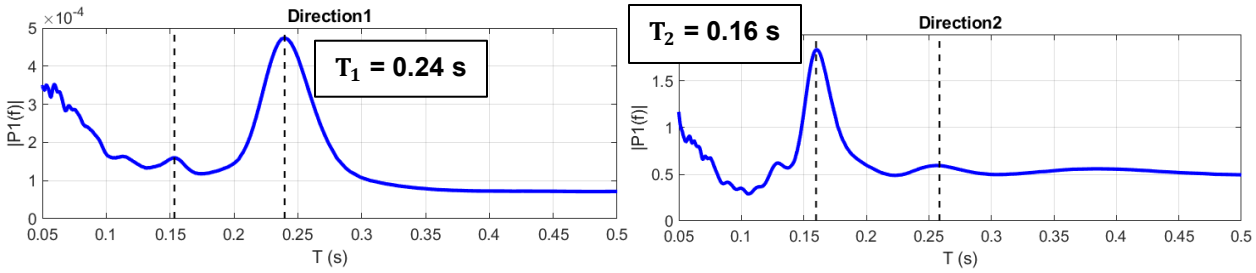

(b) Single-sided amplitude spectrum of period-content.

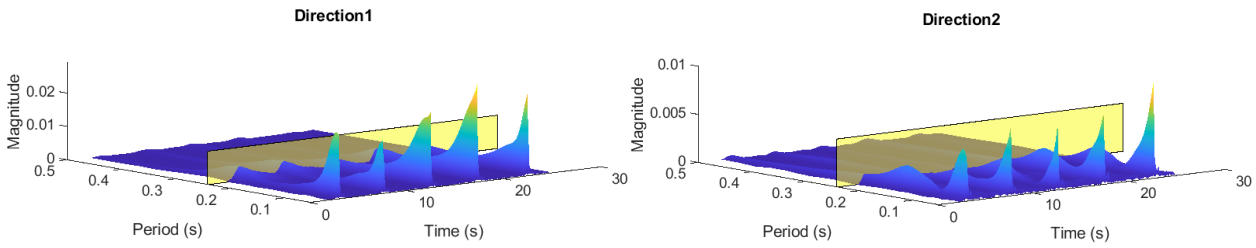

(c) Amplitude of period content versus time.

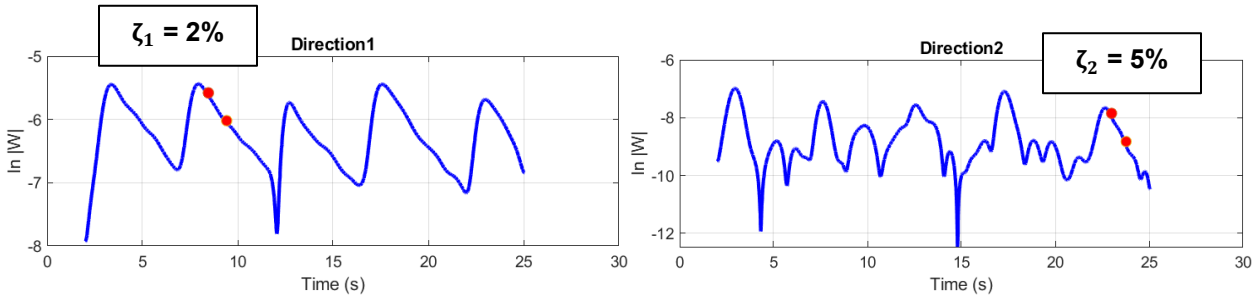

(d) Wavelet amplitude at fundamental period of vibration.

Fig. 5.29. Example frequency analysis of the Bag Corral pavilion.

5.3.7 Pool Bar pavilion (Berthoud, Colorado)

The Pool Bar pavilion is a 16.5’ by 14.5’ free-standing timber frame at a golf center in Berthoud, Colorado (Fig. 5.30). It is a single-span frame in both directions. The posts are wrapped with masonry. The gap between the posts and the masonry are filled with mortar. Each post on the frame is 4.5 ft high from the top of the pier to the spandrel beam. The mean roof height is 6.5 ft. from the top of the pier. The vibration test was conducted in March, 2022. The first period of vibration was 0.13 sec. and the corresponding damping was 2% (Fig. 5.31). The second period of vibration was 0.09 sec. The computed period of vibration for the structural model was 0.09 sec.

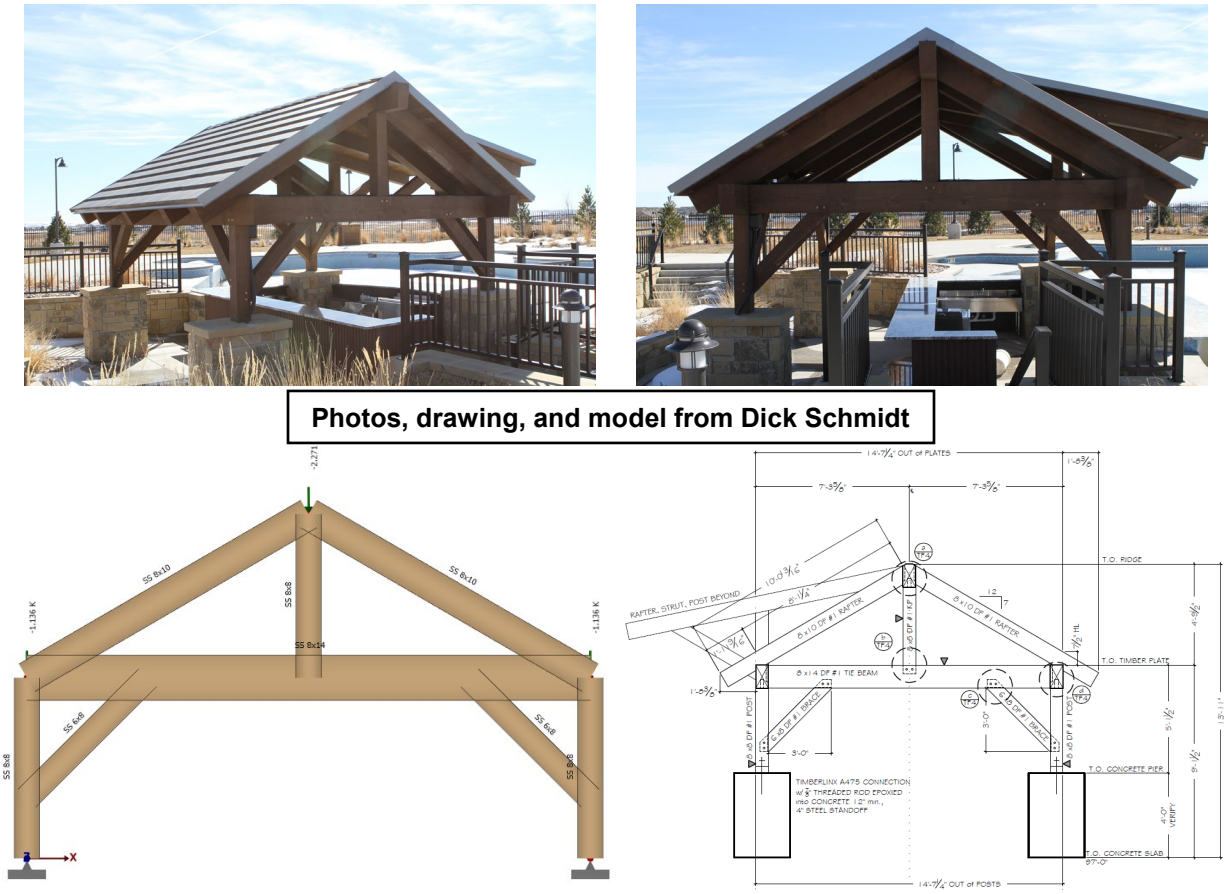

Fig. 5.30. Pool Bar pavilion in Berthoud, Colorado.

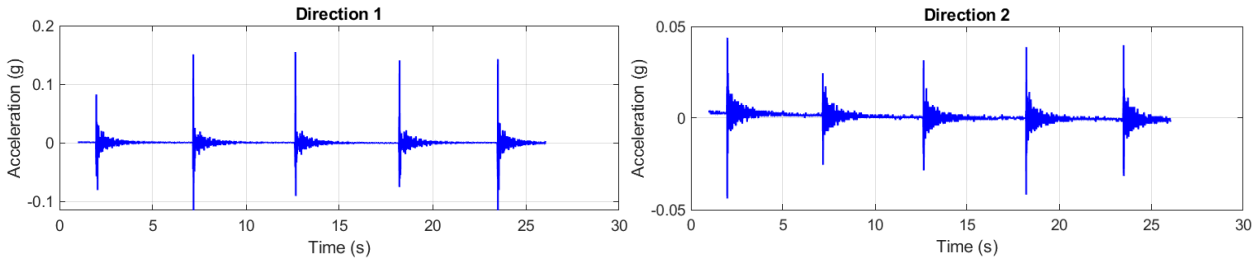

(a) Acceleration history

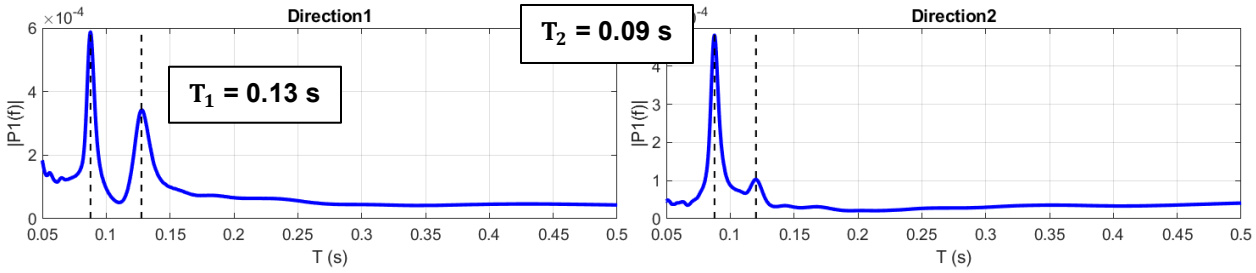

(b) Single-sided amplitude spectrum of period-content.

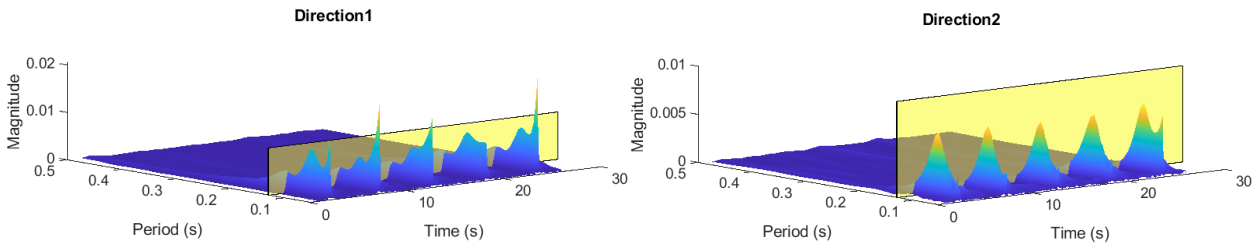

(c) Amplitude of period content versus time.

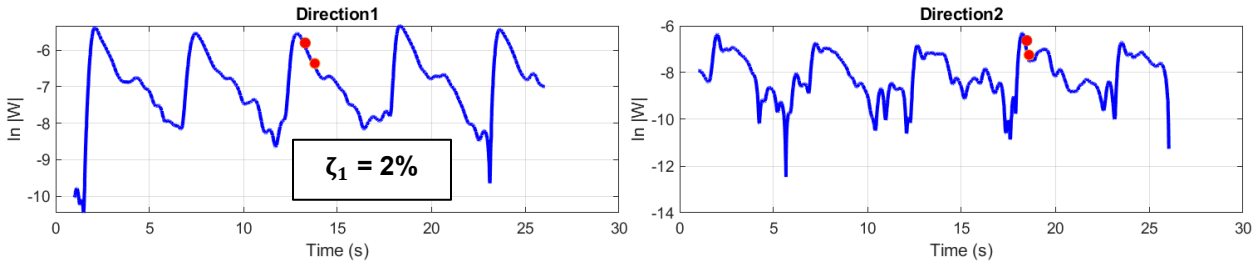

(d) Wavelet amplitude at fundamental period of vibration.

Fig. 5.31. Example frequency analysis of the Pool Bar pavilion.

5.3.8 Farghee pergola (Ft. Collins, Colorado

The Farghee pergola is a 12.5 ft by 12.8 ft free-standing timber frame in Fort Collins, Colorado. The frame is 10.5 ft tall from the base to the 8x10 wood plate (beam). The base of the posts rests on steel plates set on top of isolated stone pavers (Fig. 5.32). The vibration test was conducted in March, 2022. The first period of vibration was 0.16 sec and the corresponding damping was 2%. The second period of vibration was 0.10 sec.

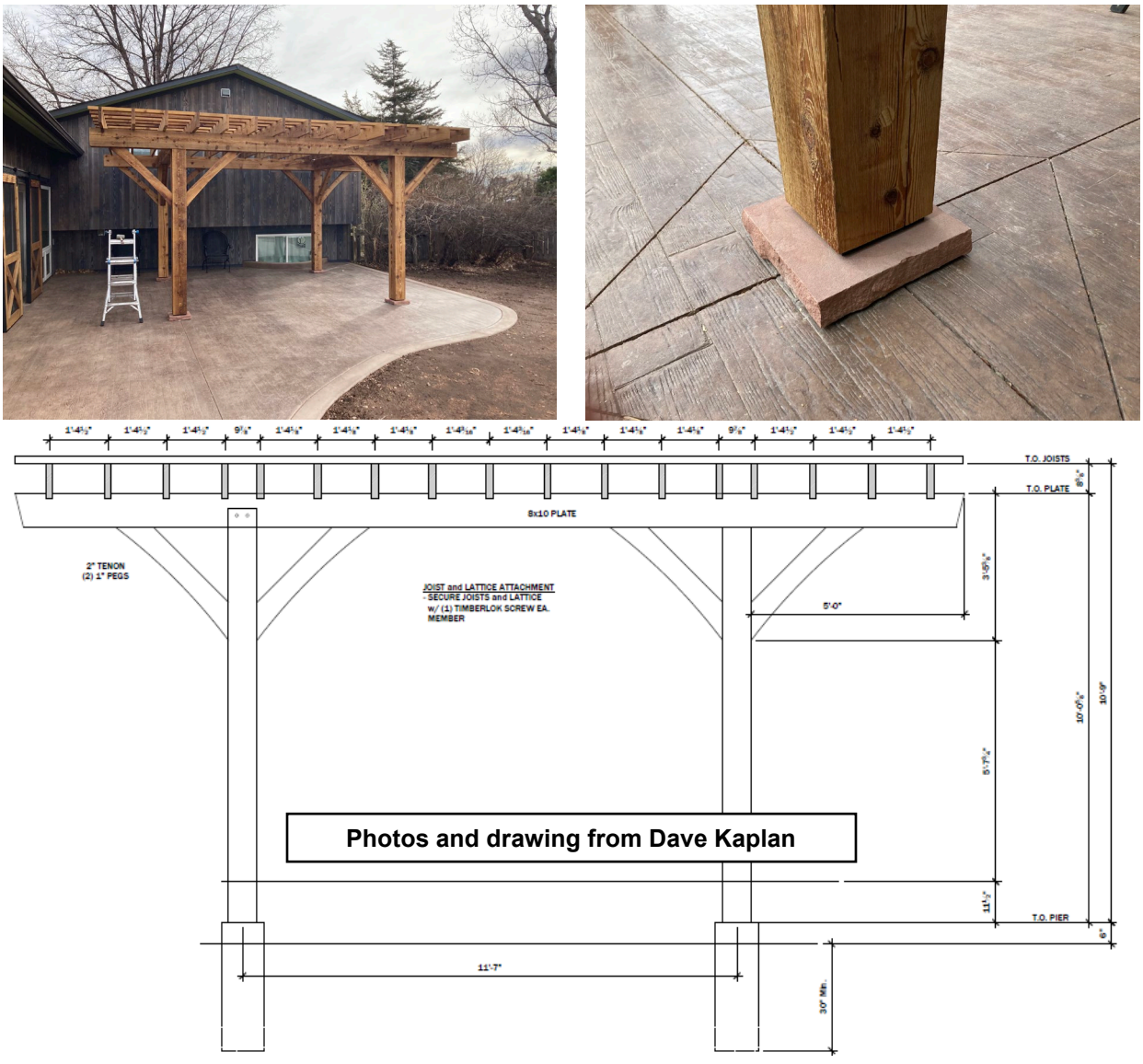

Fig. 5.32. Farghee Pergola in Ft. Collins, Colorado.

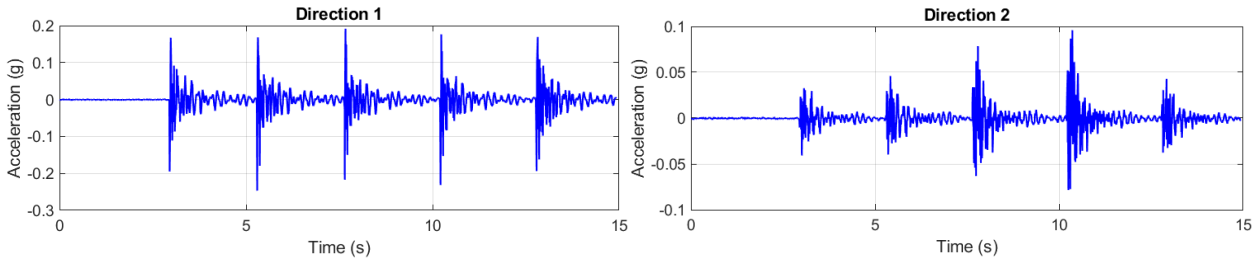

(a) Acceleration history

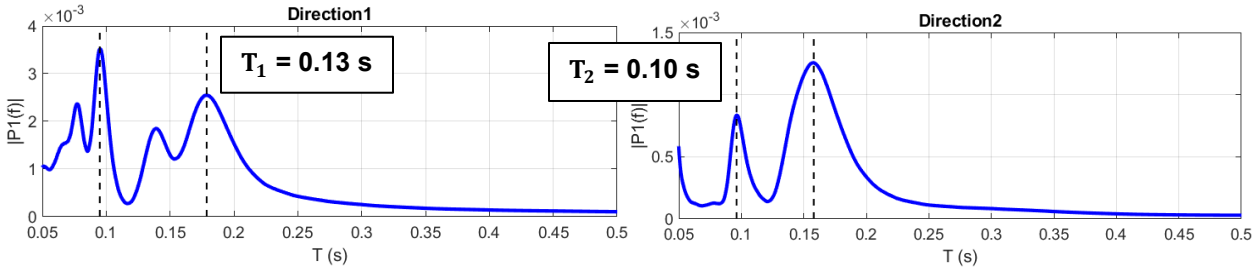

(b) Single-sided amplitude spectrum of period-content.

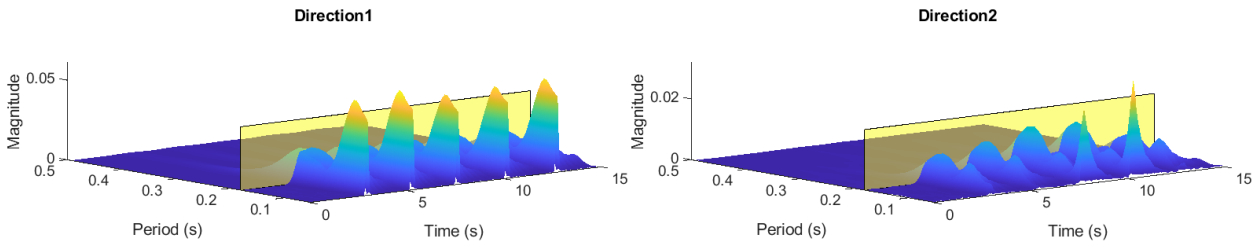

(c) Amplitude of period content versus time.

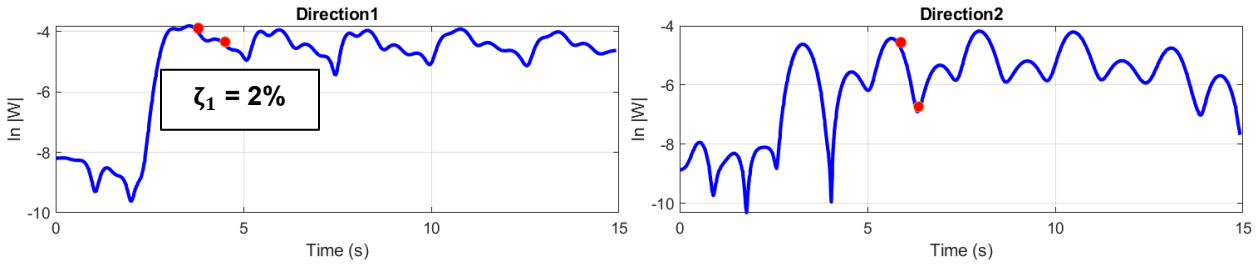

(d) Wavelet amplitude at fundamental period of vibration.

Fig. 5.33. Example frequency analysis of the Farghee pergola.

5.3.9 Cook County High School frame (Grand Marais, Minnesota)

The Cook County High School frame, in Grand Marais, Minnesota, was a 20 ft by 16 ft free-standing timber frame that was built by the students as an educational experience (Fig. 5.34). The roof was not covered. The mean roof height is 10.75 ft. The vibration test was conducted in May, 2022. The first period of vibration was 0.32 sec. and the corresponding modal damping was 2% (see Fig. 5.35). The second period of vibration was 0.25 sec.

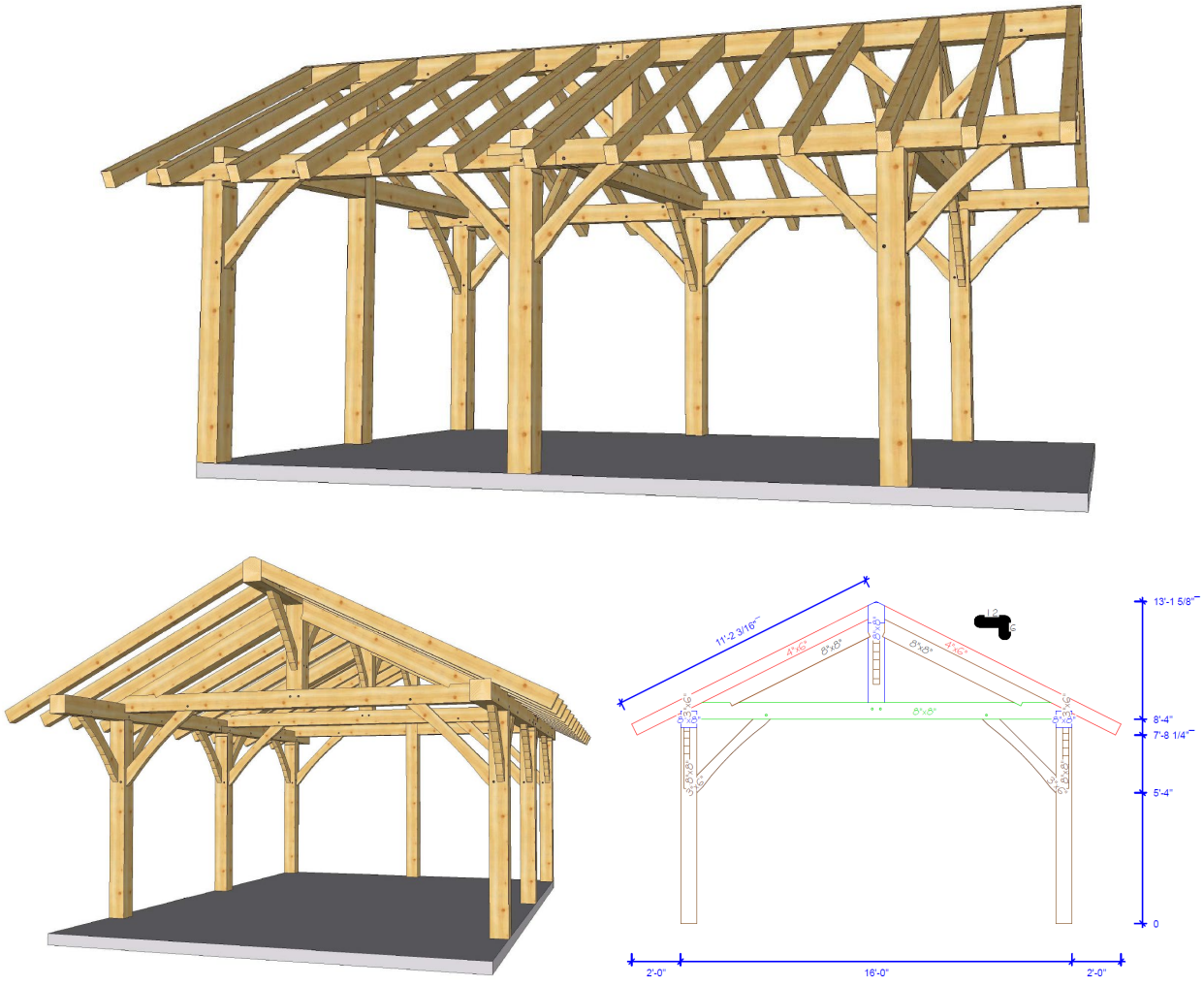

Fig. 5.34. Cook County High School frame in Grand Marais, Minnesota.

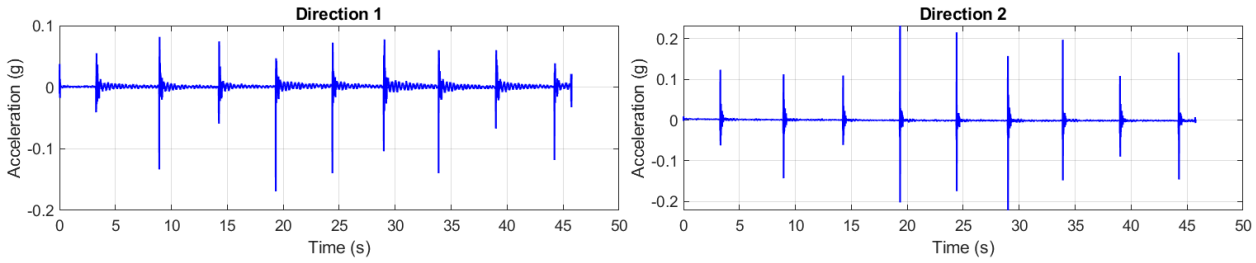

(a) Acceleration history

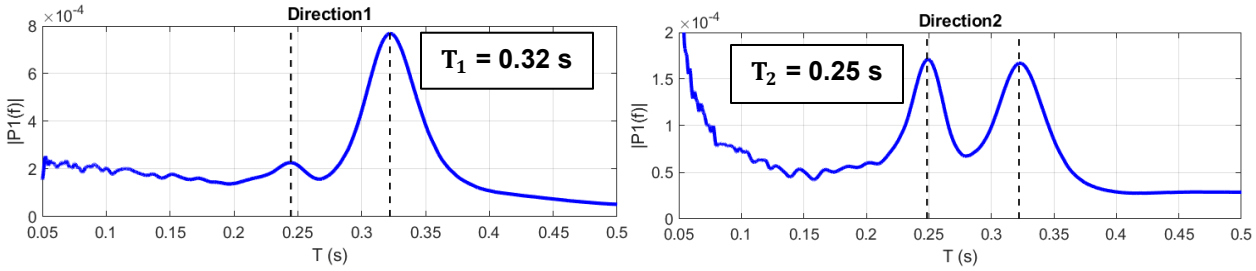

(b) Single-sided amplitude spectrum of period-content.

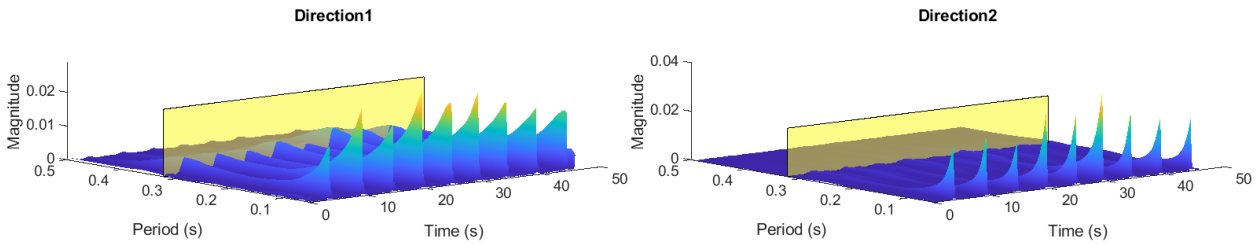

(c) Amplitude of period content versus time.

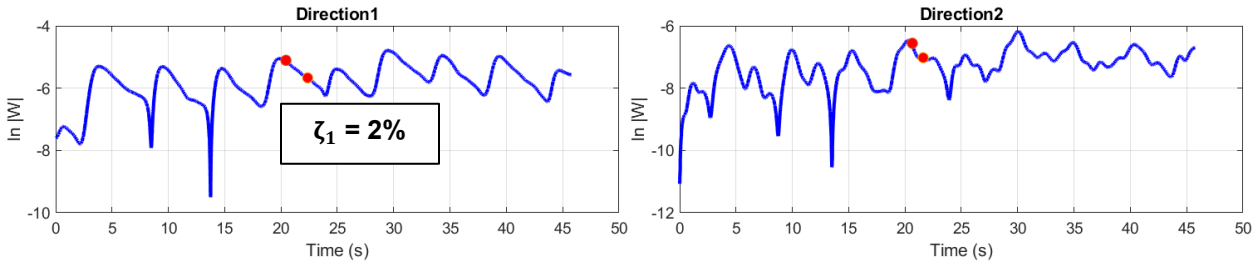

(d) Wavelet amplitude at fundamental period of vibration.

Fig. 5.35. Example frequency analysis of the Cook County High School frame.

5.3.10 Farmers Market pavilion (Vicksburg, Michigan)

The Farmers Market pavilion is a 121 ft long by 36 ft wide free-standing timber frame in Vicksburg, Michigan (Fig. 5.36 to Fig. 5.38). The frame spans across 10 posts longitudinally. The mean roof height is approximately 17.5 ft. The footings rest on steel plates embedded into the concrete footings, with a bolted base connection into the post. The vibration test was conducted in March, 2022. Similar to the Legacy bridge, the vibration data is noisy. With this in mind, the fundamental periods of vibration were 0.34 sec. and 0.31 sec. The first-mode damping was approximately 10% (Fig. 5.39).

Fig. 5.36. Farmers Market pavilion in Vicksburg, Michigan.

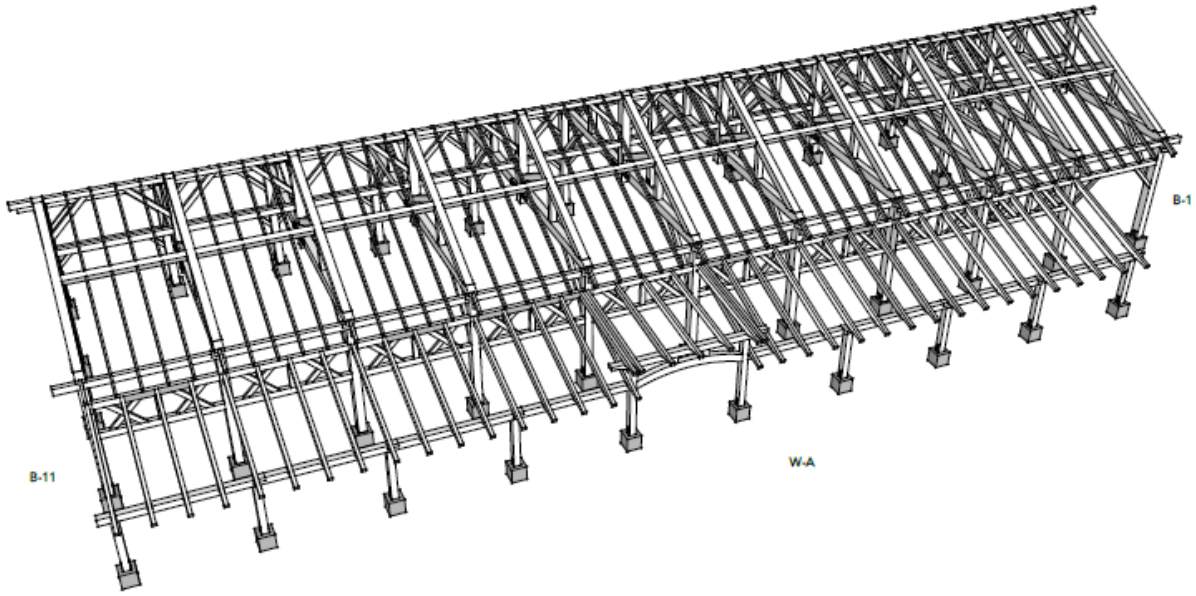

Fig. 5.37. Isometric drawing of the Farmers Market pavilion.

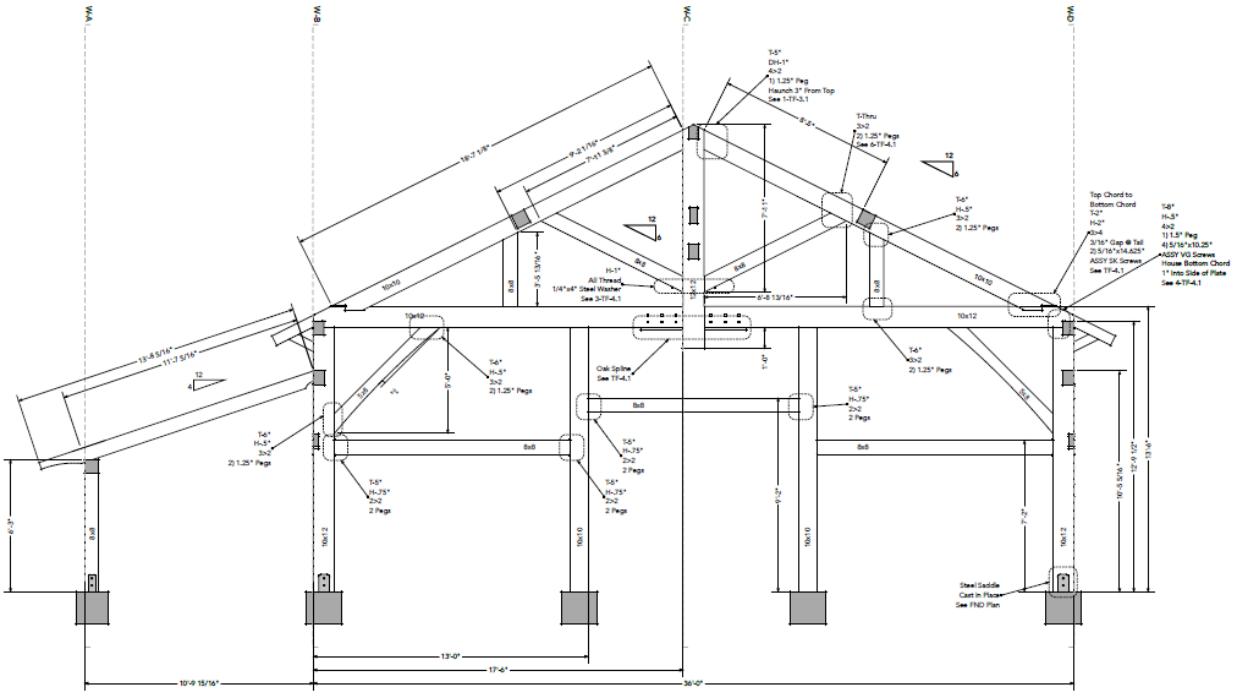

Fig. 5.38. Profile drawing of the Farmers Market pavilion.

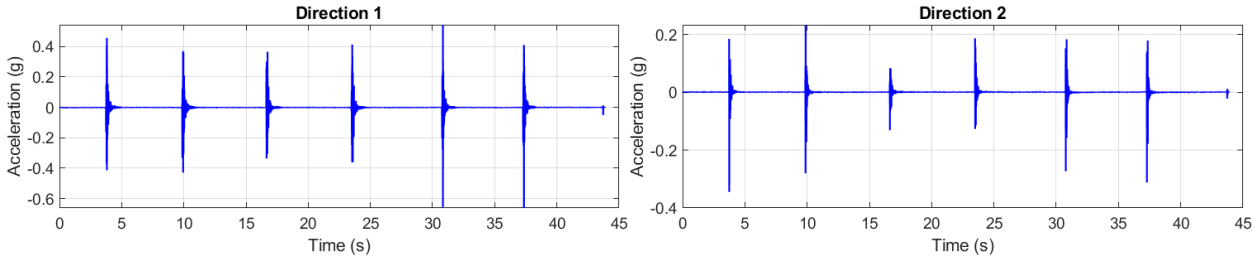

(a) Acceleration history

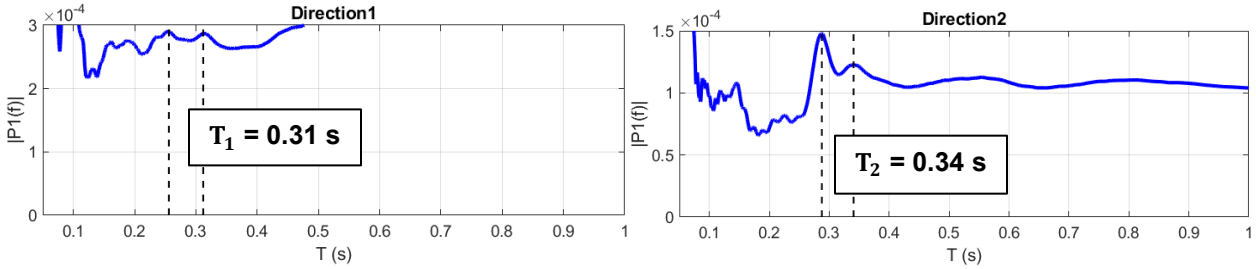

(b) Single-sided amplitude spectrum of period-content.

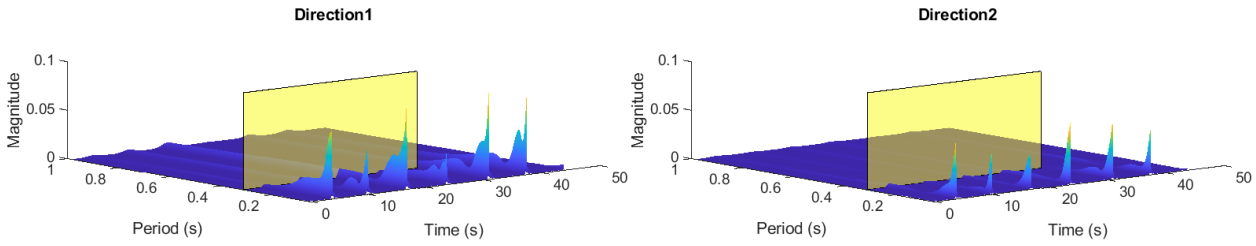

(c) Amplitude of period content versus time.

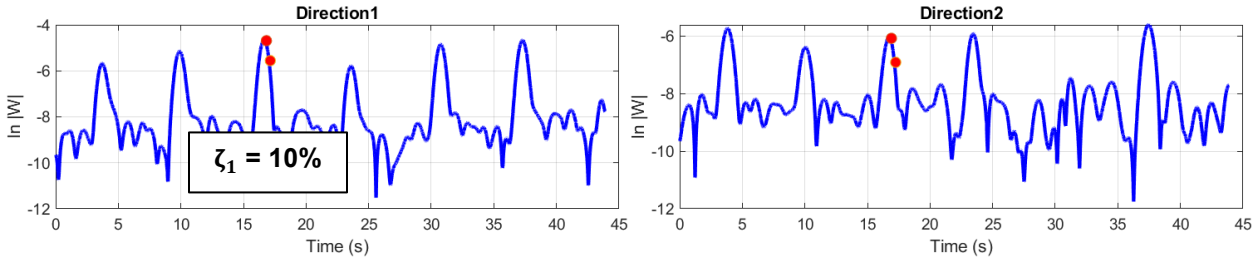

(d) Wavelet amplitude at fundamental period of vibration.

Fig. 5.39. Example frequency analysis of the Farmers Market pavilion.

5.3.11 Independence Farmers Market pavilion (Independence, Virginia)

The Independence Farmers Market pavilion is a 132-ft long by 20-ft wide (drip line of about 136 ft by 40 ft) free-standing timber frame in Independence, Virginia (Fig. 5.40). The timber frame is supported on concrete piers and spans twelve posts longitudinally. Each span is 12 ft across. The mean roof height is approximately 17 ft. The timber frame was built as a community building workshop by the TFG.

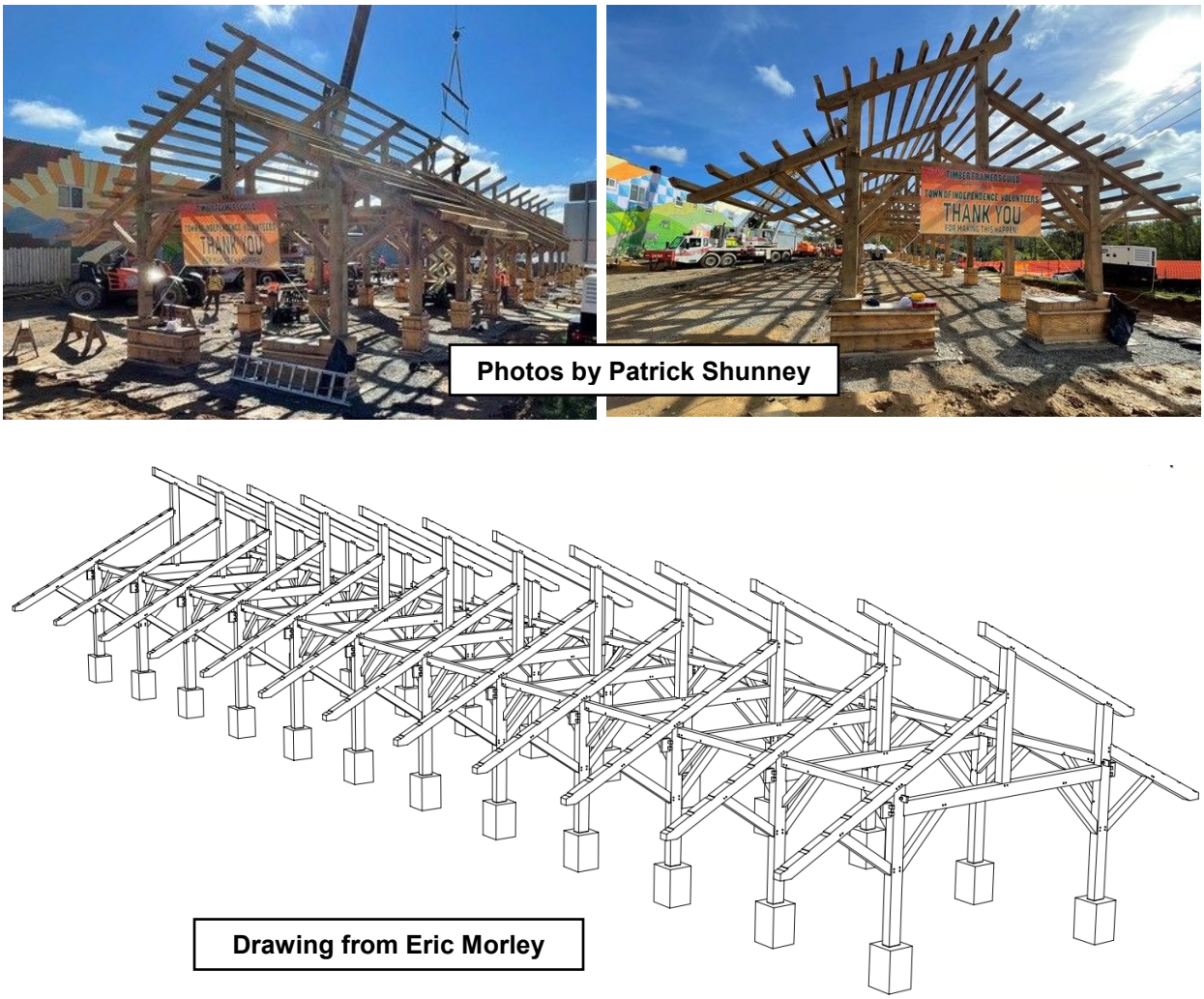

Fig. 5.40. Independence Farmers Market pavilion in Independence, Virginia.

The vibration test was conducted in November, 2021. Fig. 5.41 illustrates the field test. As was the case with other large timber frames, the fundamental period of vibration was difficult to clearly identify. For this pavilion, the period varied from 0.3 sec., 0.25 sec., and 0.18 sec. For comparison, the computed period of vibration for the structural model was 0.24 sec. (Fig. 5.42). The modal damping was 3% to 4% (Fig. 5.43).

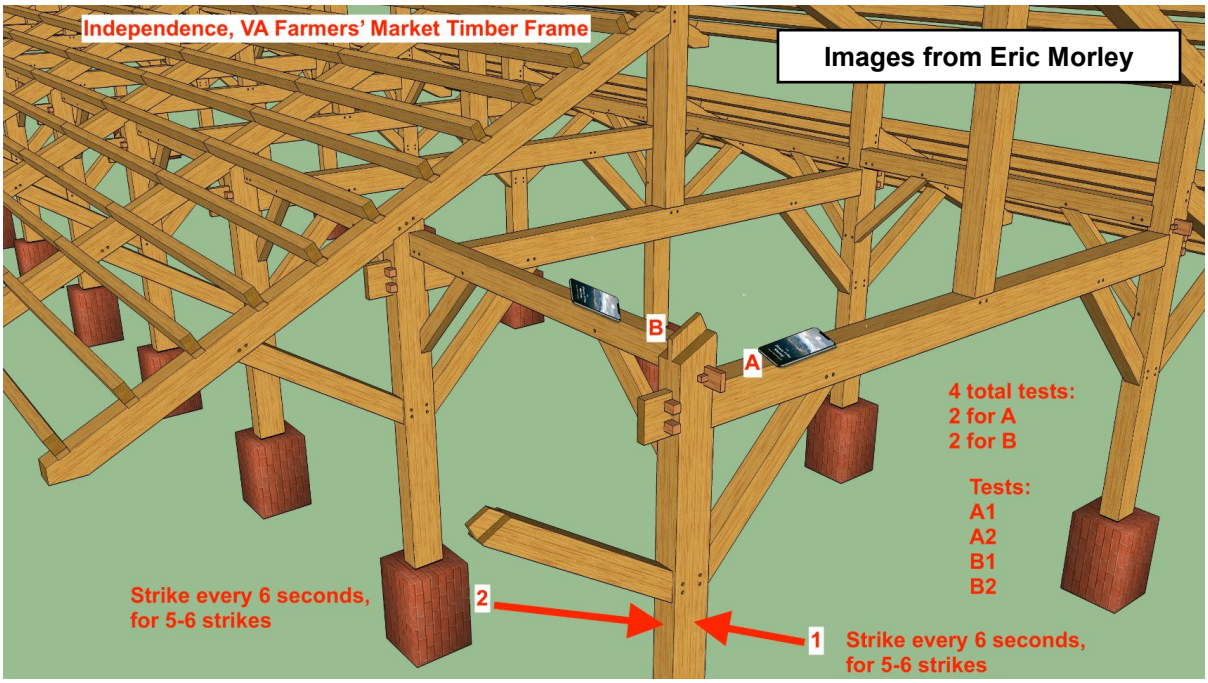

(a) Orientation of smartphone and test sequence

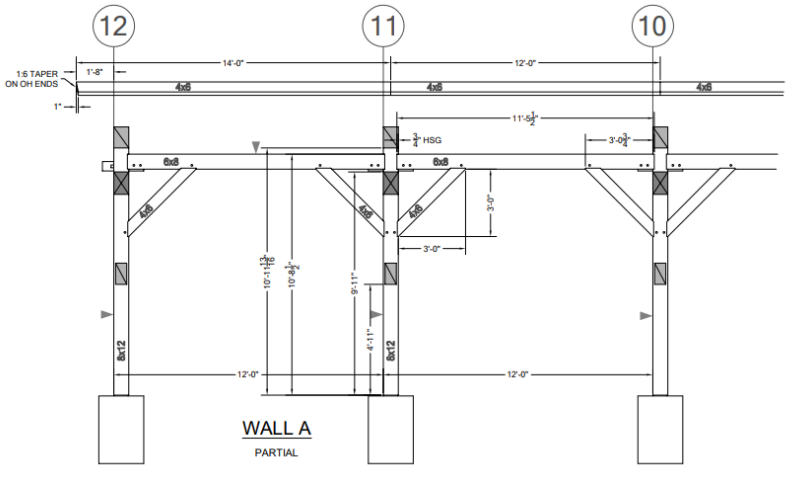

(b) Elevation drawing

(c) Hammer strike

Fig. 5.41. Independence Farmers Market pavilion field test.

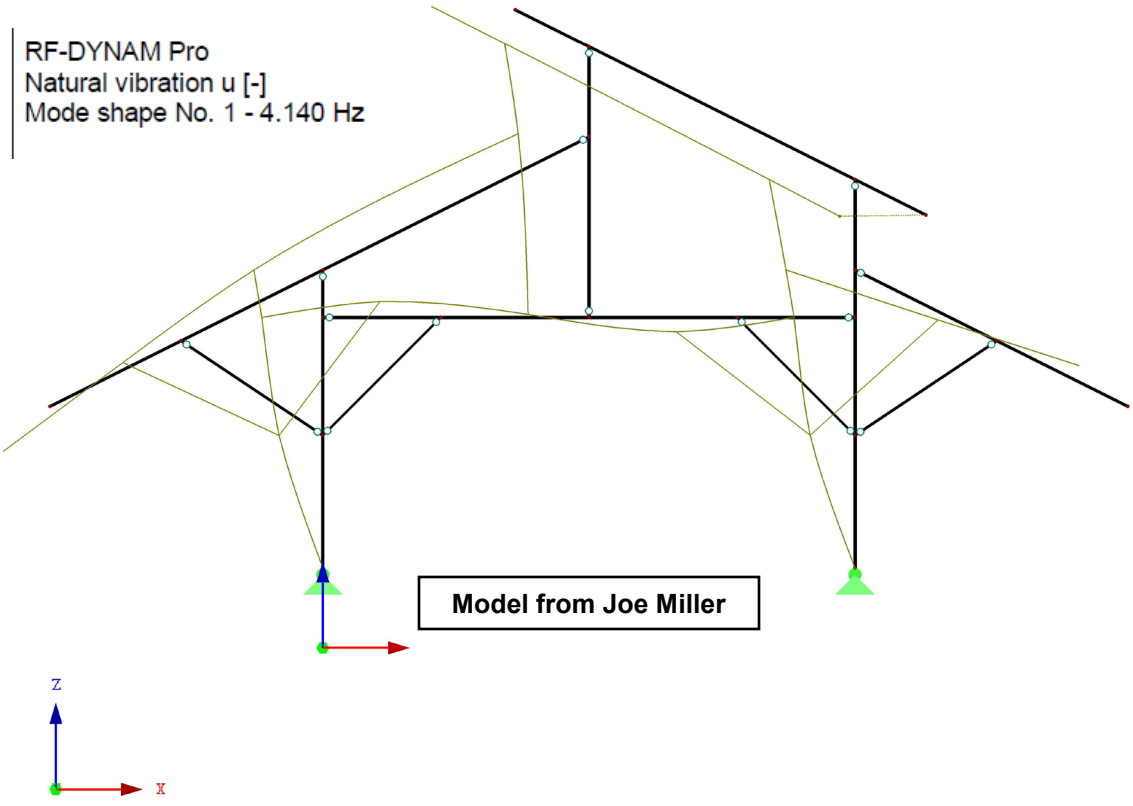

Fig. 5.42. Mode shape of structural model of Independence Farmers Market pavilion.

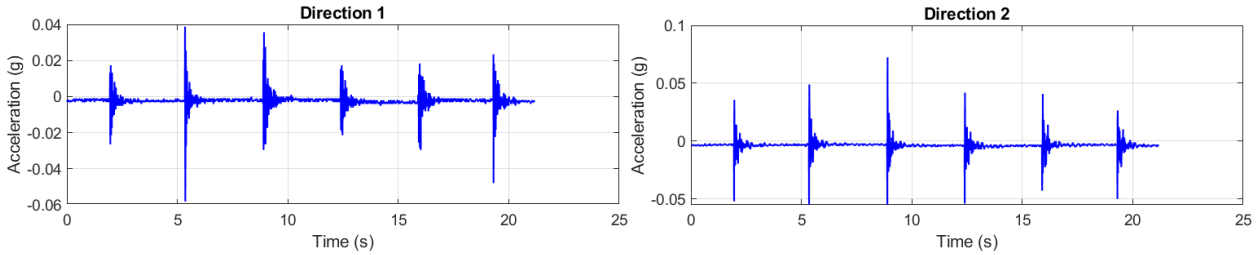

(a) Acceleration history

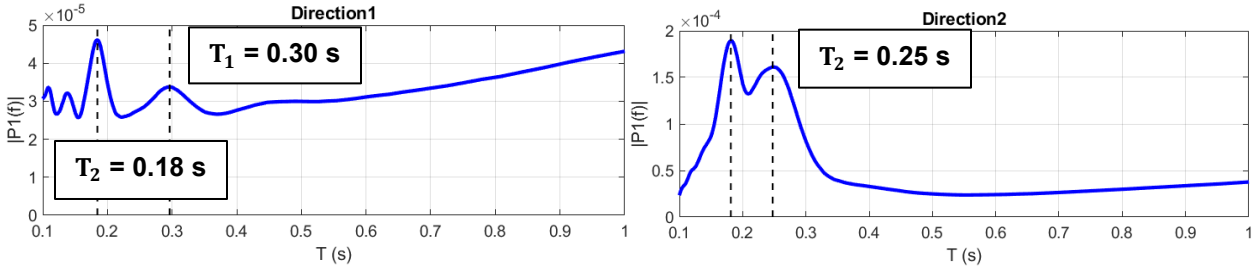

(b) Single-sided amplitude spectrum of period-content.

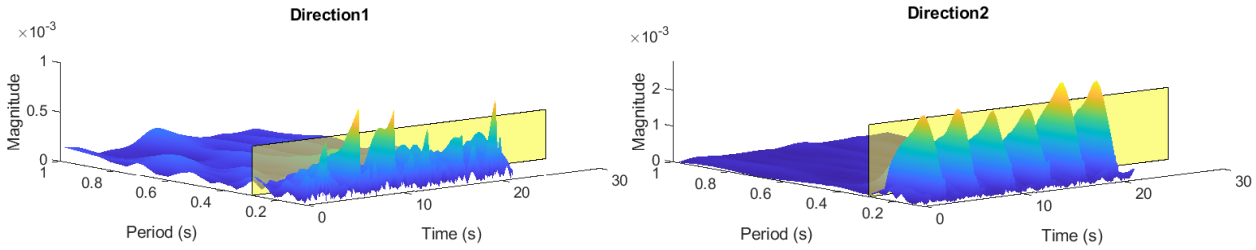

(c) Amplitude of period content versus time.

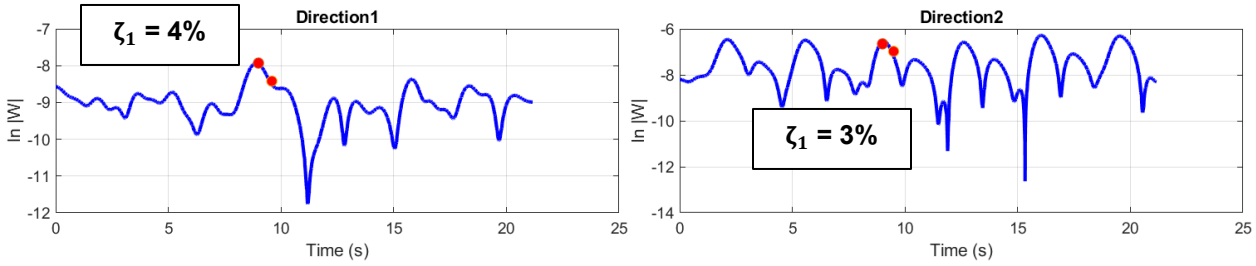

(d) Wavelet amplitude at fundamental period of vibration.

Fig. 5.43. Example frequency analysis of the Independence Farmers Market pavilion.

5.3.12 Sunflower Meadows pavilion (Newton, North Carolina)

The Sunflower Meadows pavilion is a 60-ft long by 30-ft wide free-standing timber frame in Newton, North Carolina (Fig. 5.44). The mean roof height is approximately 16 ft. The timber frame was made using White Oak. The posts are connected to the concrete slab below, and it spans across six posts longitudinally.

The vibration test was conducted in March, 2022 (Fig. 5.45). As was the case with other large timber frames, the fundamental period of vibration was difficult to clearly identify. For this pavilion, the fundamental periods were 0.48 sec. and 0.21 sec. For comparison, the computed period of vibration of the structural model was 1.26 sec. for the primary axis (Fig. 5.46), 0.57 sec. for mode 17, and 0.28 for mode 20. The modal damping was 3% to 4% (Fig. 5.47).

Fig. 5.44. Sunflowers Meadows pavilion in Newton, North Carolina.

Fig. 5.45. Sunflower Meadows Pavilion field test.

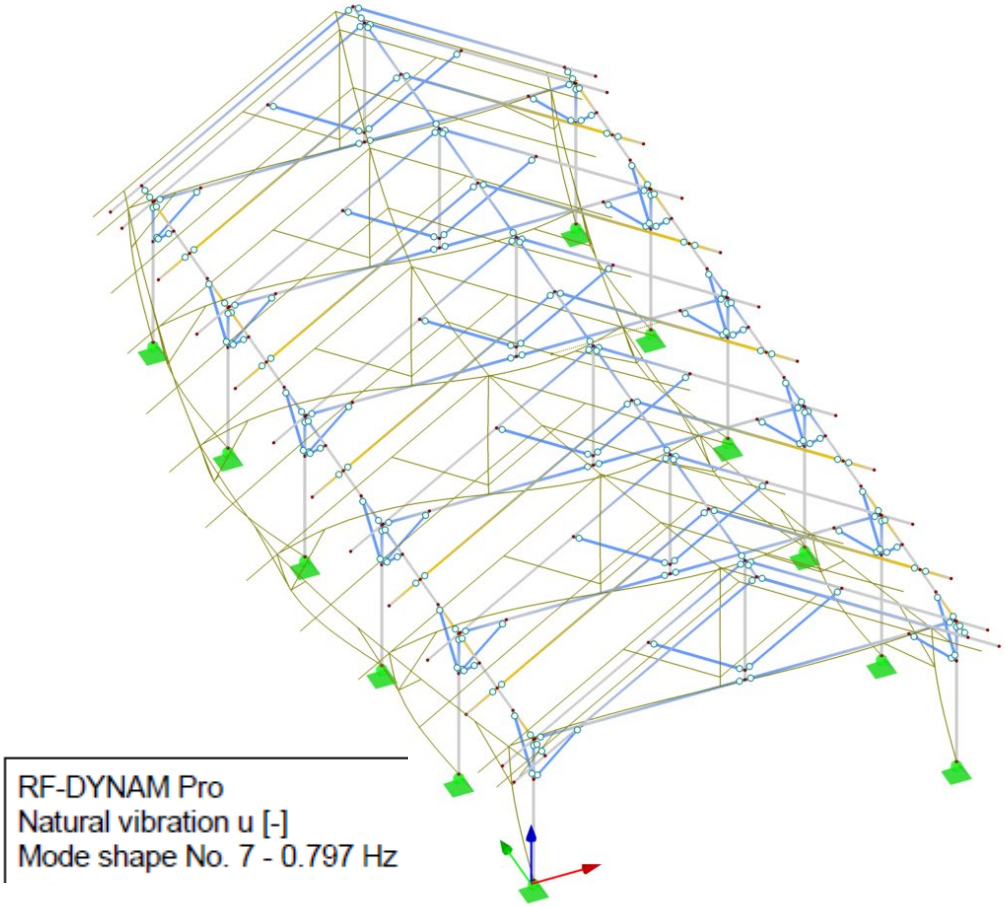

Fig. 5.46. Mode shape of structural model of Sunflower Meadows Pavilion.

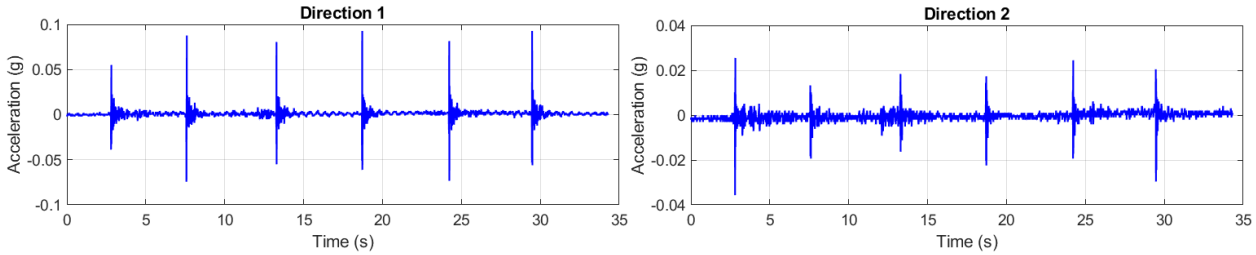

(a) Acceleration history

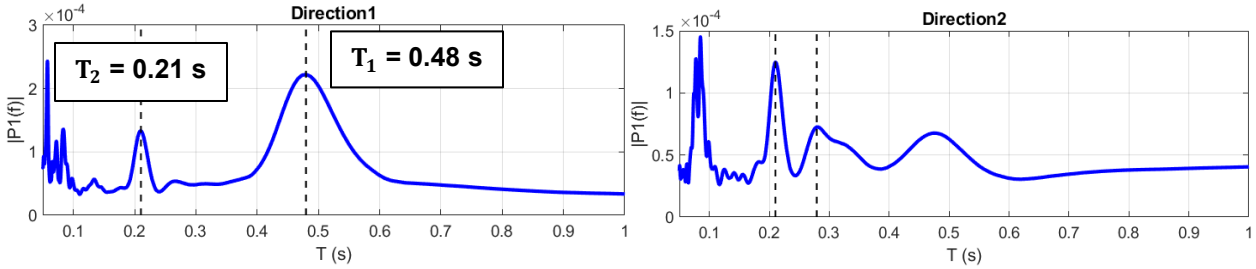

(b) Single-sided amplitude spectrum of period-content.

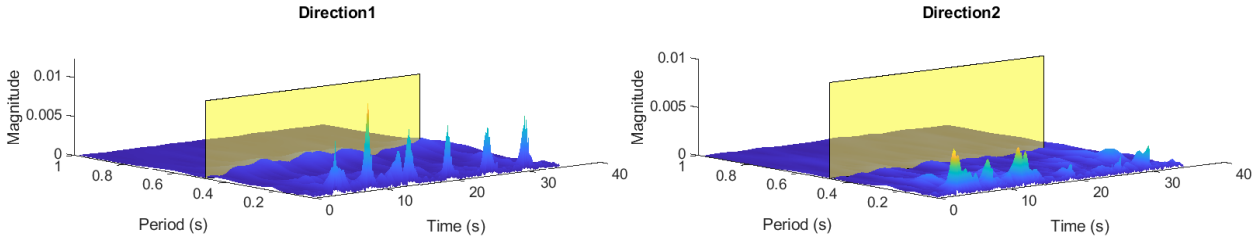

(c) Amplitude of period content versus time.

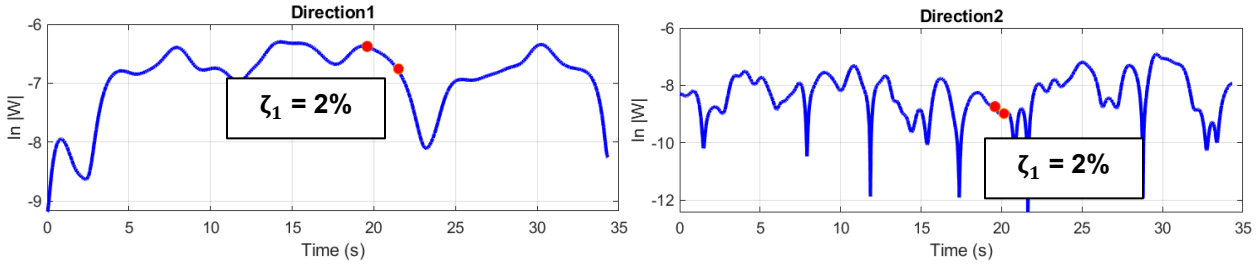

(d) Wavelet amplitude at fundamental period of vibration.

Fig. 5.47. Example frequency analysis of the Independence Farmers Market pavilion.

5.3 Fundamental Period of Vibration

The fundamental period of vibration and damping are essential parameters that can be used to estimate seismic loads and wind loads. For seismic loads, the fundamental period is used in ASCE 7 to determine the base shear using a response spectrum. For wind loads, the inverse of the fundamental period (the natural frequency) is used in ASCE 7 to determine dynamic wind effects via the gust effect factor. In addition to seismic and wind loads, the fundamental period is also useful to estimate loads for free-standing structures, such as climbing loads (e.g. during structural maintenance), and vandalism loads (e.g. human excitation of a structure).

In Fig. 5.48, the measured periods of vibration (sec.) is plotted against the mean roof height (ft). Each dot in the plot is a test data point. The data points show an increasing trend (taller timber frames generally correlate with longer periods), but there is no clear mathematical relationship.

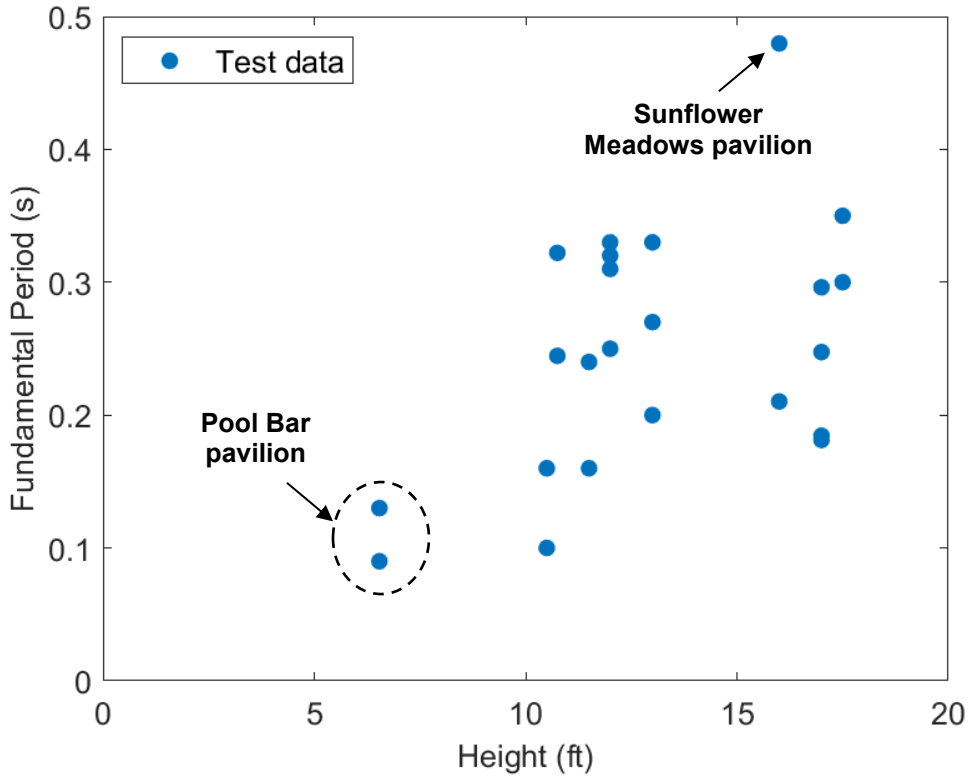

Fig. 5.48. Measured fundamental period of vibration versus mean roof height.

A regression analysis was used to better understand the relationship between the fundamental period of vibration and the mean roof height. In the literature, various equations for fundamental period have been proposed (e.g. Smith and Uang 2013, Bertero 2022). In ASCE 7, for steel and concrete buildings the approximate fundamental period of vibration (T_a) is estimated using a power function:

$$T_a = C_t h_n^x \quad \text{(Eq. 5.1)}$$

where C_t and x are regression parameters determined using ASCE 7 Table 12.8.2, and h_n is the mean roof height in feet. Eq. (5.1) and the corresponding regression parameters were based on vibration test data of instrumented steel and concrete buildings in southern California (Goel and Chopra 1997). Based on the test data, either a linear or a power function could provide a good fit for free-standing timber frames. The power function was chosen for this study.

For timber frames, the parameters for Eq. (5.1) were determined using the following process. First, a random set of positive parameters were selected. Second, the sum of the squared errors between a test data point and the curve fit was computed. Third, the parameters were then adjusted to minimize the sum of the squared errors. This produced the "best" parameters for the mean curve fit. However, for seismic design the parameters in ASCE 7 correspond to the mean minus one standard deviation ("the lower bound" curve). Therefore, the curve fitting process was repeated by fitting the points for the mean minus one-standard deviation curve. Similarly, for wind design the parameters in ASCE 7 correspond to the mean plus one standard deviation (the "upper bound" curve), and a third set of parameters was fit to the mean plus one standard deviation. The resulting parameters are shown in Fig. 5.49. For reference, the ASCE 7 curve fit for typical buildings is also shown. The measured fundamental period was generally longer compared to the values using the ASCE 7 equation.

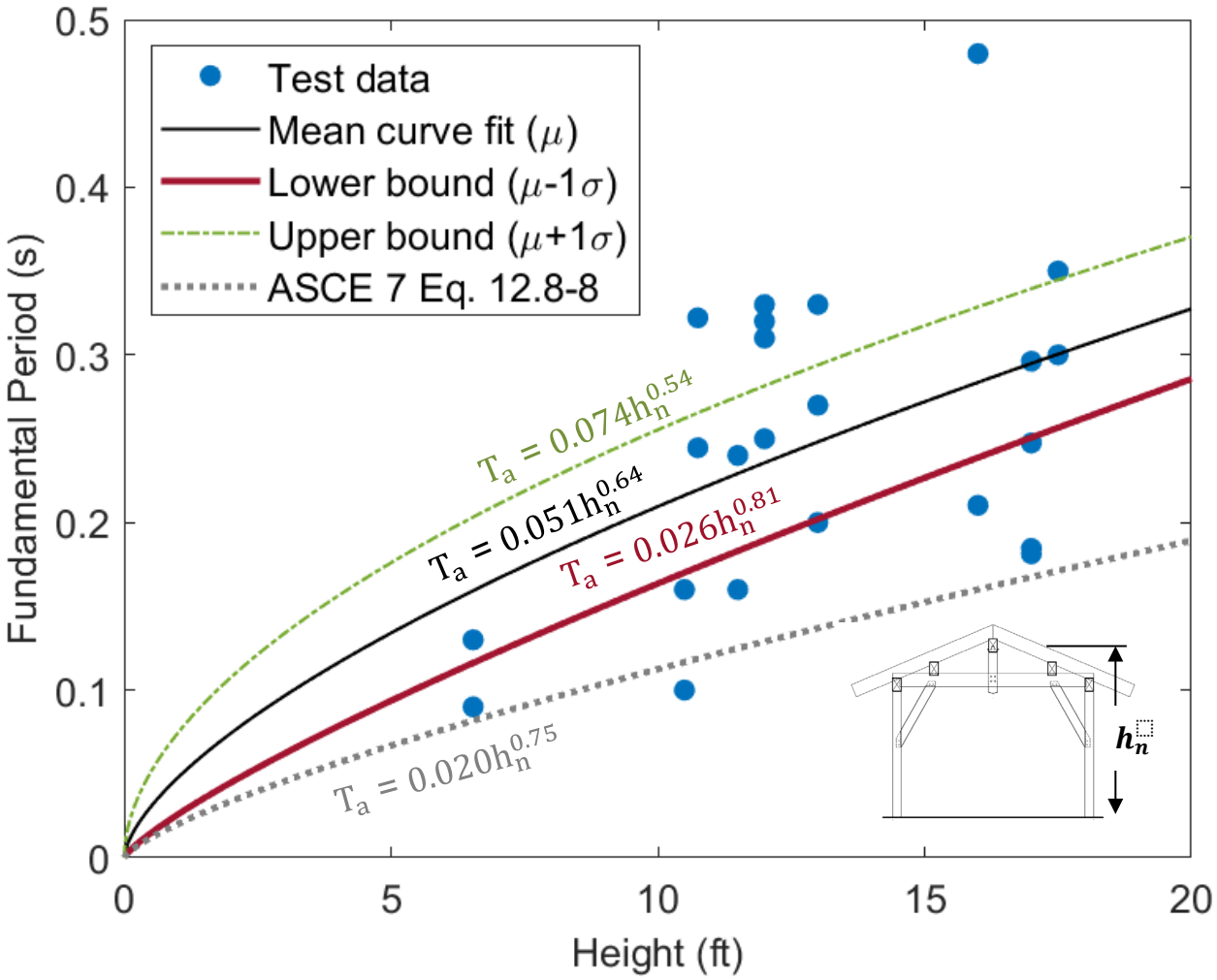

Fig. 5.49. Fundamental period of vibration versus mean roof height.

In general, the plot shows that the power function curve fit provides a reasonable approximation to the test data, especially considering the scatter in the test data. Previous research shows that the fundamental period of vibration measured in a test depends on the amplitude of the vibration (Skolnik et al. 2006). Low-amplitude vibrations, such as those from ambient sources, lead to shorter periods, whereas high-amplitude vibrations lead to relatively longer periods. In other words, larger structures require higher-amplitude vibrations to determine the period of vibration. Therefore, the approach to vibration tests used in this study are not appropriate for determining the fundamental period of buildings or larger structures.

5.4 Modal Damping

In Fig. 5.50, the measured estimate of modal damping is plotted against the mean roof height (ft). Each dot in the plot is a test data point. The data points show an increasing trend (taller timber frames generally correlate with increased damping), but as was the case with the fundamental period of vibration, there is no clear mathematical relationship. The damping varied between 1% and 10%, with 2% being the mostly common value. Therefore, based on the data the damping in a bare-frame model of a free-standing timber frame with knee braces can be taken as 2% for low-amplitude excitation, unless there is significant cladding or other building components that would contribute additional damping.

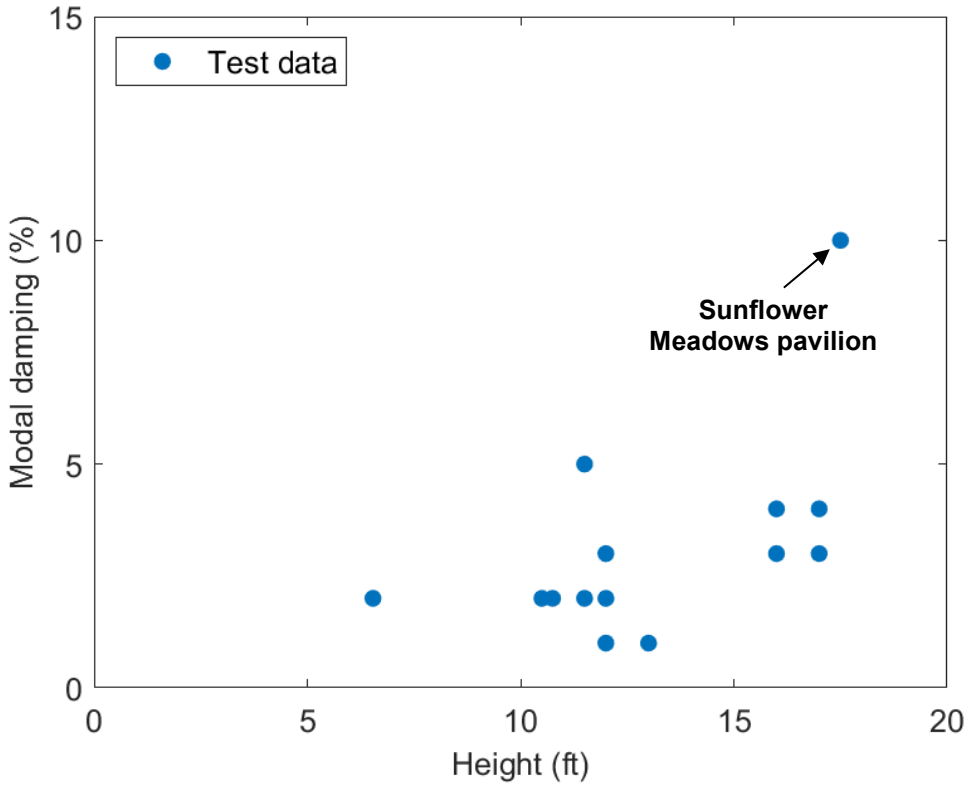

Fig. 5.50. Modal damping versus mean roof height.

To understand the impact of damping on human induced excitation on free-standing timber frames, such excitation caused by climbing on the frame for maintenance, or excitation caused by vandalism (e.g. teenagers rocking the frame), in Fig. 5.51 the dynamic magnification factor (DMF) for displacement (R_d) for single-degree-of-freedom (SDOF) system is plotted versus the ratio of the forcing frequency (Ω) to the system's fundamental frequency (ω_n). The response is shown for two levels of damping, 2% and 10%. The plot shows that the equivalent elastic force (F) would be 5 to 25 times the static elastic force ($k\,\Delta_{st}$). If the static force is taken as the "crowd" force of 50 lb/ft defined in ASCE 7 Section 4.5.1.1, the corresponding design force would be 250 lb/ft to 1250 lb/ft. The mean curve fit for the period of vibration, determined previously, could be used in computing the frequency ratio for this purpose.

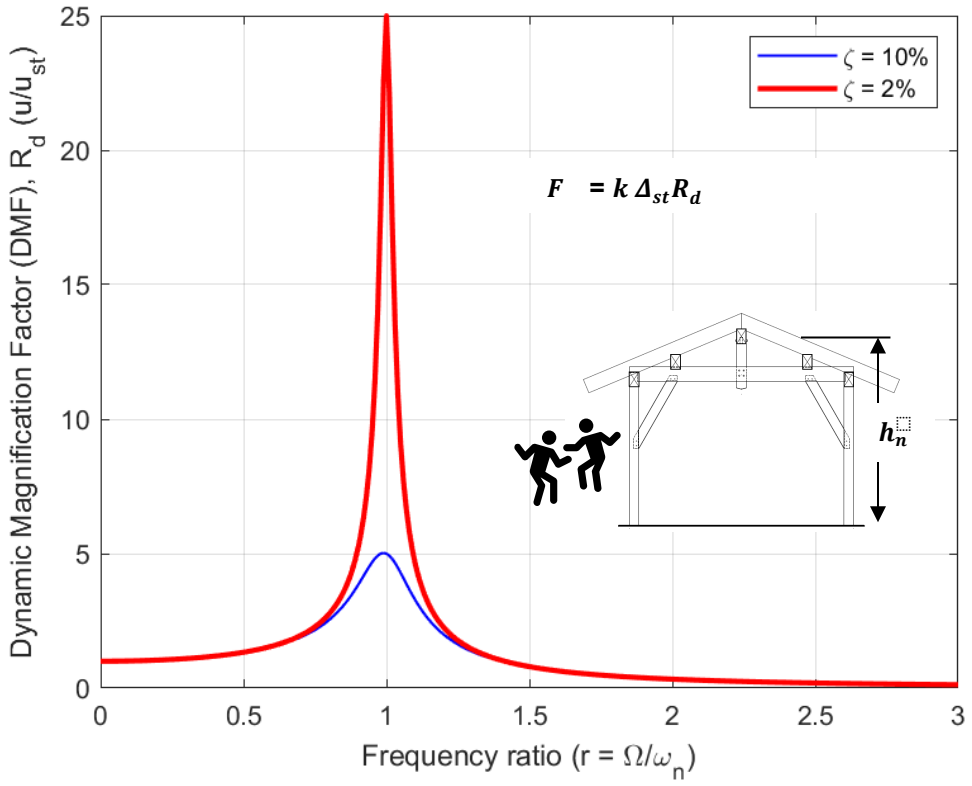

Fig. 5.51. Dynamic magnification factor for a SDOF system versus frequency ratio.

5.5 Summary

Twelve free-standing timber frames with knee braces, located at various sites across the United States, were tested in the field to determine their fundamental period of vibration and to estimate the corresponding modal damping. A relationship between the mean roof height of the timber frame and the fundamental period was fit to the test data using a power-law equation, similar to the approach used in ASCE 7 for steel, concrete, and masonry structures. The parameters for the equation were determined using a regression analysis. Three sets of parameters were determined: a lower-bound equation for seismic loads, an upper-bound equation for wind loads, and mean equation for human-induced vibration performance criteria:

- For seismic, $T_a = 0.026\ h^{0.81}$ for $h \leq 20$ ft is recommended. The upper bound coefficient, C_u is determined using ASCE 7 Table 12.8-1.
- For wind, $n_a = 13.5/\ h^{0.54}$ for $h \leq 20$ ft is recommended, where n_a is the natural frequency (Hz).
- For climbing/vandalism, it is suggested to use $T_a = 0.051\ h^{0.64}$ and 2% damping for a bare frame, 10% damping for an enveloped frame.

The curve fits are intended for smaller timber frames, and they may not be appropriate for larger structures. In the next chapter, an approach to life cycle analysis for timber frames and performance assessment is discussed.

CHAPTER 6 LIFE-CYCLE ANALYSIS AND FRAGILITY CURVES

This chapter describes the life-cycle analysis and presents component fragility curves. A life-cycle analysis was used to determine the embodied carbon and the damage states for knee-brace connection. Component fragilities for performance assessment were established based on data from a survey of practicing timber framers.

6.1 Life Cycle Analysis

Regarding the environmental consequences of the failure modes, values for the embodied carbon and embodied energy of wood were found. It was assumed that the wood type was Douglas-fir, which is about 50.5% carbon (Lamlom and Savidge 2003). There isn't significant variance in this value for other types of softwood commonly used in timber frame construction.

The Bag Corral pavilion described in Chapter 5 (see Fig. 5.28) was used for an example life cycle analysis. For the Bag Corral timber frame, the mass of wood needed to repair the various failure was calculated and multiplied by 50.5% to get the mass of carbon in the wood. Carbon emissions in production and transportation of wood were not included in the embodied carbon calculations. Wood has an embodied energy of about 2.4 MJ/kg (Lenzen and Treloar 2002), and

this was multiplied by the same weight as the percent carbon to get the embodied energy of the wood used in each repair.

As for the post failure mode that uses steel self-tapping screws to repair the split post, MTC Solutions was contacted to get a quote for 25 screws, the minimum quantity they sell, which was $103.44 including tax. This is similar to the cost of a brace, so the cost of repairing the brace was also used for repairing the post because the values included labor costs. Steel has an embodied energy of around 40 MJ/kg (Menzies et al. 2007). The screws used are made of hardened steel, which hast a density of 7750 kg/m^3 and high-carbon steel is around 0.61-1.5% carbon (AmesWEB 2022). To be conservative, 1.5% carbon was assumed. According to world counts, producing one ton of steel produces 1.83 tons of carbon dioxide. CO_2 is 27.27% carbon. This information was used to calculate the carbon emissions produced and embodied energy of the screws.

6.2 Component Fragilities

The FEMA P-58 methodology (FEMA 2018a) was applied to timber frames to predict performance (repair costs, repair time, the probability of unsafe placarding, and the embodied carbon) during the life-cycle of the structure. PACT software (FEMA 2018b) was used to develop component fragilities that could be used to perform a life-cycle analysis of a free-standing timber frame or on their own to predict how a structure will perform under various lateral loads. Parts of this process included gathering test and survey data to determine failure modes and repair measures, synthesizing this data to find usable values, and creating new fragilities to simulate various failure modes based on those values.

Tests showed that the main failure modes for a free-standing timber frame included peg shear, tenon plug shear, and post splitting. Fragilities were developed around these failures as well as failure requiring the replacement of timber frame bay. Fragilities include the cost to repair, time to repair, and environmental consequences of repairing the damaged frame element. At the Timber Frame Engineering Council 2022 Symposium, a survey was carried out to gather information on the monetary and time costs to repair a peg, a brace, and a bay.

Engineers and builders who completed the survey were from various locations in the United States and Canada. Fig. 6.1 shows the variety of areas represented on a map. Due to the wide range of professionals and geographic areas, the information gathered was useful in creating widely applicable fragilities. The data collected in the survey is summarized in Table 6.1.

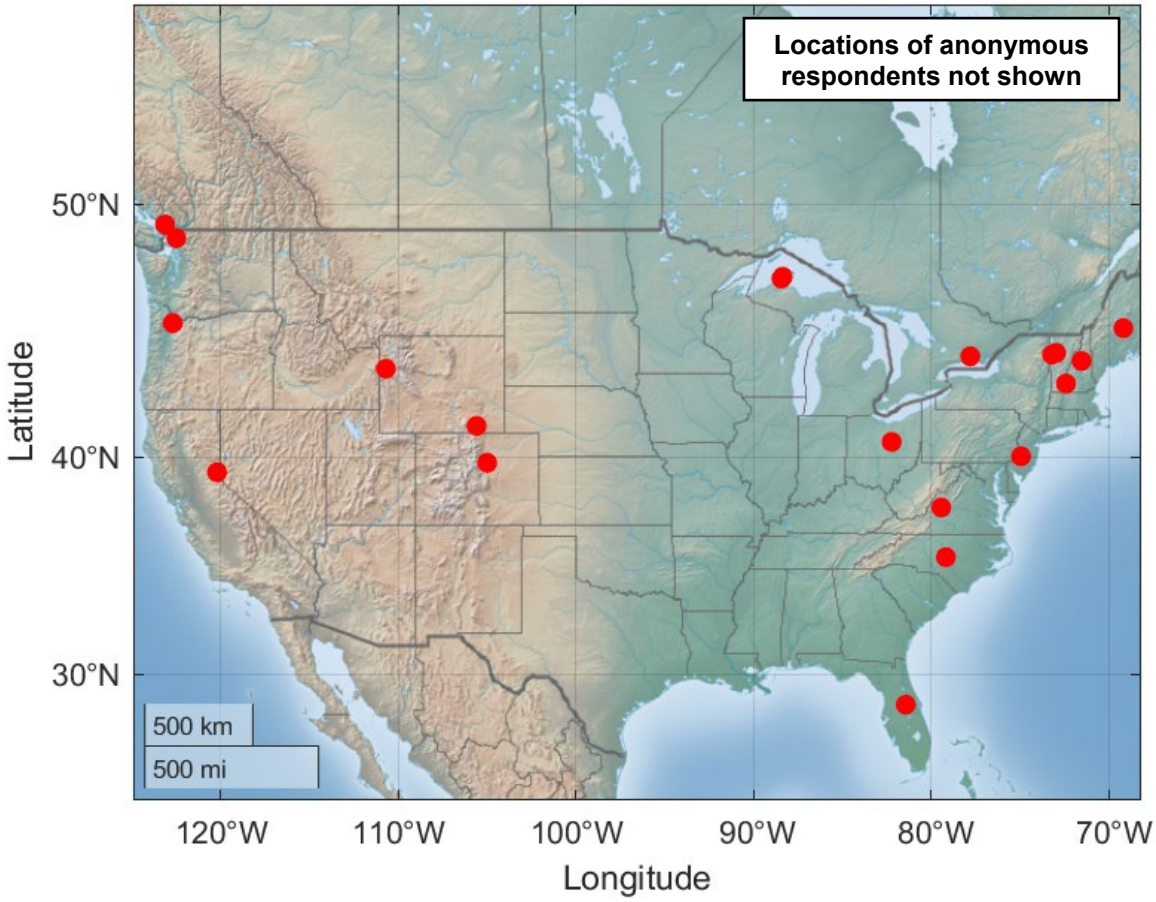

Fig. 6.1. Home locations of respondents in the survey.

Since some respondents included travel costs in their estimates and others did not, the following four component fragilities were developed (letter/number sequence is the PACT ID, where "B" is for the superstructure and shell, and 107 is for wood structures.):

- B1071.032 – Timber frame bay (travel not included)
- B1071.033 – Single-sided knee brace (travel not included)
- B1071.034 - Single-sided knee brace (travel included)
- B1071.35 – Timber frame bay (travel included).

Table 6.1 Survey data (Timber Frame Engineering Council 2022 Symposium).

	Cost ($)			Time (days)		
Respondent	Peg	Brace	TF (/bay)	Peg	Brace	TF (/bay)
1	$ 25.00	$ 500.00	$ 5,000.00	0.013889	1	30
2	$ 50.00	$ 3,750.00	$20,000.00	1	60	180
3	$ 10.00	$ 100.00	$10,000.00	0.006944	0.041667	7
4	$ 10.00	$ 250.00	$ 3,500.00	0.006944	0.020833	2
5	$ 100.00	$ 500.00	$ 3,000.00	7	14	60
6	$ 100.00	$ 2,300.00	---	0.013889	1	---
7	$ 31.64	$ 450.00	$18,900.00	0.013889	0.208333	---
8	---	---	---	2	5	14
9	$ 5.00	$ 500.00	$50,000.00	0.041667	1	7
10	$ 5.00	$ 250.00	$15,000.00	0.020833	0.125	21
11	$ 50.00	$ 2,000.00	$10,000.00	0.333333	14	180
12	$ 337.00	$ 410.00	$ 5,000.00	0.020833	0.041667	4
13	---	---	---	1	2	5
14	$ 200.00	$ 2,000.00	$25,000.00	0.25	1	3
15	$ 750.00	$ 3,250.00	$75,000.00	0.002083	0.166667	21
16	$ 40.00	$ 225.00	$ 5,500.00			
17	$ 500.00	$ 3,000.00	$22,500.00	1	7	45
18	$ 500.00	$ 1,500.00		7	21	75
19	$ 2.00	$ 1,000.00	$ 320.00	0.003472	0.5	7
19	$2,000.00	$30,000.00		0.041667	7	30
20	---	---	---	---	---	---
21	$ 30.00	$ 500.00	$ 1,000.00	1	1	3
22	$ 310.00	$ 550.00	$20,000.00	1	1	4
23	$1,517.50	$ 1,650.00	$20,000.00	---	---	---
24	$1,000.00	$ 5,000.00	$15,000.00	14	35	180
25	$1,000.00	$ 2,000.00	$10,000.00	7	14	28

Respondents also had the opportunity to give a description of repair measures. The component fragilities and corresponding damage states and repair descriptions based on their responses are described in Table 6.2. Averages of the estimated repair times and repair costs for each failure mode were used in the fragilities along with the coefficient of variation each data set.

Histograms of the survey data are shown in Fig. 6.2 through Fig. 6.7 to better understand the distribution of estimated repair costs and time for pegs (Fig. 6.2 and Fig. 6.3), braces (Fig. 6.4 and Fig. 6.5), and frames (Fig. 6.6 and Fig. 6.7). Two histograms are shown in each figure, one with travel included in the estimate of cost and time, and one without.

The component fragilities can be used in PACT to predict consequences (in terms of cost and time) for a given level of lateral force on the timber frame. Each damage state has a corresponding drift ratio at which failure occurs, and based on the drift created by an intensity, certain components fail. PACT enables engineers and builders to project how their structure will perform over time and how costly repairs are likely to be.

Table 6.2 Fragilities and corresponding damage states and repair descriptions.

Fragility ID	Damage State(s)	Repair Description
B1071.033 & B1071.034	1) Peg shear in brace connection	Shore member, drive out old peg, drive in new peg.
	2) Tenon plug shear	Shore member, remove old brace, cut new brace, disassemble frame enough to allow brace installation (if necessary), install new brace, insert block to support new brace (if necessary).
	3) Splitting of the post or beam	Rehabilitate members by clamping split member together, install layout of self-tapping scews, remove clamp.
B1071.032 & B1071.035	1) Failure of timber frame bay	Shore existing structure, disassemble damaged frame, cut new members and pegs as needed, assembed new bay, raise and fasten.

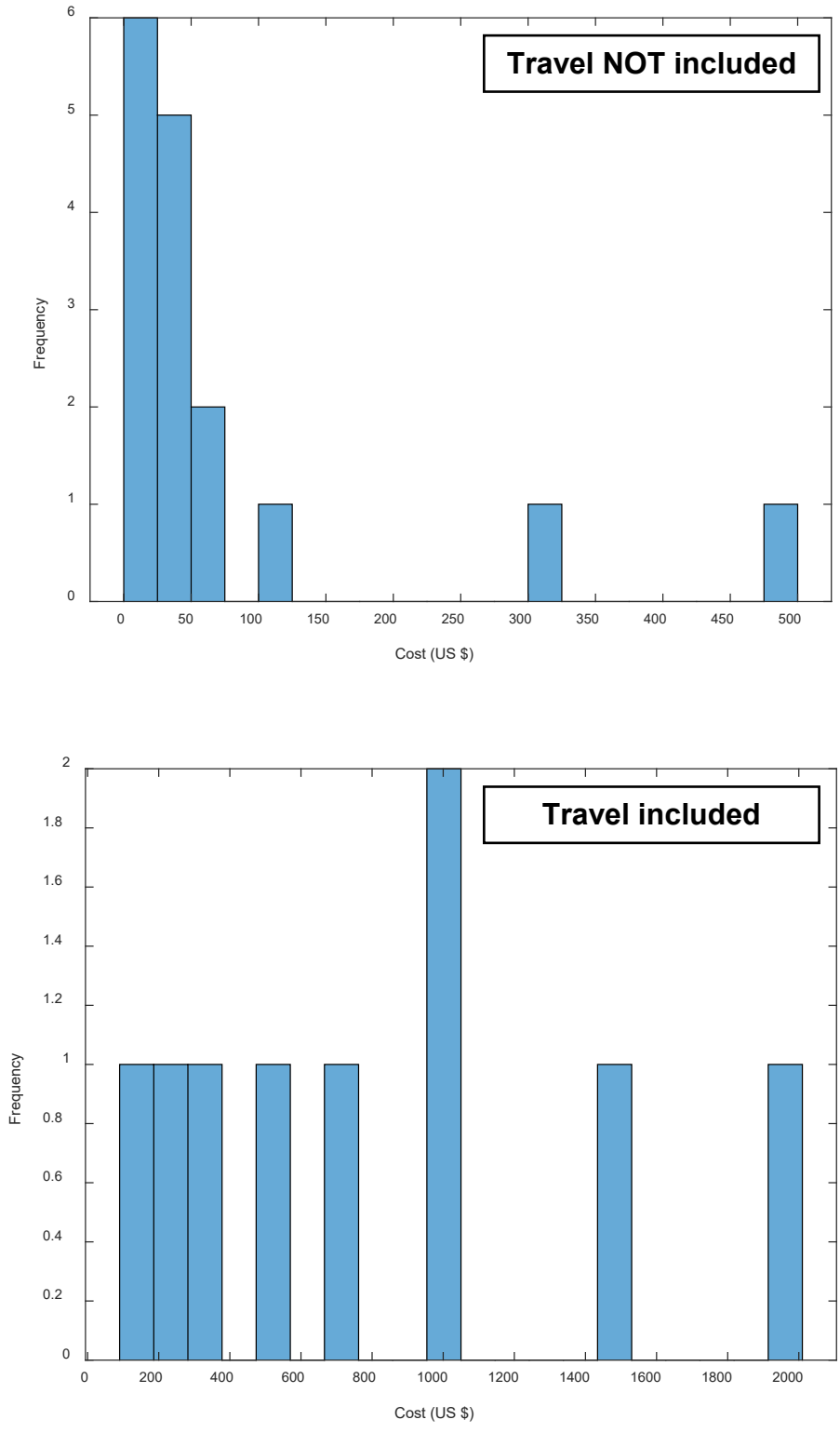

Fig. 6.2. Peg replacement cost.

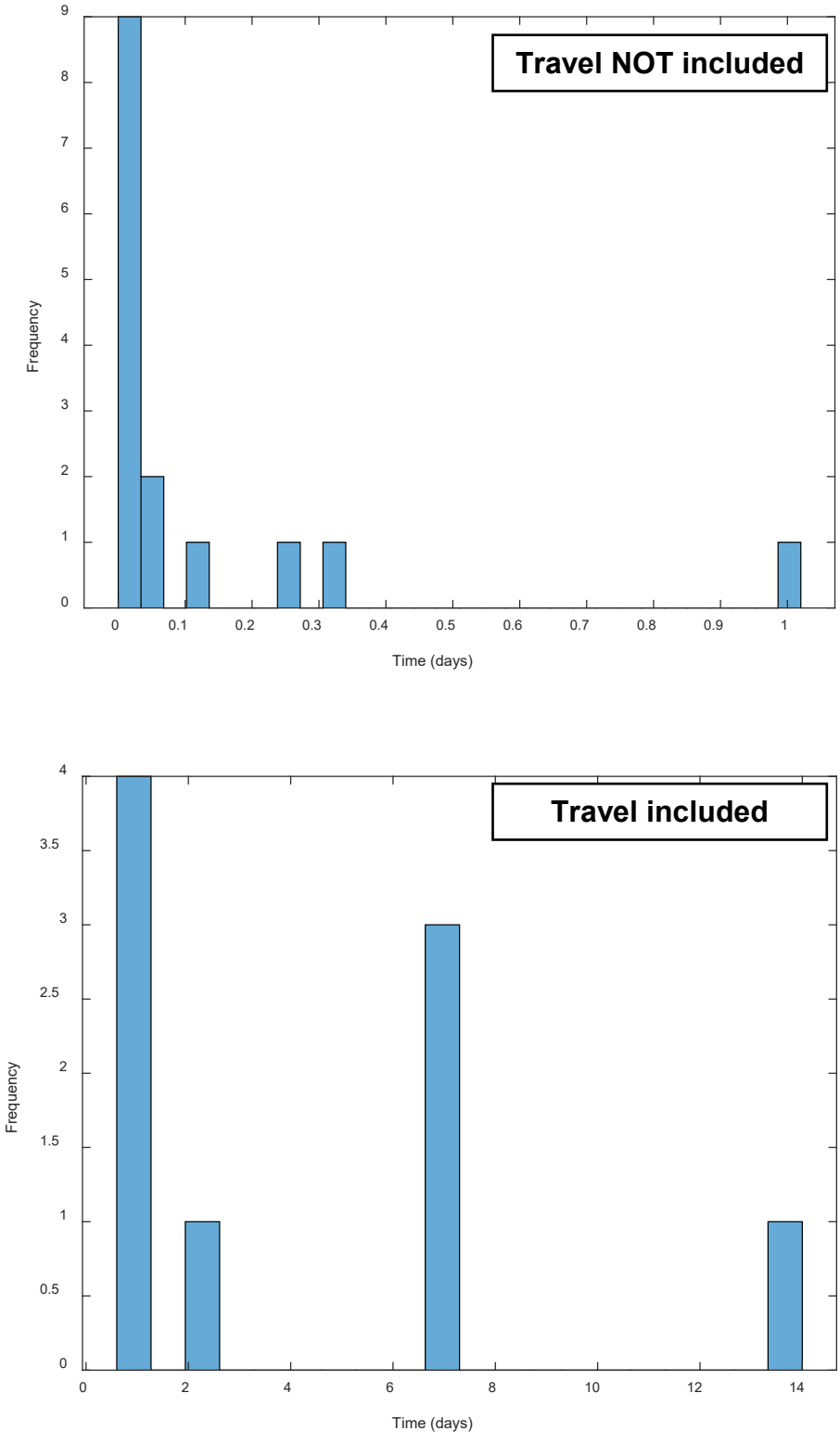

Fig. 6.3. Peg replacement time.

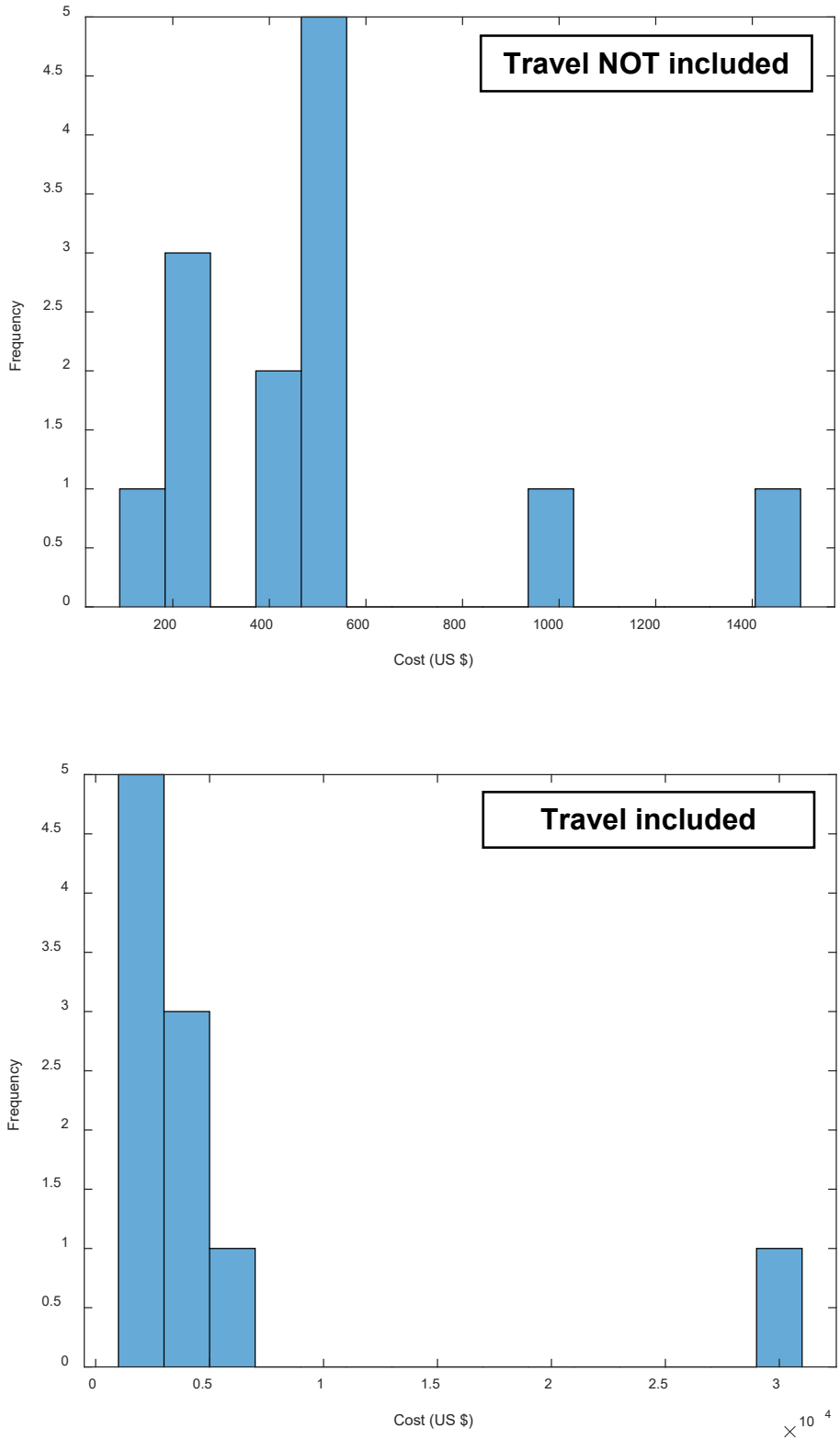

Fig. 6.4. Knee brace replacement cost.

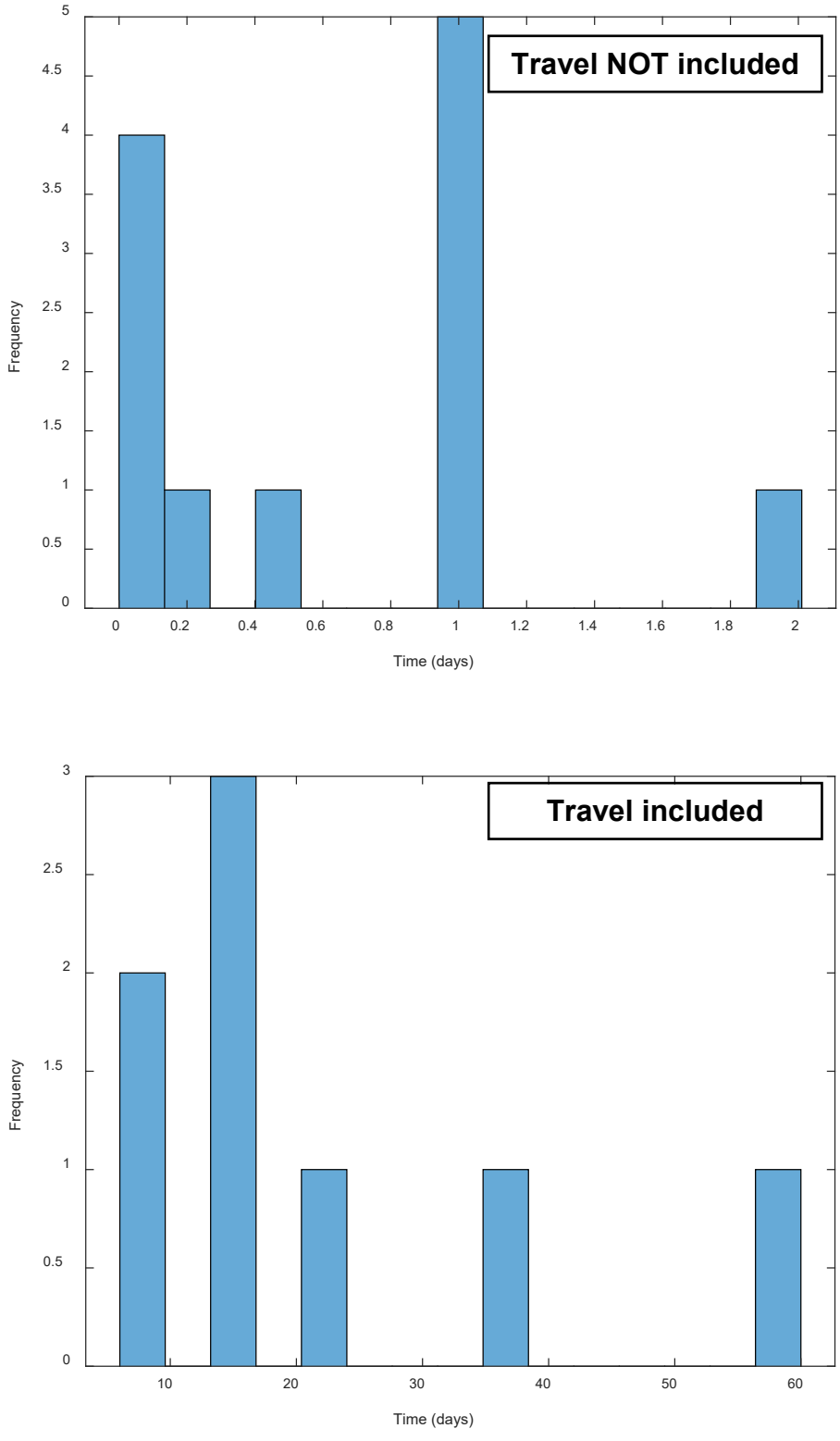

Fig. 6.5. Knee brace replacement time.

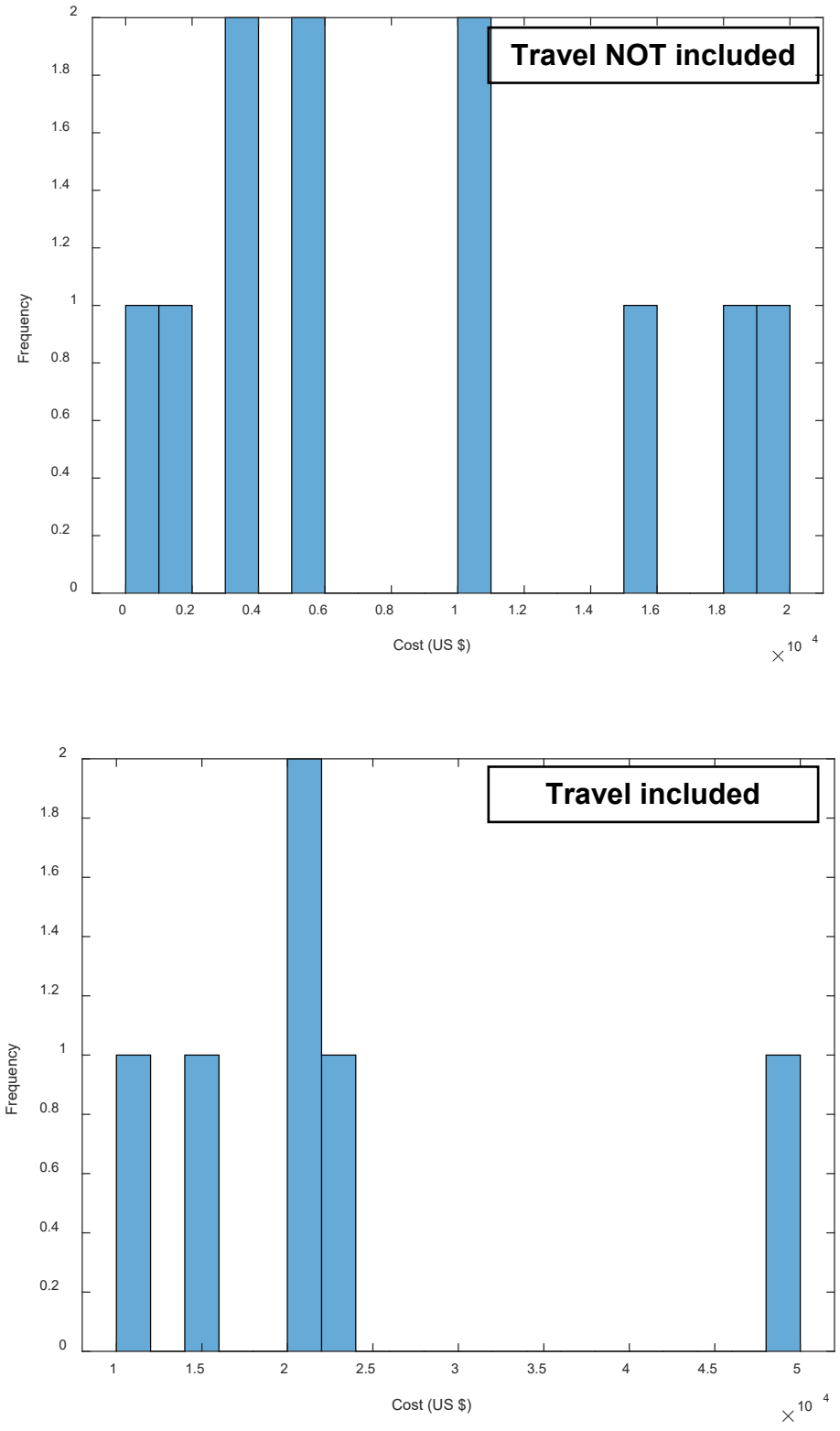

Fig. 6.6. Timber frame bay replacement cost.

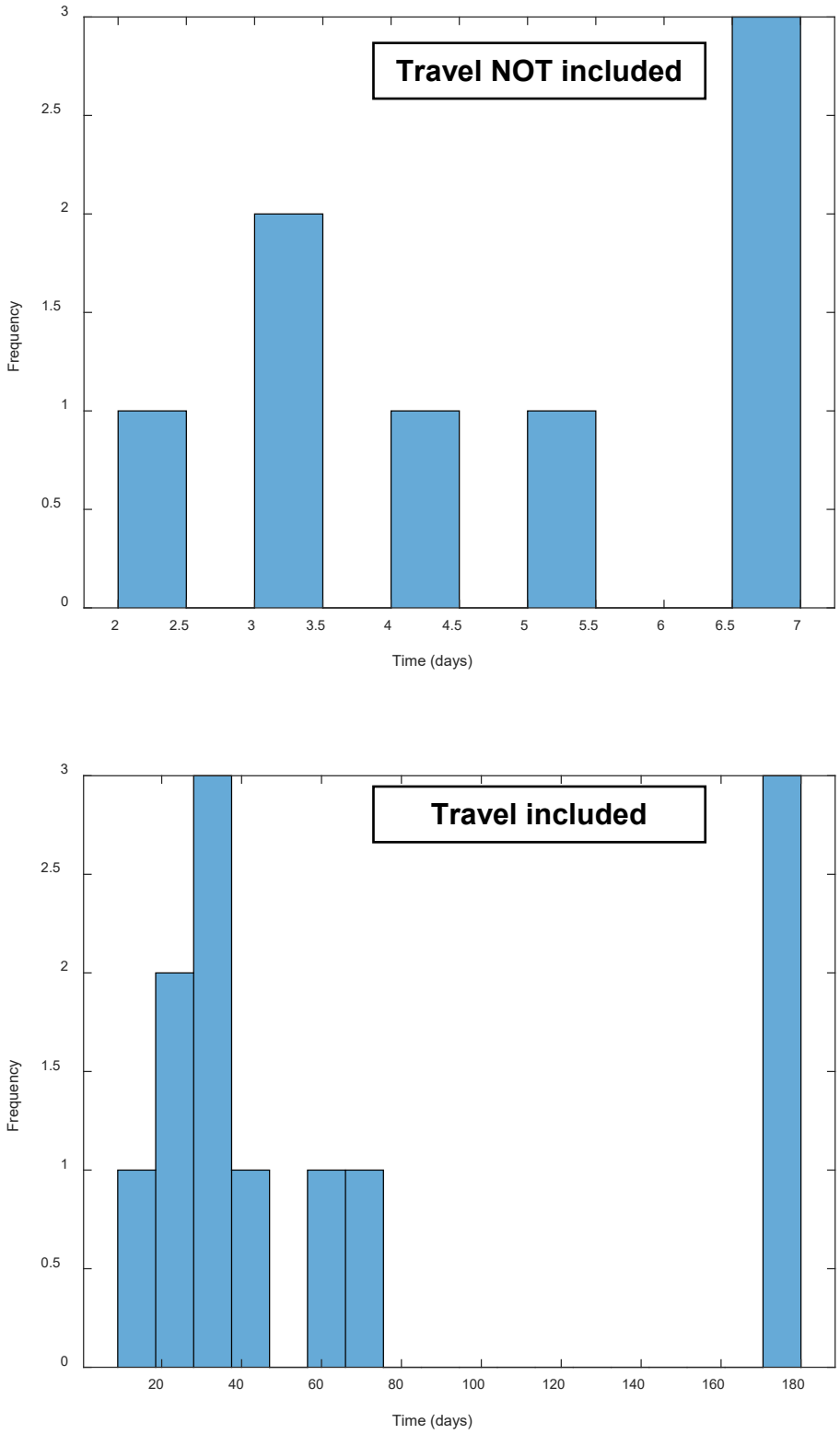

Fig. 6.7. Timber frame bay replacement time.

Fig. 6.8 through Fig. 6.11, show what fragility B1707.033 looks like, with a particular focus on the peg shear damage state. The other fragilities are similar in appearance and creation. Fig. 6.8 shows the main screen of B1071.033. The name of the fragility and description are found here, along with the demand parameter that the fragility corresponds to, which in this case is story drift. The fragility is directional because lateral forces could come from multiple directions and the direction could impact the outcome.

Fig. 6.9 shows the Damage State Type screen. This fragility is sequential because some of the damage states occur at lower drift ratios than others, as shown by the graph. Peg shear and tenon plug shear both occur at an average ratio of 0.02 radians, while posts and beams tend to crack around a drift ratio of 0.05 radians.

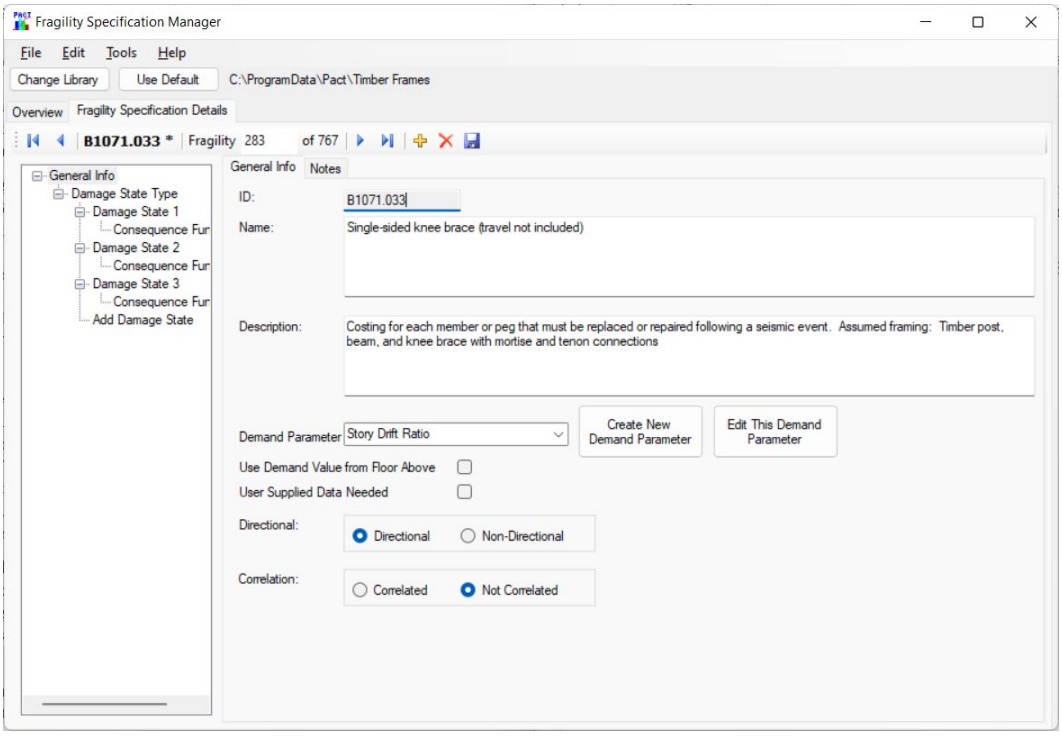

Fig. 6.8. Timber frame fragility B1071.033 general info.

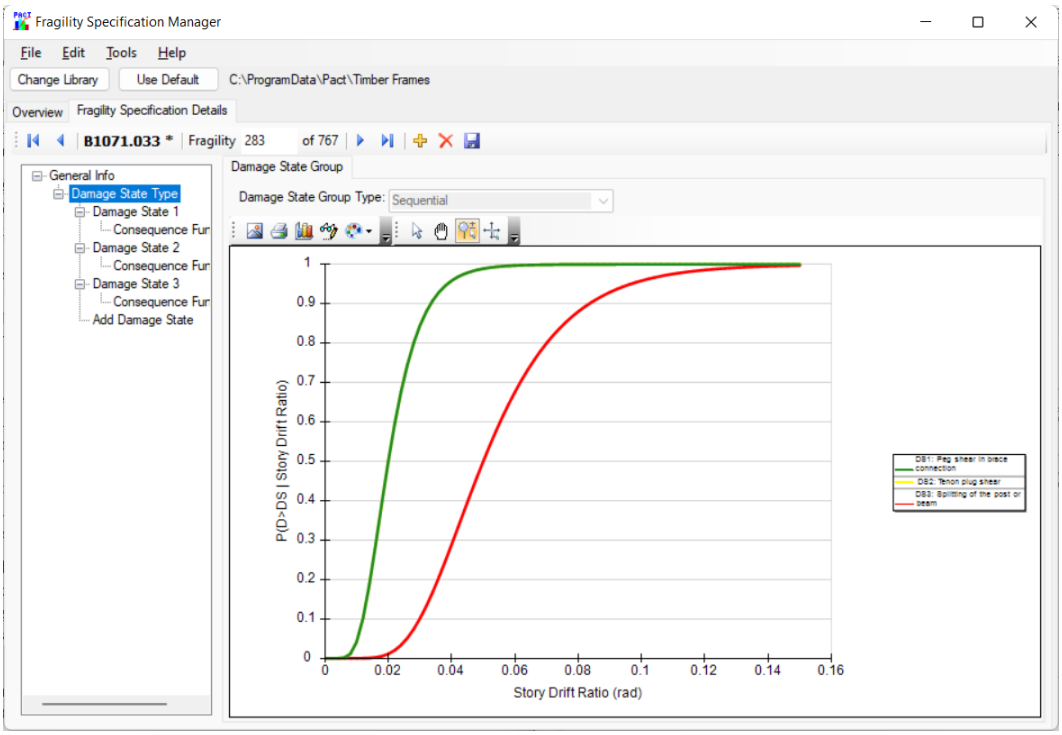

Fig. 6.9. Timber frame fragility B1071.033 Damage State group.

The screen shown by Fig. 6.10 gives an overview of the damage state as well as the drift ratio that failure occurs at. This value was taken from test data. There are four tabs under Consequence Functions. The first shows repair measures (Fig. 6.11), the second gives repair cost consequences (Fig. 6.12), the third gives repair time consequences (Fig. 6.13), and the fourth gives environmental and other consequences not covered in the second and third tabs (Fig. 6.14). Due to the relative simplicity of a free-standing timber frame, unsafe placard consequences and non-collapse casualties were not included in the fragility analysis. When a dispersion for a value was not known during the fragility creation process, a dispersion of 0.4 was assumed.

Table 6.3 compiles the standard deviation, coefficient of variation, and continuous probability distribution of each failure and consequence function shown by the histograms. These values can be used with the timber frame fragilities to predict behavior without requiring a PACT model.

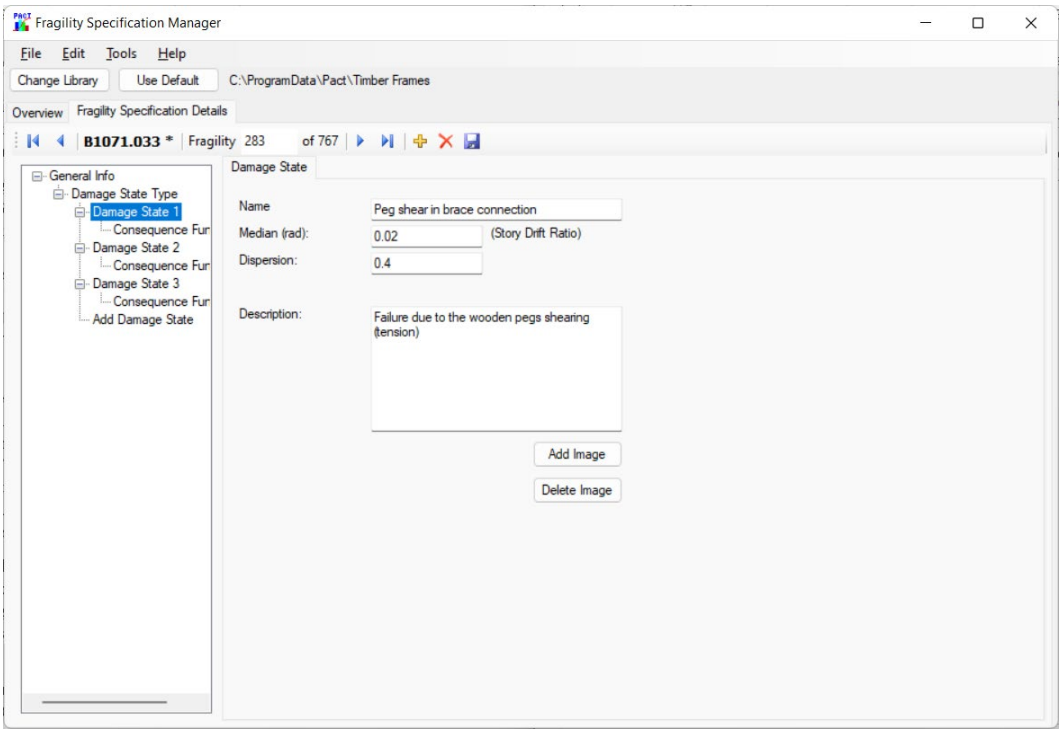

Fig. 6.10. Timber frame fragility B1071.033 Damage State 1 (peg shear).

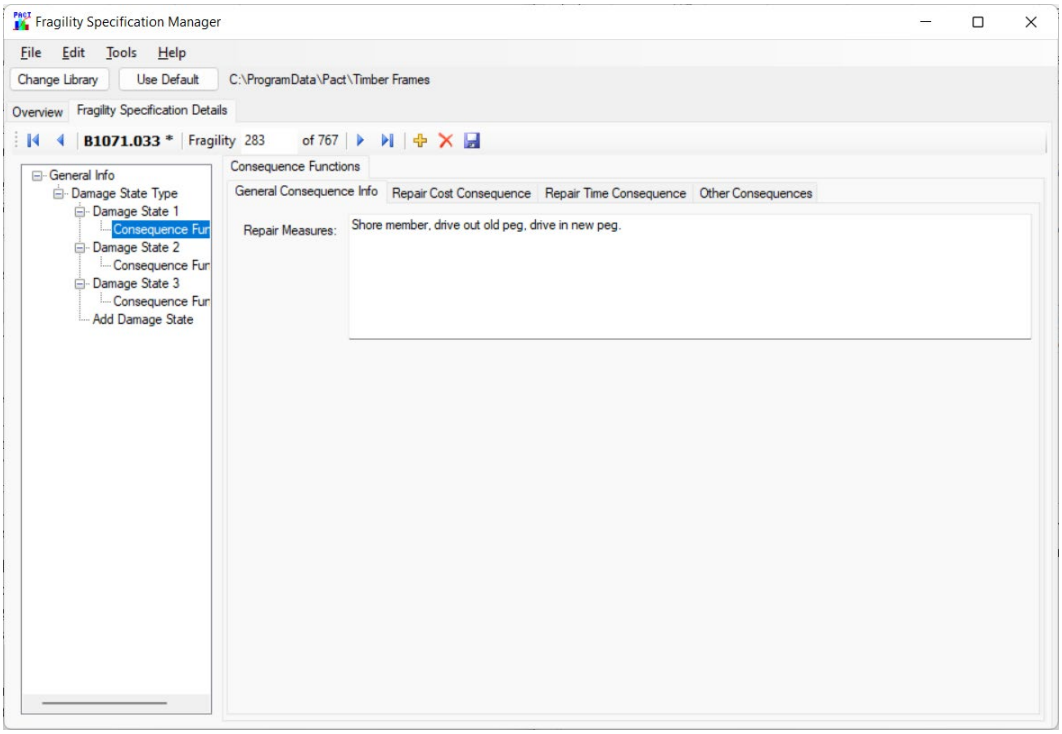

Fig. 6.11. Timber frame fragility B1071.033 Damage State 1: consequence information.

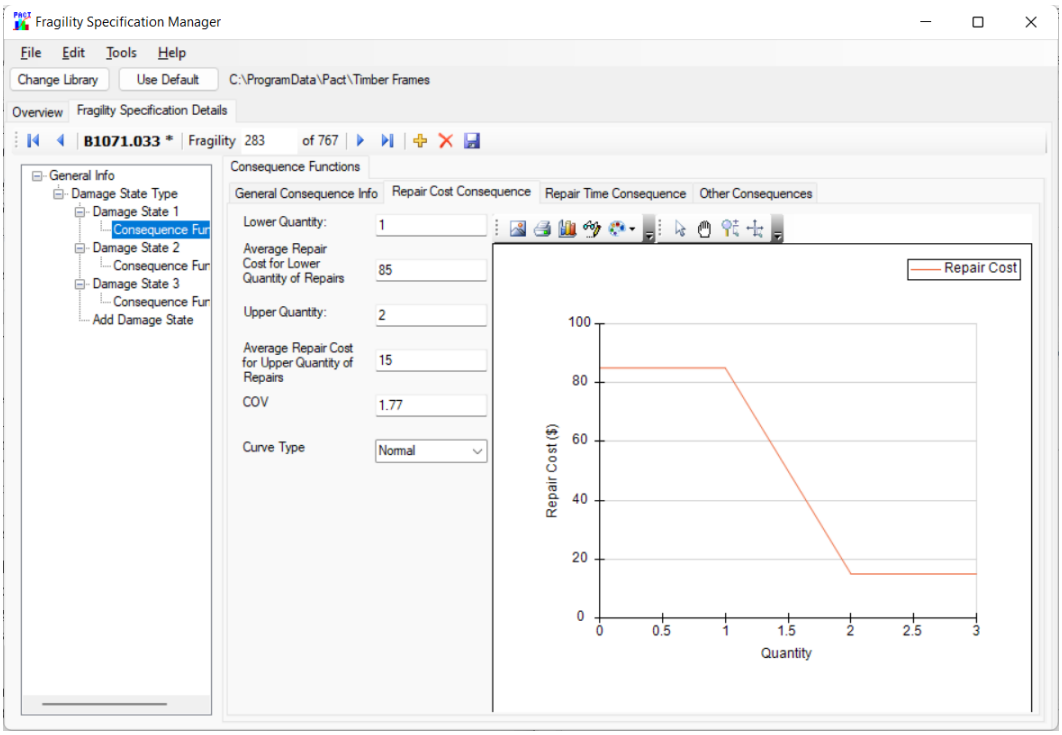

Fig. 6.12. Timber frame fragility B1071.033 Damage State 1: repair cost consequences.

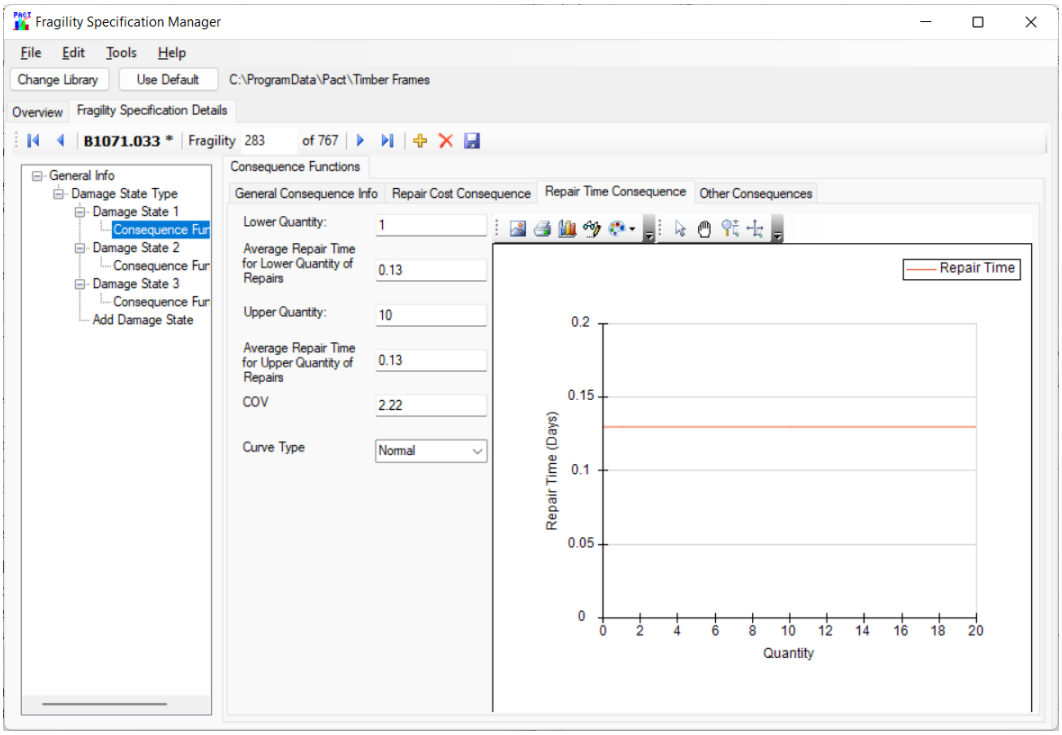

Fig. 6.13. Timber frame fragility B1071.033 Damage State 1: repair time consequences.

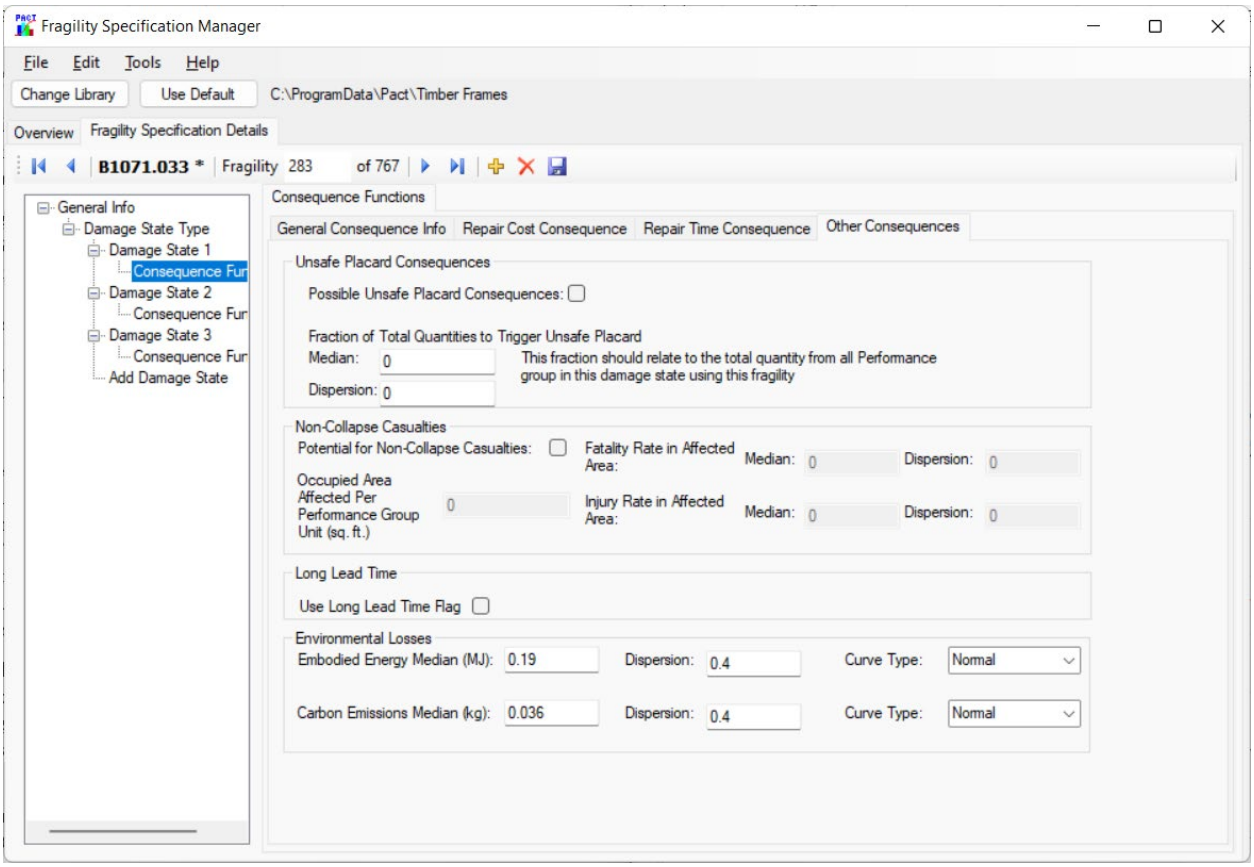

Fig. 6.14. Timber frame fragility B1071.033 Damage State 1: other consequences.

Table 6.3 Results of statistical analysis of survey data.

Failure Location	Consequence function	Travel Included?	σ	COV	β
Peg	Cost	N	147.4	1.77	0.68
		Y	631.2	0.77	0.42
	Time	N	0.3	2.22	0.77
		Y	4.5	0.99	0.47
Brace	Cost	N	367.4	0.71	0.30
		Y	1088.0	0.39	0.16
	Time	N	0.6	0.93	0.68
		Y	17.9	0.83	0.32
Bay	Cost	N	6998.5	0.84	0.56
		Y	14001.5	0.61	0.23
	Time	N	2.1	0.43	0.21
		Y	67.4	0.94	0.40

6.3 Summary

A life cycle analysis of an example timber frame was used to demonstrate a method to determine the embodied carbon in free-standing timber frames. The embodied energy was calculated per mass of wood, as was carbon emissions. A 10% reduction in carbon emissions was assumed based on 10% of the timber being recycled or reused. Carbon emissions produced in wood production was not included, but it can be included if the information is available.

The FEMA P-58 methodology was applied to timber frames to predict performance (repair costs, repair time, the probability of unsafe placarding, and the embodied carbon) during the life-cycle of the structure. Component fragilities for PACT were developed to determine the performance of timber frames. Based on test data (Chapter 3 and Chapter 4), three damage states were defined. The damage states were determined to be sequential. The damage was correlated to story drift ratios based on test data. A survey of timber framers was conducted to determine the anticipated procedures required to repair the damage in each state is described, and to determine the corresponding repair cost and repair time.

CHAPTER 7 CONCLUSIONS

This chapter contains a summary of the research project (cyclic tests, durability tests, vibration tests, and life-cycle analysis) and the implications of the main findings from the research. Areas for future research are also identified.

7.1 Summary

Cyclic tests of timber frames were conducted in the structures laboratory to determine hysteretic behavior and to explore rehabilitation schemes for improved performance after damage due to a lateral-loading event. Two types of free-standing timber frames with knee braces were tested under cyclic loading. Three damage states for were identified: (1) peg shear and (2) tenon tearout at approximately 0.02 rad. joint rotation, and (3) splitting of the post or beam at approximately 0.05 rad. joint rotation. The post base connection of the 3-peg frame was destroyed, so the 3-peg frame was not rehabilitated. The beam in the 2-peg frame split, so the 2-peg frame was rehabilitated by installing an array of self-tapping screws perpendicular to the plane of the split. The test results showed that the self-tapping screws restored the strength of the 2-peg timber frame with the damaged beam, but the stiffness of the 2-peg frame was only partially restored.

Durability tests of brace connections were conducted in the structures laboratory to determine the effect of joint details on the tensile strength and behavior of typical knee-brace connections. Two types of mortise and tenon connections, “drained” and “undrained”, were subjected to damp conditions in a fog room for six months, removed from the fog room, and then tested under monotonic (tensile) load. The monotonic behavior of the joints confirmed the failure modes (peg shear and tenon tearout) that were observed in the cyclic tests. The drained connection did not enhance or diminish the strength or stiffness of the brace connection.

Vibration tests of free-standing timber frames were conducted in the field to determine the fundamental period of vibration and modal damping. Twelve free-standing timber frames with knee braces, located at various sites across the United States, were tested. A relationship between the mean roof height of the timber frame and the fundamental period was fit to the test data using a power-law equation:

- For seismic, $T_a = 0.026\ h^{0.81}$ for $h \leq 20$ ft is recommended. The upper bound coefficient, C_u is determined using ASCE 7 Table 12.8-1.
- For wind, $n_a = 13.5/\ h^{0.54}$ for $h \leq 20$ ft is recommended, where n_a is the natural frequency (Hz).
- For climbing/vandalism, it is suggested to use $T_a = 0.051\ h^{0.64}$ and 2% damping for a bare frame, 10% damping for an enveloped frame.

The curve fits are intended for smaller timber frames, and they may not be appropriate for larger structures.

A life-cycle analysis was conducted to determine the embodied carbon and the damage states for knee-brace connection and to establish component fragilities for performance assessment. The embodied energy was calculated per mass of wood, as was carbon emissions. A

10% reduction in carbon emissions was assumed based on 10% of the timber being recycled or reused. Carbon emissions produced in wood production was not included. The FEMA P-58 methodology was applied to timber frames to predict performance during the life-cycle of the structure. Component fragilities for PACT were developed to determine the performance of timber frames based on the cyclic and monotonic test data. Damage was correlated to story drift ratios. A survey of timber framers was conducted to determine the anticipated procedures required to repair the damage in each state is described, and to determine the corresponding consequences in terms of repair cost and repair time.

7.2 Research implications

The cyclic test results indicate that timber frames with knee braces are relatively flexible for a braced frame system, and that most of the strength and stiffness is developed when the brace is in compression and bears against the post and beam. The brace that is in tension is susceptible to peg shear and tenon tearout. Thus, the test results suggest that a sufficient number of pegs need to be installed to resist the demands, and the end distance in the tenon needs to be sufficiently long to prevent tearout. It should be noted that the tenons in this research were intended to represent current construction details for a typical knee-brace and therefore the tenon was not designed to meet end distance requirements for tensile loading. The rehabilitation study suggests that self-tapping screws have the potential to restore the strength of a timber frame. Restoring stiffness may require another rehabilitation strategy.

The results from the monotonic tests suggest that moisture content does not diminish the tensile strength of mortise and tenon connections more that would be otherwise predicted using

standard procedures (e.g. using the moisture content adjustment factor in the NDS). Although two types of connections were tested (an "undrained" connection that allowed moisture to collect and remain in the joint, and a "drained" connection that had a slope cut at the front of the post/beam and a weep hole at the opposite side to drain water) the approach used in the durability tests did not allow these types of connections to be fully evaluated because the wood in both connections was fully saturated (i.e. near the fiber saturation point). Thus, it is not clear yet if there is an advantage to draining the mortise and tenon connection for the knee brace.

The vibration tests suggest that a power-law equation can be used to determine the period of vibration in a preliminary analysis of a free-standing timber frame. It is understood that for wind and seismic loads the fundamental period would need to be confirmed using a properly substantiated analysis as indicated in ASCE 7, and the equations proposed in this report are only for preliminary sizing, similar to the approach used for buildings in ASCE 7 Chapter 12. For vibration due to human excitation not covered in ASCE 7, such as dynamic loads that occur during maintenance of the timber frames or dynamic loads due to vandalism, the equations proposed in this report represent a first attempt. For all types of loads, the equations are intended for smaller timber frames, not larger timber frames. Damping is particularly difficult to estimate accurately, and the damping range determined in this study were recognized to be estimates for preliminary analysis.

Lastly, the component fragilities developed in this study can be employed with or without the FEMA P-58 software, PACT. The carbon emissions produced in wood production was not included in these fragilities, but it can be added if the information is available.

7.3 Areas for Future Research

The following areas of research are recommended to further understand performance criteria of traditional timber frames:

- This study examined the rehabilitation of one type of knee-braced timber frame with splitting failure using self-tapping screws and tested under a racking load, but further research is recommended to explore different other types of rehabilitation, other configurations of self-tapping screws, and the effect of rehabilitate on other types of members in timber frames, such as the brace or post.

- The approach used in the durability tests employed constant moisture exposure for all of the specimens. Future specimens tested for drainage may be tested in different intervals of moisture exposure or with a different method than utilizing a water vapor-curing room in order to prevent over-saturation of the knee-brace. Erosive materials such as sand or dirt composites could be used to test their impact on joint durability.

- Vibration tests were performed on a limited number of free-standing timber frames that were located in different regions of the United States. Testing additional timber frames is recommended to increase the confidence in the relationship between mean roof height and the fundamental period, or to provide data to substantiate an alternative relationship.

REFERENCES

ACI (American Concrete Institute). 2014. *Building code requirements for structural concrete and commentary*. ACI 318-14, ACI 318R-14, ACI, Farmington Hills, Michigan.

Aejaz, S.A., A.R. Dar, and J.A. Bhat. 2021. Numerical study on the nonlinear behavior of full-scale timber framed joints. *Pract. Period. Struct. Des. Constr.*, 26 (1): https://doi.org/10.1061/(ASCE)SC.1943-5576.0000539

AISC (American Institute of Steel Construction). 2022. *Specification for structural steel buildings*. ANSI/AISC 360-22, AISC, Chicago, Illinois.

AMESWeb. 2022. "Density of steel." Accessed October 28, 2022. https://amesweb.info/Materials/Density_of_Steel.aspx

ASCE (American Society of Civil Engineers). 2022. *Minimum design loads and associated criteria for buildings and other structures*. ASCE/SEI 7-22, ASCE, Reston, Virginia.

Avent, R. R., 1985. "Decay, weathering and epoxy repair of timber." *J. Struct. Eng.*, 111(2), 328-342, https://doi.org/10.1061/(ASCE)0733-9445(1985)111:2(328).

Bertero, S. 2022. Towards a better understanding of the fundamental period of metal building systems. M.S. thesis, Virginia Polytechnic Institute and State University, Blacksburg, Virgina.

Browne, R. D. 1980. "Mechanisms of corrosion of steel in concrete in relation to design, inspection and repair of offshore and coastal structures." ACI Publ. SP-65, V. M. Malhotra, ed., American Concrete Institute, Detroit, 169– 204.

Brungraber, R.L. 1985. Traditional timber joinery: a modern analysis. Ph.D. thesis, Stanford University, Palo Alto, California.

Bulleit, W.M., L.B. Sandberg, M.W. Drewek, and T.L. O'Bryant. 1999. "Behavior and modeling of wood-pegged timber frames." *J. Struct. Eng.*, 125 (1): https://doi.org/10.1061/(ASCE)0733-9445(1999)125:1(3)

Chen, L.-K., S.-C. Li, K.-P. Zhao, Z.-Y. Chen, T.S., L. Zhang, and Z.-J. Jang. 2020. "Experimental and numerical investigation on seismic performance of one-way straight mortise–tenon joints based on a novel method to simulate damage of deteriorated ancient Chinese timber buildings." *J. Perform. Const. Fac.*, 34 (2): https://doi.org/10.1061/(ASCE)CF.1943-5509.0001390

Chen, H. L., and Choi, J. H. 2002. "Effects of GFRP reinforcing rebars on shrinkage and thermal stresses in concrete." *15th ASCE Engineering Mechanics Conf.*, New York.

Courtenay, L.T. 2022. "The roofs of Notre-Dame de Paris: the wider context." *Timber Framing*, 144, 4-13.

Church, J.R., and B.W. Tew. 1997. "Characterization of bearing strength factors in pegged timber connections. *J. Struct. Eng.*, 123 (3): https://doi.org/10.1061/(ASCE)0733-9445(1997)123:3(326)

Dien, N.P. 2008. "Damping identification using the wavelet-based demodulation method: application to gearbox signals." *Technische Mechanik* 28(3-4), 324-333: https://journals.ub.ovgu.de/index.php/techmech/article/view/853

Erikson, R.G., Schmidt, R.J., 2003. "Behavior of traditional timber frame structures subjected to lateral load." Research Report, University of Wyoming, Laramie, Wyoming.

Feio, A.O., P.B. Lourenço, and J.S. Machado. 2014. "Testing and modeling of a traditional timber mortise and tenon joint." *Mater. Struct.* 47: https://doi.org/10.1617/s11527-013-0056-y

Federal Emergency Management Agency (FEMA). 2018a. *Seismic performance assessment of buildings, volume 1—methodology* (FEMA P-58-1). FEMA, Washington, D. C.

Federal Emergency Management Agency (FEMA). 2018b. *Seismic performance assessment of buildings, volume 3— supporting electronic materials* (FEMA P-58-3). FEMA, Washington, D. C.

Frigo, M., and Johnson, S.G. 1998. "FFTW: An adaptive software architecture for the FFT." *International Conference on Acoustics, Speech, and Signal Processing*, 3:1381-1384.

Goel, R. K. and Chopra, A. K. (1997). "Period formulas for moment-resisting frame buildings." *J. of Struct. Eng.*, 123(11):1454–1461. https://doi.org/10.1061/(ASCE)0733-9445(1997)123:11(1454)

Harries, K. A., B. M. Shahrooz, and A. Soltani. 2012a. "Flexural crack widths in concrete girders with high-strength reinforcement." *J. Bridge Eng.* 17 (5): 804–812, https://doi.org/10.1061/(ASCE)BE.1943-5592.0000306

Heitz, J. 2016. "The Resurgence of Heavy Timber Construction." In: *Fire Resistance in American Heavy Timber Construction*. Springer, Cham. https://doi.org/10.1007/978-3-319-32128-8_7

Hindman, D.P. 2019. "Predicting the bending yield strength of timber frame pegs." *J. of Mat. in Civil Eng.* 31(3): 06018027: https://doi.org/10.1061/(ASCE)MT.1943-5533.0002585

Hindman, D., and Mohamadzadeh, M. 2016. "Splitting strength of mortise members in timber frame joints. *J. of Mat. in Civil Eng.*, 28(12), 04016167.

Hochwalt, J. M., and J.E. Amrhein. 2012. *Reinforced masonry engineering handbook*, 7th ed., Masonry Institute of America and International Code Council, Torrance, California.

Jiang, S. F., Wu, M. H., Ma, S. L., & Lin, D. Y. 2018. "Structural stiffness identification of traditional mortise-tenon joints based on statistical process control chart." *J. of Aerospace Eng.,* 31(5), 04018066.

Johansen, K.W. 1949. "Theory of timber connections." Intl. association for Bridge and Structural Engineering. 9: 249-262.

Judd, J.P., Fonseca, F.S., and Leidy, J. 2018. *Seismic performance factors for free-standing timber frame structures.* Structural Engineering and Materials Report No. 18/05, Department of Civil and Architectural Engineering, University of Wyoming, Laramie, Wyoming.

Judd, J.P., Fonseca, F.S., Walker, C.R., and P.R. Thorley. 2012. "Tensile strength of varied-angle mortise and tenon connections in timber frames." *J. Struct. Eng.*, 138 (5): https://doi.org/10.1061/(ASCE)ST.1943-541X.0000468

Kasal, B., Pospisil, S., Jirovsky, I., Heiduschke, A., Drdacky, M. and Haller, P. 2004. "Seismic performance of laminated timber frames with fiber-reinforced joints." *Earthquake Engng. Struct. Dyn.,* 33: 633-646. https://doi.org/10.1002/eqe.368

Lenzen, M. and G. Treloar. 2002. "Embodied energy in buildings: wood versus concrete—reply to Börjesson and Gustavsson." *Energy Policy*, 30 (3), 249-255. https://doi.org/10.1016/S0301-4215(01)00142-2

Lamlom, S.H. and R.A. Savidge. 2003. "A reassessment of carbon content in wood: variation within and between 41 North American Species." *Biomass and Bioenergy,* 24 (4), 381-388. https://doi.org/10.1016/S0961-9534(03)00033-3

Leung, Christopher K. Y. 2001. "Modeling of concrete cracking induced by steel expansion." *J. of Mat. in Civil Eng.,* 13(3), https://doi.org/10.1061/(ASCE)0899-1561(2001)13:3(169)

MATLAB. 2021. MATLAB, version 9.11.0.1837725 (R2021b) Update 2. The MathWorks Inc., Natick, Massachusetts.

Menzies, G.F., Turan, S., and P. F. G. Banfill. 2007. "Life-cycle assessment and embodied energy: a review." *Proceedings of the Ice – Construction Materials,* 160, 135-143. https://doi.org/10.1680/coma.2007.160.4.135

Miller, J.F., R.J. Schmidt, and W.M. Bulleit. 2010. "New yield model for wood dowel connections." *J. Struct. Eng.*, 136 (10): https://doi.org/10.1061/(ASCE)ST.1943-541X.0000224

AWC (American Wood Council). *2018 National design specification (NDS) for wood construction*. AWC, Leesburg, Virginia.

Page, A.W. 2001. "The serviceability design of low-rise masonry structures." *Prog. Struct. Eng. Mater.,* 3: 257-267. https://doi.org/10.1002/pse.86

Palka, L.C., 1981. "Effect of load duration upon timber fasteners: a selective literature review." Canadian Forestry Service 50-57-009, Vancouver, B.C., Canada.

Pedersen, J., Olesen, L., and D. Reinhardt. 2023. "Timber Framing 2.0." In: Gengnagel, C., Baverel, O., Betti, G., Popescu, M., Thomsen, M.R., Wurm, J. (eds) *Towards Radical Regeneration. DMS 2022*. Springer, Cham. https://doi.org/10.1007/978-3-031-13249-0_27

Pierce, P.C., R.L. Brungraber, A. Lichtenstein, and S. Sabol. 2005. *Covered Bridge Manual*. Report No. FHWA-HRT-04-098, Federal Highway Administration, McLean, Virginia.

Richards, P.W. 2012. *Build with steel: a companion to the AISC Manual*. CreateSpace Independent Publishing.

Rosowsky, D.V., and T.A. Reinhold. 1999. “Rate-of-load and duration-of-load effects for wood fasteners.” *J. Struct. Eng.*, 125 (7): https://doi.org/10.1061/(ASCE)0733-9445(1999)125:7(719)

Sandberg, L.B., W.M. Bulleit, and E.H. Reid. 2000. “Strength and stiffness of oak pegs in traditional timber-frame joints.” *J. Struct. Eng.*, 126 (6): https://doi.org/10.1061/(ASCE)0733-9445(2000)126:6(717)

Schmidt, R.J., and C.E. Daniels. 1999. Design considerations for mortise and tenon connections. Research Report, University of Wyoming, Laramie, Wyoming.

Schmidt, R.J., and R.G. Erikson. 2003. Behavior of traditional timber frame structures subjected to lateral load. Research Report, University of Wyoming, Laramie, Wyoming.

Schmidt, R.J., and R.B. MacKay. 1997. Timber Frame Tension Joinery. Research Report, University of Wyoming, Laramie, Wyoming.

Schmidt, R.J., and J.F. Miller. 2004. Capacity of pegged mortise and tenon joinery. Research Report, University of Wyoming, Laramie, Wyoming.

Schmidt, R.J., and G.F. Scholl. 2000. Load duration and seasoning effects on mortise and tenon connections. Research Report, University of Wyoming, Laramie, Wyoming.

Skolnik, D., Ying, L., Yu, E., and J.W. Wallace. 2006. “Identification, model updating, and response prediction of an instrumented 15-story steel-frame building.” *Earthquake Spectra*, 22(3), 781–802. https://doi.org/10.1193/1.2219487

Smith, M. D. and Uang, C.-M. 2013. *Approximate natural periods for metal building moment frames*. Technical Report No. SSRP–12/07, University of California, San Diego, La Jolla, California.

Soltis, L.A., and T.L. Wilkinson. 1991. "United States adaption of European yield model to large-diameter dowel fastener specification." *Int. Timber Engineering Conf.*, London, 3.43-3.49.

Stalker, I.N. 1971. "Protection of timber from fire and weathering." Chem Indus London, Dec 11, 1971, 50, 1427-1431.

The World Counts. 2022. "Environmental impact of steel production." Accessed October 28, 2022. https://www.theworldcounts.com/challenges/planet-earth/mining/environmental-impact-of-steel-production

Timber Frame Engineering Council. 2019. *Standard for design of timber frame structures and commentary*. TFEC 1-2019, Timber Framers Guild, Bellingham, Washington.

Ulewicz, R., and Mazur, M. 2013. "Fatigue testing structural steel as a factor of safety of technical facilities maintenance." *Prod. Eng. Arch.*, 1(1), 32-34. https://doi.org/10.30657/pea.2013.01.10

Van Beerschoten, W., Palermo, A., and D. Carradine. 2012. "Gravity design of post-tensioned timber frames for multi-storey buildings." *Structures Congress 2012*, 1733-1744.

Van der Put, T. A. C. M., and A. J. M. Leijten, 1999. "Evaluation of perpendicular to grain failure of beams caused by concentrated loads of joints." Proceedings of CIB-W18/paper, 33-7.

Vu, K. A. T., and Stewart, M. G. 2005. "Predicting the likelihood and extent of reinforced concrete corrosion-induced cracking." *J. Struct. Eng.*, 131(11), 1681-1689, https://doi.org/10.1061/(ASCE)0733-9445(2005)131:11(1681)

Wilkinson, T.L. 1988. "Duration of load on bolted joints: a pilot study." (Vol. 488). US Department of Agriculture, Forest Service, Forest Products Laboratory, Madison, Wisconsin.

Wilkinson, T.L. 1991. “Dowel bearing strength.” (Vol 505). US Department of Agriculture, Forest Service, Forest Products Laboratory., Madison, Wisconsin.

Wu, G., Zhong, Y., Gong, Y., and Ren, H. 2019. “Application of modern wood product glulam in timber frame with tenon-mortise joints and its structural behavior. *Journal of Renewable Materials*, 7(5), 451–461.

Zhang, L., Zhang, S., Chui, Y.H. 2021. “Analytical evaluation to the timber-concrete composite beam connected with notched connections.” *Engineering Structures*, 227(15):111466.